Check for updates

ADVANCED MATERIALS
www.advmat.de

Remote Control of Energy Transformation-Based Cancer Imaging and Therapy

Hai Xu, Dahee Kim, Yuan-Yuan Zhao, Chowon Kim, Guosheng Song, Qiongzheng Hu,* Heemin Kang,* and Juyoung Yoon**

Cancer treatment requires precise tumor-specific targeting at specific sites that allows for high-resolution diagnostic imaging and long-term patient-tailorable cancer therapy; while, minimizing side effects largely arising from non-targetability. This can be realized by harnessing exogenous remote stimuli, such as tissue-penetrative ultrasound, magnetic field, light, and radiation, that enable local activation for cancer imaging and therapy in deep tumors. A myriad of nanomedicines can be efficiently activated when the energy of such remote stimuli can be transformed into another type of energy. This review discusses the remote control of energy transformation for targetable, efficient, and long-term cancer imaging and therapy. Such ultrasonic, magnetic, photonic, radiative, and radioactive energy can be transformed into mechanical, thermal, chemical, and radiative energy to enable a variety of cancer imaging and treatment modalities. The current review article describes multimodal energy transformation where a serial cascade or multiple types of energy transformation occur. This review includes not only mechanical, chemical, hyperthermia, and radiation therapy but also emerging thermoelectric, pyroelectric, and piezoelectric therapies for cancer treatment. It also illustrates ultrasound, magnetic resonance, fluorescence, computed tomography, photoluminescence, and photoacoustic imaging-guided cancer therapies. It highlights afterglow imaging that can eliminate autofluorescence for sustained signal emission after the excitation.

1. Introduction

Energy transformation ushered in the history of the development of modern industry, starting from the transformation of thermal energy into mechanical energy and the launch of human society into the "Age of Steam." Subsequently, the advent of more convenient and transformable electrical energy created the Second Industrial Revolution. Therefore, the diversity of energy transformation methods has led to the vigorous development of science and technology.[1,2] However, cancer, one of the deadliest diseases in the world, has accompanied humankind for centuries. Although tumor-targeted therapy and immunotherapy have made many breakthroughs in the past few decades, there are still many limitations in their precise diagnosis and treatment of tumors. Interestingly, new cancer diagnosis and treatment modalities that utilize tissue-penetrative remote energy stimulation have received widespread attention and exploration due to their unique advantages of targeted local activation for deep tumors.[3–7]

H. Xu, Y.-Y. Zhao, J. Yoon
Department of Chemistry and Nanoscience
Ewha Womans University
Seoul 03760, Republic of Korea
E-mail: jyoon@ewha.ac.kr

D. Kim, C. Kim, H. Kang
Department of Materials Science and Engineering
Korea University
Seoul 02841, Republic of Korea
E-mail: heeminkang@korea.ac.kr

G. Song
State Key Laboratory of Chemo/Biosensing and Chemometrics
College of Chemistry and Chemical Engineering
Hunan University
Changsha 410082, China
E-mail: songgs@hnu.edu.cn

Q. Hu
Qilu University of Technology (Shandong Academy of Sciences)
Shandong Analysis and Test Center
Jinan 250014, China
E-mail: huqz@qlu.edu.cn

H. Kang
College of Medicine
Korea University
Seoul 02841, Republic of Korea

The ORCID identification number(s) for the author(s) of this article can be found under https://doi.org/10.1002/adma.202402806

© 2024 The Authors. Advanced Materials published by Wiley-VCH GmbH. This is an open access article under the terms of the Creative Commons Attribution-NonCommercial License, which permits use, distribution and reproduction in any medium, provided the original work is properly cited and is not used for commercial purposes.

DOI: 10.1002/adma.202402806

With the rapid development of nanotechnology, nanomaterial-mediated energy transformation has attracted much attention in cancer treatment.[8–12] Meanwhile, in order to adapt to various external environments or tumor microenvironments (TMEs), nanomaterials can coordinate the transformation of different energies through tissue penetration and remote energy stimulation so as to achieve efficient, precise, and controllable treatment.[13,14] Moreover, the mutual transformation of different energies can enable diverse cancer treatment modalities, among which the synergistic transformation of multiple energies tends to be more effective, and energy transformation processes with certain similarities can be skillfully combined together.[15–17] For example, Yong et al. constructed a phthalocyanine self-assembled nanomaterial that guided tumor treatment through imaging combining photothermal therapy (PTT, photonic-to-thermal energy transformation) and photoacoustic imaging (PAI, photonic-to-thermal-to-ultrasonic energy transformation).[18] However, in order to achieve better therapeutic effects, remote therapy combined with drug therapy or immunotherapy is a good choice.[19–24] Among them, the combination of PTT and photodynamic therapy (PDT) is still a research hotspot and its combination with immunotherapy has achieved good therapeutic effects.[25–27] Moreover, effective imaging or therapeutic methods often attract scientists to explore energy transformation further.[28] For instance, Song et al. explored the mechanism of organic photoafterglow imaging and achieved remarkable results in early disease diagnosis and cancer treatment using afterglow imaging.[29] In any case, the diversity of energy and the complexity of transformation pathways make the concept of transformation between energy types vague and inconvenient for further research.[30] Therefore, it is necessary to comprehensively summarize and elaborate on the reported remote imaging and therapy modalities in energy mode.

Here, specifically targeted imaging of tumors through remote stimulation of different energy types is summarized, including ultrasound (US), magnetic field, light, and radiation (**Figure 1**). In addition, these energies are directly or indirectly transformed by uniquely designed nanomaterials to achieve efficient diagnostic imaging and therapy of cancers. Therefore, many of the latest typical examples are discussed from the perspective of how various energies are transformed and achieve targetable, efficient, and long-term cancer imaging and therapy. To the best of our knowledge, this is the first review on the topic of "remote control of energy transformation for cancer imaging and therapy." Recent review articles have discussed specific energy transformation alone for either cancer imaging or therapy, but no review articles have fully described various kinds of energy transformation for cancer imaging and therapy. For example, relevant review articles have focused only on energy application (without energy transformation), piezoelectric energy transformation, and fluorescent energy transformation.[31–33] In this review, we describe multimodal energy transformation where a serial cascade or multiple types of energy transformation occur. In addition, we highlight ultrasensitive afterglow imaging that can eliminate autofluorescence for sustained signal emission after the excitation. Finally, subdividing the categories and advantages between different energies provides new ideas for further designing and improving remote diagnostic and therapeutic technology for enhanced practical applicability.

2. Single Energy Transformation for Cancer Therapy

2.1. Ultrasonic-to-Chemical Energy Transformation: Sonodynamic Therapy

US—mechanical vibration waves with frequencies beyond human hearing (>20 kHz)—has a high penetration depth (≥10 cm) in soft tissues.[34,35] High- and low-intensity US are classified based on the US wave intensity. Low-intensity US can generate reactive oxygen species (ROS) through sonosensitizers to kill malignant tumors.[36,37] This type of therapy, which transforms US energy into chemical energy, is called sonodynamic therapy (SDT). Compared with lasers used for PDT, US can reach deep organs such as the liver and pancreas and selectively kill tumors without damaging the surrounding healthy tissues, which is very effective in the treatment of deep malignant tumors.[38] Therefore, the unique advantages of SDT, such as non-invasiveness and strong penetrability, provide new options for cancer treatment and are expected to become a promising non-invasive cancer treatment method.[39]

In SDT, sonosensitizers are the necessary media for transforming ultrasonic energy into chemical energy. Among them, porphyrin derivatives and some clinical chemotherapy drugs (doxorubicin [DOX] and curcumin) are commonly used sonosensitizers.[40,41] However, most of these compounds have issues, such as high dose-dependent toxicity or inherent skin sensitivity in the clinical application of SDT. In addition, most sonosensitizers result in a significant reduction in the effectiveness and accuracy of SDT due to poor hydrophobicity aggregation, poor pharmacokinetics, and poor targeting of lesion sites. Excitingly, advances in nanotechnology offer hope for this dilemma. For instance, Lin et al. reported highly efficient nano-sonosensitizers (TBP@MOL) consisting of iridium-based linkers and Hf-oxo secondary building units (SBUs), in which 5,10,15,20-tetra(*p*-benzoato)porphyrin (TBP) sensitizers anchored to the SBU (**Figure 2**a).[42] Under US irradiation, TBP@MOL produced 14.1- and 7.4-fold more cytotoxic singlet oxygen ($^1O_2$) than TBP and Hf-TBP alone, respectively (Figure 2b). At the same time, the lethality and the SDT therapeutic effect of TBP@MOL were significantly better than those of other groups in the tumor mouse model experiment (Figure 2c), showing that SDT had a good killing effect on tumors in vivo.

Compared with inorganic nano-sonosensitizers that may have problems such as biosafety and biodegradation, organic sonosensitizers can be synthesized in a controlled manner by rationally designing the molecular structure, thereby making them good biocompatible materials.[43,44] Based on this, Chen et al. designed and synthesized high-efficiency organic sonosensitizers BAnTh and BTeTh based on triarylboron-doped acenethiophene scaffolds (Figure 2d).[45] Under US irradiation, it had a high ROS (hydroxyl radical, $^{\bullet}OH$) production efficiency, which avoided the potential skin phototoxicity problem in cancer treatment. Moreover, in biological experiments, BTeTh nanoparticles (NPs) could effectively inhibit tumor growth without causing obvious damage to normal tissues. These results indicated that B(0)-doped organic sonosensitizers had a broad application prospect in the efficient, non-toxic, and high-safety SDT.

© 2024 The Authors. Advanced Materials published by Wiley-VCH GmbH

15214095, 2024, 27, Downloaded from https://onlinelibrary.wiley.com/doi/10.1002/adma.202402806 by Ewha Womans University Library, Wiley Online Library on [13/11/2024]. See the Terms and Conditions (https://onlinelibrary.wiley.com/terms-and-conditions) on Wiley Online Library for rules of use; OA articles are governed by the applicable Creative Commons License

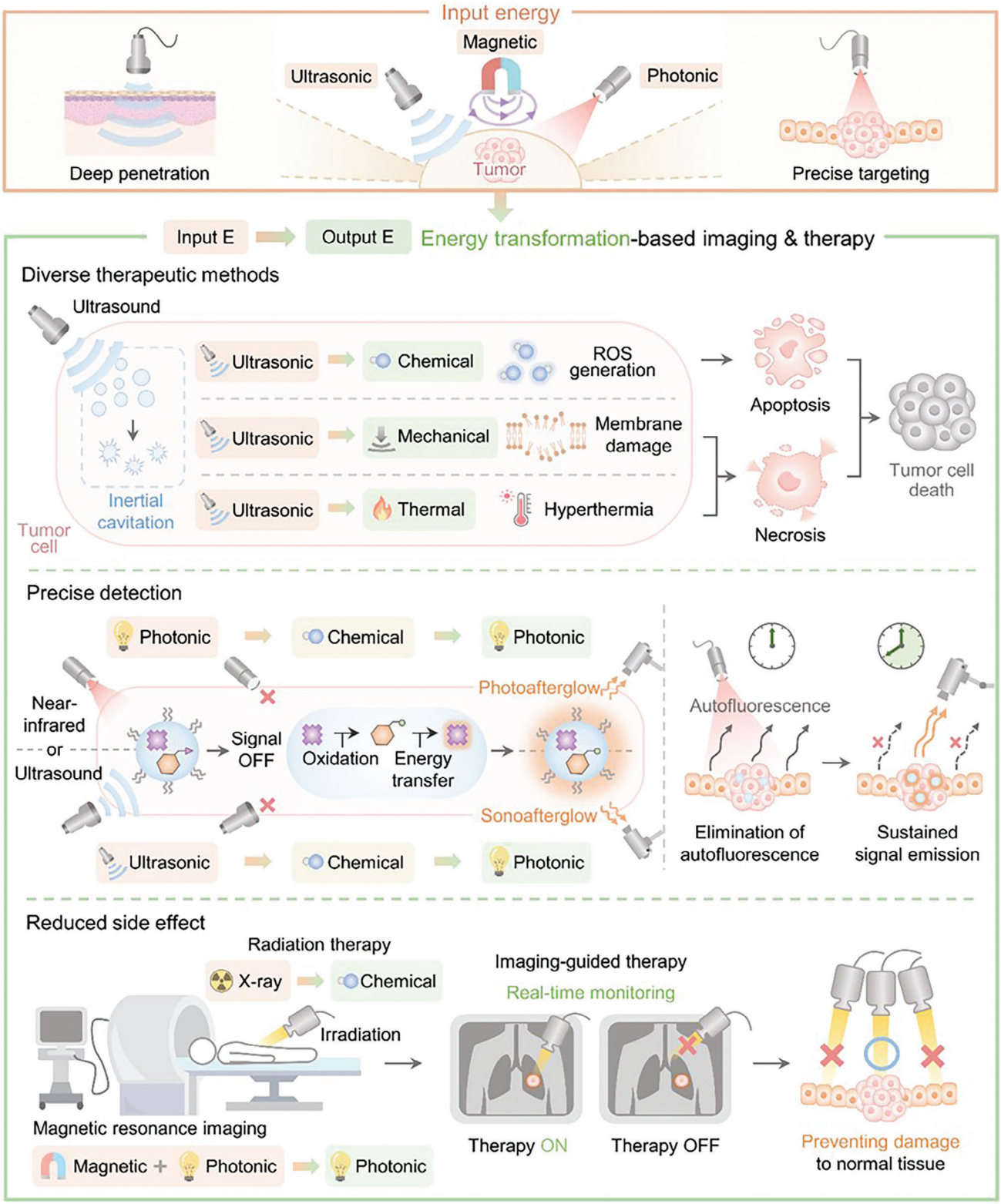


Figure 1. A schematic illustration of various energy transformation-based cancer imaging and therapies.

© 2024 The Authors. Advanced Materials published by Wiley-VCH GmbH

15214095, 2024, 27, Downloaded from https://onlinelibrary.wiley.com/doi/10.1002/adma.202402806 by Ewha Womans University Library, Wiley Online Library on [13/11/2024]. See the Terms and Conditions (https://onlinelibrary.wiley.com/terms-and-conditions) on Wiley Online Library for rules of use; OA articles are governed by the applicable Creative Commons License

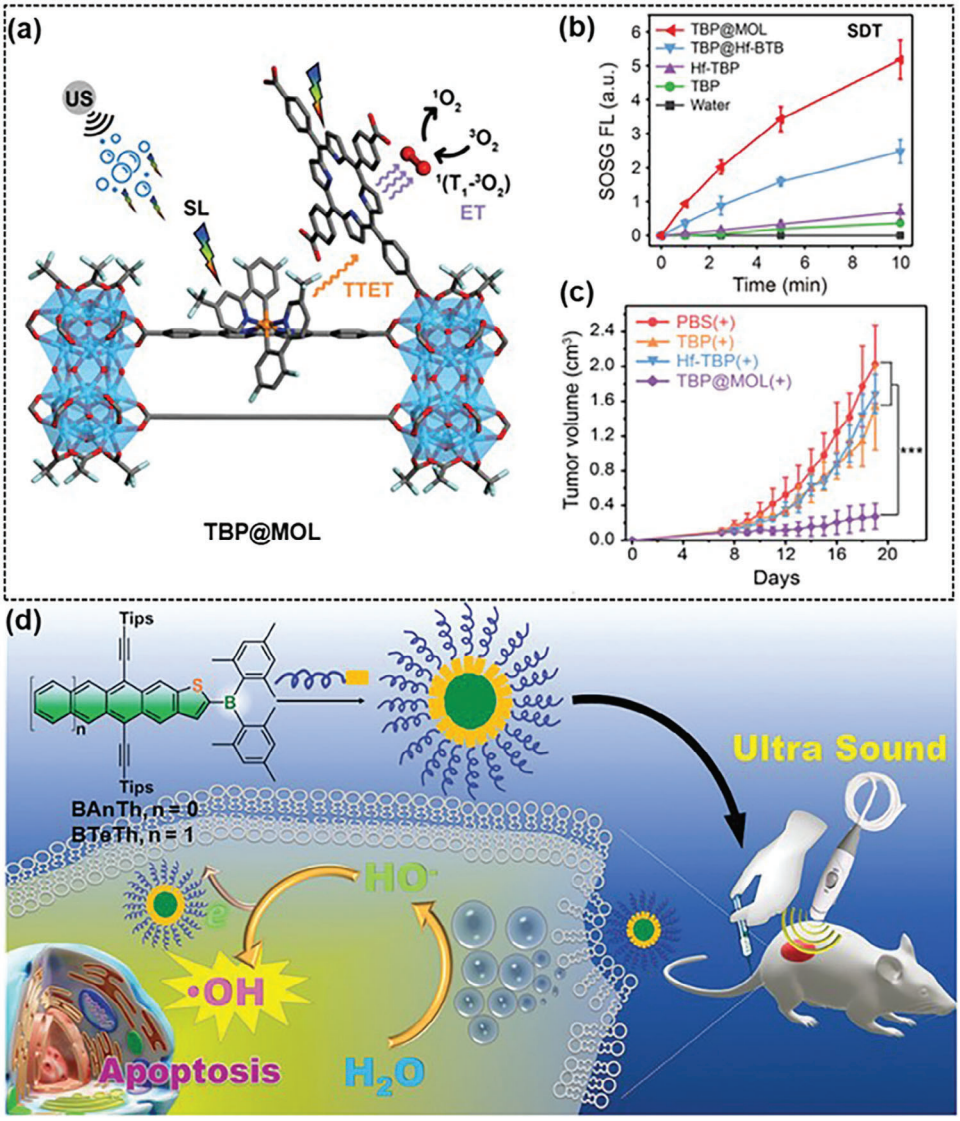


Figure 2. a) Schematic illustration of the $^1O_2$ generation of TBP@MOL. b) $^1O_2$ generation of different TBP systems upon US. c) SDT anticancer efficacy in subcutaneous. Reproduced with permission.[42] Copyright 2023, Wiley-VCH. d) Schematic illustration of B(0)-doped acenethiophenes for efficient SDT. Reproduced with permission.[45] Copyright 2022, Wiley-VCH.

Although SDT has clear advantages in tumor treatment, it leads to a low immune response and is difficult to inhibit tumor recurrence due to the insufficient tumor targeting of sonosensitizers and the influence of the TME. Therefore, the combination of SDT and drug therapy deserves attention.[46,47] For example, Yang et al. developed an SDT–nanovaccine integration platform (cMn-MOF@CM) consisting of a manganese porphyrin-based metal-based organic framework (Mn-MOF) and the immune adjuvant CpG that were encapsulated in melanoma B16 cell membranes (**Figure** 3a).[48] Meanwhile, cMn-MOF@CM could effectively alleviate the hypoxic environment of tumors and reduce intracellular glutathione (GSH) by prolonging blood circulation time and enhancing tumor targeting, resulting in a strong SDT effect and immunogenic cell death (ICD) (Figure 3b). Moreover, tumor-associated antigens of orthotopic SDT and overexpressing ovalbumin (OVA), as well as the immune adjuvant CpG, could effectively enhance antitumor immunity. Finally, the combination of cMn-MOF@CM-triggered SDT and anti-programmed death-1 (anti-PD-1) antibody induced a stronger systemic immune response and long-term immune memory function, preventing tumor growth and recurrence. Similarly, immunosuppression of the TME is also worthy of attention.[49,50] For instance, Dai et al. synthesized an artificial polyphenol derivative conjugated to the sonosensitizer chlorine e6 (PEG-Ce6 polyphenols) and cross-linked with Fe^{2+} ions to form nanocarriers (PALF), along with introduced lactate oxidase (LOX) and the mitochondrial respiratory inhibitor atovaquone (ATO) (Figure 3c).[51] It is particularly worth noting that the introduction of ATO could reduce the oxygen demand of mitochondria, effectively alleviate tumor hypoxia, accelerate LOX to reverse the acidic TME, enhance the SDT effect, and inhibit tumor proliferation and metastasis.

© 2024 The Authors. Advanced Materials published by Wiley-VCH GmbH

15214095, 2024, 27, Downloaded from https://onlinelibrary.wiley.com/doi/10.1002/adma.202402806 by Ewha Womans University Library, Wiley Online Library on [13/11/2024]. See the Terms and Conditions (https://onlinelibrary.wiley.com/terms-and-conditions) on Wiley Online Library for rules of use; OA articles are governed by the applicable Creative Commons License

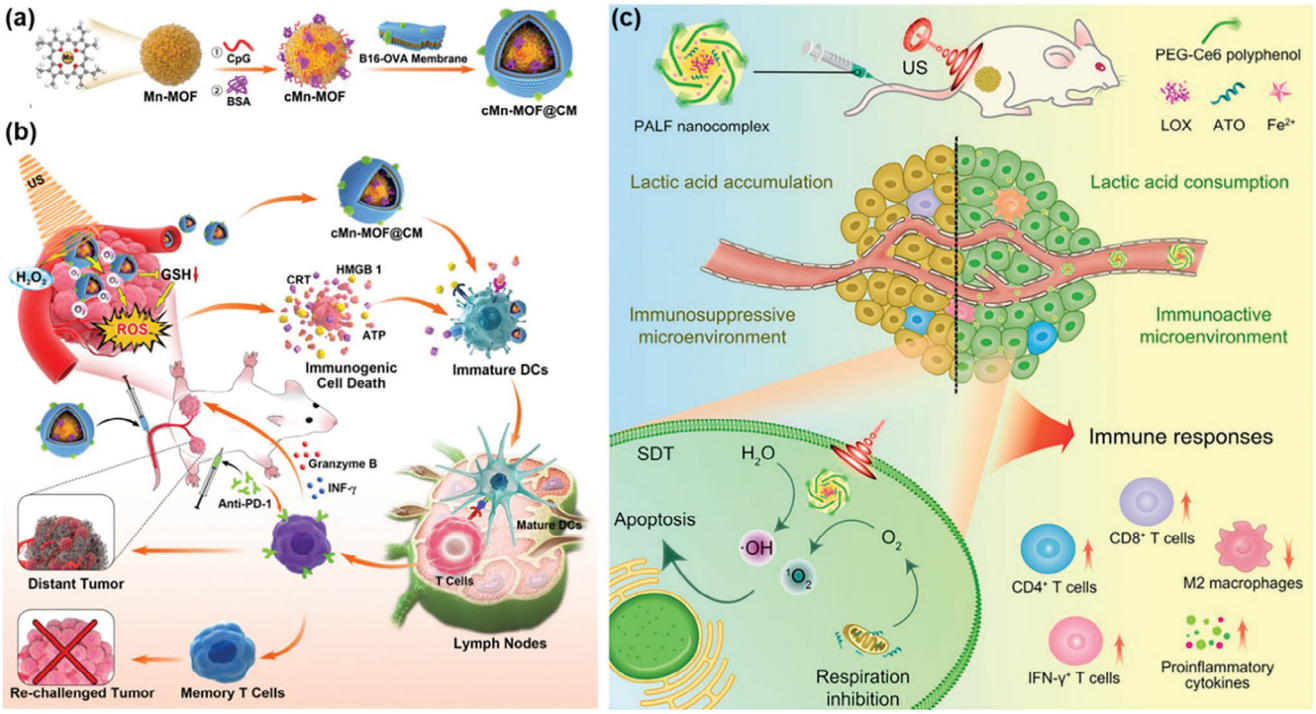


Figure 3. a) Schematic illustration of the synthesis of cMn-MOF@CM. b) Schematic illustration of SDT–nanovaccine integration platform to improve anti-PD-1 efficacy. Reproduced with permission.[48] Copyright 2021, Elsevier. c) Schematic illustration of the co-loading and antitumor effect of PALF. Reproduced with permission.[51] Copyright 2021, American Chemical Society.

2.2. Ultrasonic-to-Mechanical Energy Transformation: Ultrasonic Mechanical Therapy

Although nanocarriers have some effect in chemotherapy drug therapy, nanocarriers need to rely on the enhanced permeability and retention (EPR) effect to deliver drugs to tumor tissues.[52] However, the EPR effect can only deliver ≈0.7% of the drug to tumor tissue, which means that finding better delivery methods is urgent.[53] It is worth noting that under the action of US of a certain intensity and frequency, the mechanical pressure of the tissue fluid increases rapidly, resulting in a large number of cavitation microbubbles (MBs) with a diameter of ≈1–10 μm.[54] At the same time, the cavitation MBs will undergo the mechanical dynamic process of oscillation, expansion, and even bursting, resulting in the collapse of the cell membrane and the increase of permeability. Therefore, the process of transforming US energy into mechanical energy can efficiently promote the transport of drugs to tumor cells.

Based on the drug delivery capability of focused ultrasound (FU), Kim et al. developed nanocomplexes (siRNA-NP-PTX-MBs) consisting of paclitaxel (PTX)-loaded MBs and RNA hydrogel-based NPs (siRNA-NPs) (**Figure 4a**).[55] The nanocomplex enhanced the penetration and aggregation ability of siRNA-NPs and PTX in tumor tissues, and the strong mechanical energy of FU relaxed the extracellular matrix of cancer, which resulted in an excellent chemo-gene therapeutic effect (Figure 4b). In addition, Lux et al. developed a US-guided cancer immunotherapy platform based on nanocomposites (ncMBs). The platform was composed of 2′3′-cyclic guanosine monophosphate–adenosine monophosphate (cGAMP) that was electrostatically bound to a biocompatible branched cationic biopolymer that bound to antigen-presenting cells (APC)-targeted MBs (Figure 4c).[56] Further, US-guided cancer MB immunotherapy delivered the immune transmitter cGAMP, which was involved in anticancer immunity, to APCs (Figure 4d). Within APCs, MBs released cGAMP to activate the cyclic GMP–AMP synthase-stimulator of interferon genes (cGAS-STING) pathway, which stimulated the type I interferon response crucial for initiating tumor-specific T cells. In short, the platform could generate systemic antitumor immunity and improve the therapeutic effects of immune checkpoint blockade.

2.3. Ultrasonic-to-Thermal Energy Transformation: High-Intensity Focused Ultrasound

High-intensity focused ultrasound (HIFU) therapy utilizes the tissue penetration and energy deposition characteristics of US to focus US that occurs outside the body on the diseased tissue and achieves the goal of treating tumors through the thermal effect of US. It is important to note that the energy of FU in the non-treatment area through which it passes is not enough to cause tissue damage. Meanwhile, the temperature of the focal point can reach 60–100 °C, resulting in coagulative necrosis of the tissues at the focal point without damaging the normal tissue outside the focal point.[57,58] However, due to the energy attenuation of deep lesions, it is difficult for HIFU to

© 2024 The Authors. Advanced Materials published by Wiley-VCH GmbH

15214095, 2024, 27, Downloaded from https://onlinelibrary.wiley.com/doi/10.1002/adma.202402806 by Ewha Womans University Library, Wiley Online Library on [13/11/2024]. See the Terms and Conditions (https://onlinelibrary.wiley.com/terms-and-conditions) on Wiley Online Library for rules of use; OA articles are governed by the applicable Creative Commons License

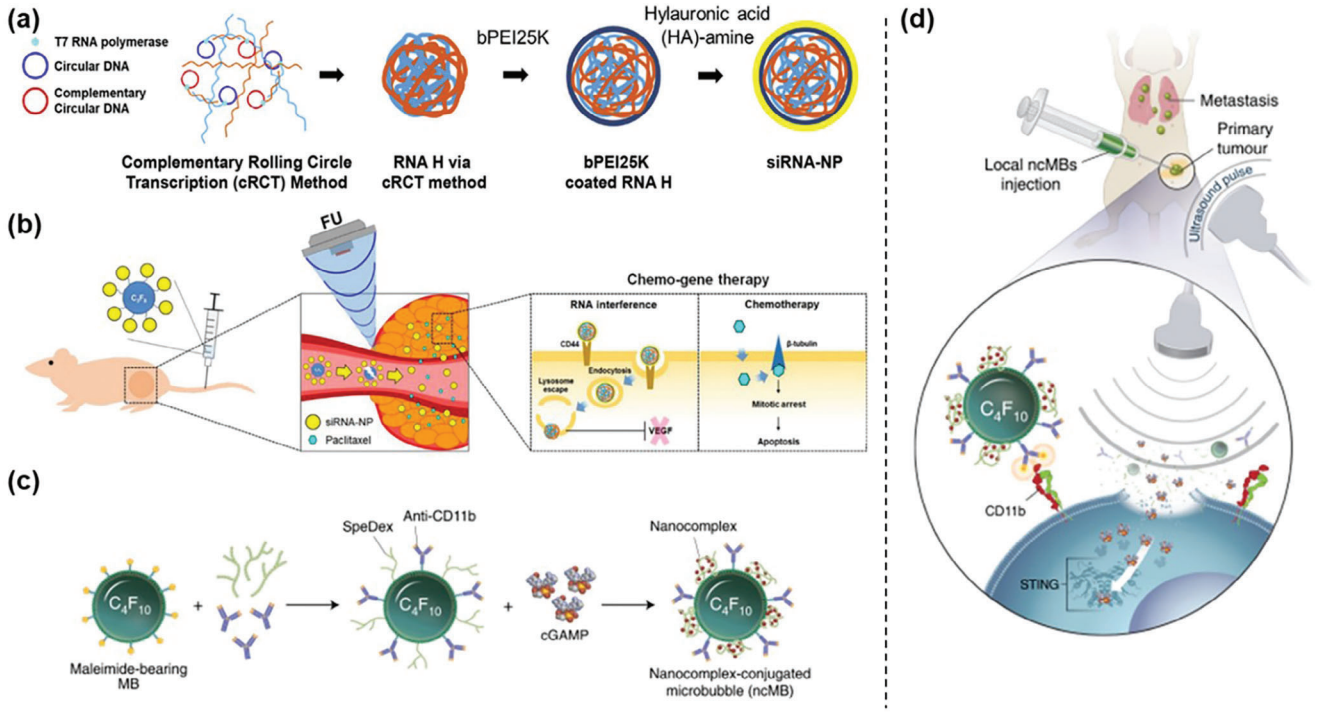


Figure 4. a) Schematic illustration of the preparation of siRNA-NPs. b) Schematic illustration of therapy using FU-responsive siRNA-NP-PTX-MBs. Reproduced with permission.[55] Copyright 2020, Elsevier Ltd. c) Schematic illustration of the preparation of ncMBs. d) Schematic illustration of US-activated STING. Reproduced with permission.[56] Copyright 2022, Springer Nature.

eradicate tumors completely. A great number of clinical data have shown that this ability to transform ultrasonic into thermal energy has a good synergistic effect on radiotherapy, chemotherapy, and chemoradiotherapy. HIFU has been reported to be used in combination with heat-sensitive drug carrier systems such as liposomes as a trigger for local drug delivery.[59] For instance, Grüll et al. used a thermosensitive liposome (TSL) of phosphatidyldiglycerol to encapsulate DOX and released DOX locally under the influence of HIFU (**Figure 5a**).[60] The cycle time of DOX with HIFU was prolonged, and the concentration of intramuscular drug for hyperthermia at 10 min was increased 15-fold compared to that of DOX without HIFU (Figure 5b). Meanwhile, it was expected that the optimal time point for TSL infusion would be determined through the HIFU drug release experiment, which was of great significance for clinical translation.

HIFU can be thermally ablated from the lesion site, but the phenomenon of energy decay with increasing tissue depth makes it difficult to ablate tumors in deeper tissues completely. To ameliorate the above shortcomings, Jing et al. developed temperature-sensitive plateletsomes (TSPs) for the integration of HIFU tumor ablation and chemotherapy in vivo (Figure 5c).[61] During HIFU hyperthermia, TSPs provided high drug utilization at the tumor site and targeted the postoperative tumor site due to their high drug loading efficiency and temperature-sensitive permeability, which had effective integration into the surgical process. In short, the nanoplatform of HIFU and chemotherapy combination therapy has certain application prospects.

2.4. Magnetic-to-Mechanical Energy Transformation: Magnetic Mechanical Therapy

In addition to US, magnetic therapy is also considered to be an emerging patient-friendly and effective treatment strategy using mechanical stimulation with deep tissue penetration and focusable energy sources.[62–65] Magnetic nanomaterials (MNMs) are widely used in the biomedical field, especially in the field of cancer treatment, due to their unique magnetic properties. In addition, the combination of MNMs with alternating magnetic fields is an emerging physiotherapy method, mainly including magnetic mechanical therapy (MMT) and magnetic hyperthermia therapy (MHT). Between them, MMT is a powerful mechanical force generated by placing MNMs in a low-frequency alternating magnetic field, thereby destroying the structure of tumor cells and ultimately leading to apoptosis.[66,67]

In 2021, Cheng et al. modified MNM with a Cyanine5-tagged (Cy5-tagged) caspase-3-specific peptide to adaptively control the MNM swarms in lysosomes under a rotating magnetic field, thereby inducing apoptosis in cancer cells (**Figure 6a**).[68] It was found that the step-out frequency was the main parameter of synchronous rotation, which played a key role in the efficient transformation of magnetic energy into mechanical energy.[69] Moreover, Cy5 could detect and feed back the apoptotic process induced by the MNM population in real-time, thereby programming the MNM population to destroy cancer cells and perform adaptive control. In short, this study provided a reference for remote adaptive control of magnetic nanoparticles (MNPs) for cancer treatment. Similarly, considering that mitochondria

© 2024 The Authors. Advanced Materials published by Wiley-VCH GmbH

15214095, 2024, 27, Downloaded from https://onlinelibrary.wiley.com/doi/10.1002/adma.202402806 by Ewha Womans University Library, Wiley Online Library on [13/11/2024]. See the Terms and Conditions (https://onlinelibrary.wiley.com/terms-and-conditions) on Wiley Online Library for rules of use; OA articles are governed by the applicable Creative Commons License

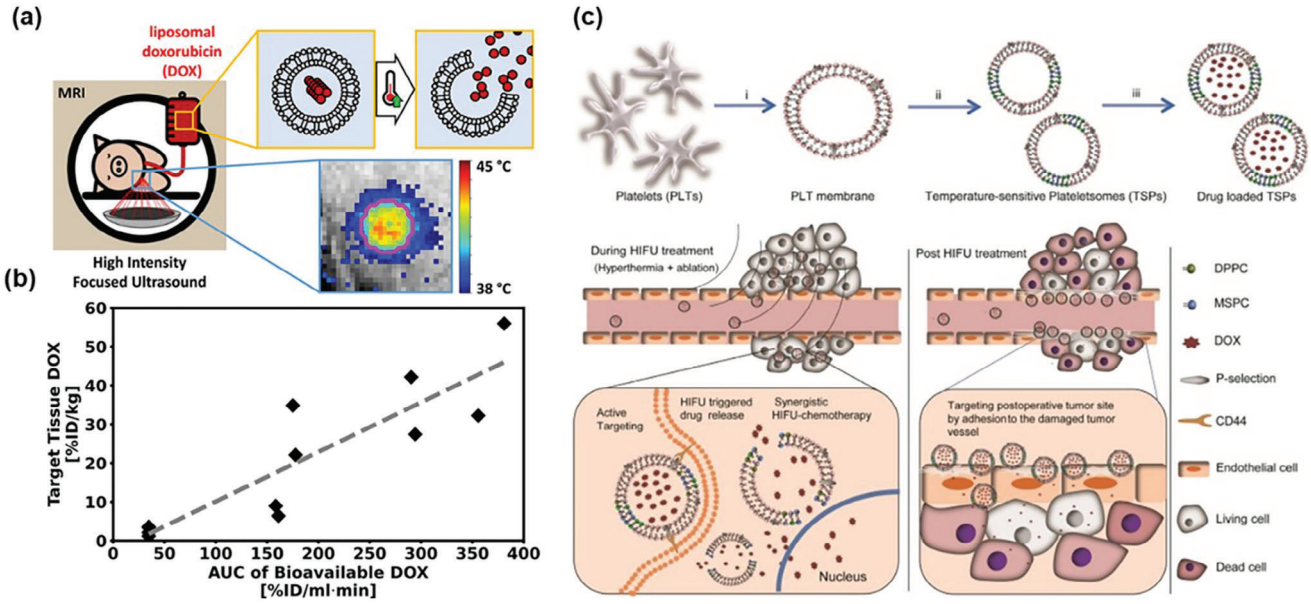


Figure 5. a) Schematic illustration of MR-HIFU hyperthermia drug delivery. b) DOX concentration versus the respective AUC of bioavailable DOX. Reproduced with permission.[60] Copyright 2022, Elsevier Ltd. c) Schematic design of TSPs combined with HIFU tumor ablation. Reproduced with permission.[61] Copyright 2019, Ivyspring International.

are important organelles influencing apoptosis, Cheng et al. designed a cube composed of zinc-doped iron oxide nanocubes and triphenylphosphine cations (TPPs) for mitochondrial targeting nanorotators (TPP-MNPs) (Figure 6b).[70] As shown in Figure 6c, TPP-MNPs had good colocalization with mitochondria and were found in some lysosomes, indicating that the nanocube underwent lysosomal escape to the mitochondria. Meanwhile, TPP-MNPs could efficiently accumulate in mitochondria and assemble by an external magnetic field to destroy mitochondria and induce cancer cell death under a rotating magnetic field. Moreover, with the deep penetration ability of magnetic fields, MNPs could destroy cancer cells through mechanical force and are expected to be combined with magnetic hyperthermia for synergistic treatment.

2.5. Magnetic-to-Thermal Energy Transformation: MHT

Tumor MHT is based on the magnetic thermal effect generated by MNPs-mediated external magnetic fields.[71,72] Compared with radiotherapy/chemotherapy, MHT has fewer toxic side effects, stronger controllability, and does not involve drug resistance. Meanwhile, compared with therapies such as PTT/PDT and US ablation, magnetic hyperthermia is safer, more penetrating, and

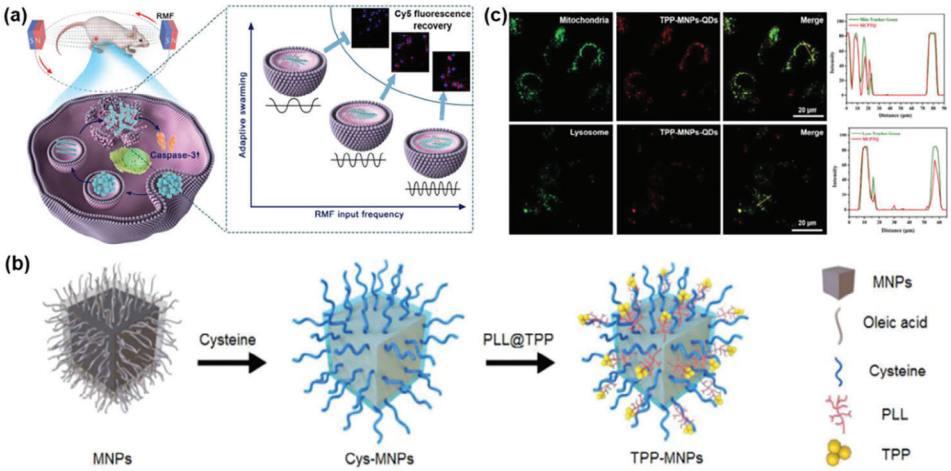


Figure 6. a) Schematic illustration of the frequency-adapted behaviors of MNM swarms and the cancer cell destruction. Reproduced with permission.[68] Copyright 2021, American Chemical Society. b) Schematic illustration of the preparation of TPP-MNPs. c) Mitochondrial and lysosomal confocal fluorescence images of U87 cells. Reproduced with permission.[70] Copyright 2019, Wiley-VCH.

© 2024 The Authors. Advanced Materials published by Wiley-VCH GmbH

15214095, 2024, 27, Downloaded from https://onlinelibrary.wiley.com/doi/10.1002/adma.202402806 by Ewha Womans University Library, Wiley Online Library on [13/11/2024]. See the Terms and Conditions (https://onlinelibrary.wiley.com/terms-and-conditions) on Wiley Online Library for rules of use; OA articles are governed by the applicable Creative Commons License

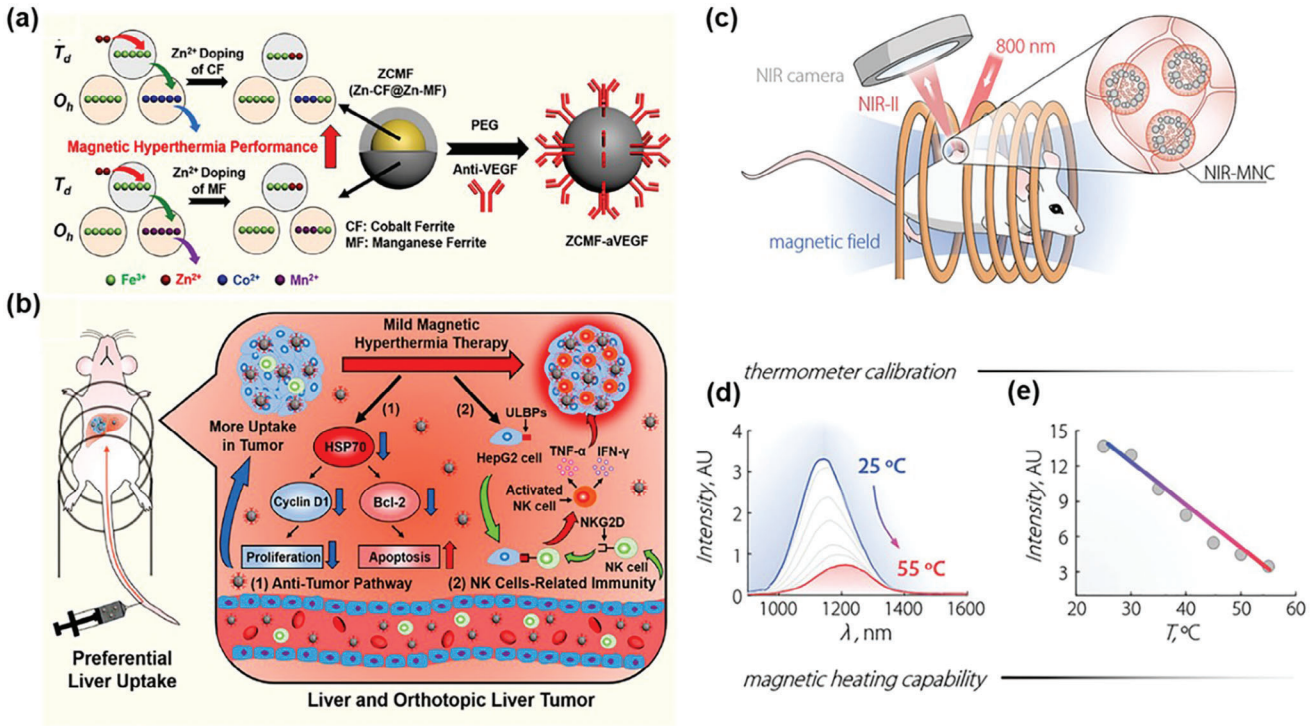


Figure 7. a) Schematic illustration of the design of ZCMF-aVEGF. b) Illustrative presentations for treating orthotopic liver tumors by mild MHT. Reproduced with permission.[79] Copyright 2021, American Chemical Society. c) Schematic illustration of the MHT experiment. d) Fluorescence spectra of NIR-MNCs at different temperatures. e) Fluorescence intensity of NIR-MNCs changes with temperature. Reproduced with permission.[83] Copyright 2021, Wiley-VCH.

unaffected by biological tissues. However, currently, MHT mediated by clinical iron oxide nanomaterials (superparamagnetic iron oxide nanomaterials) still has difficulty in meeting clinical needs.[73] In recent years, more and more research has focused on enhancing the magnetothermal efficiency of MHT materials by changing their particle size, morphology, composition, and magnetic anisotropy constant, thereby further improving the therapeutic effect of thermal ablation on tumors.[74–77]

Due to the inability to inject magnetic materials into the tumor locally, there are fewer examples of using magnetic materials for MHT clinical trials through intratumoral perfusion or local injection.[78] In order to solve this problem, Shi et al. first injected MNPs intravenously into the liver to generate magnetic hyperthermia, passively enriching MNPs in the liver for the treatment of orthotopic liver tumors.[79] In their study, Zn2+-doped Zn-CoFe2O4@Zn-MnFe2O4 core–shell structure superparamagnetic NPs (ZCMF) were synthesized and modified with antivascular endothelial growth factor (aVEGF) antibodies to obtain highly targeted ZCMF-aVEGF NPs (**Figure** 7a). They showed that mild MHT could inhibit the growth of liver tumors by inhibiting the expression of heat shock protein 70 (HSP70) and upregulating the expression of natural killer (NK) cells (Figure 7b).

Although MNPs can absorb energy under alternating magnetic fields and transform it into thermal energy, they cannot provide real-time feedback, and moreover, they pose unnecessary overheating risks.[80–82] Based on this, Jaque et al. constructed a nanocapsule containing MNPs and emission nanothermometers working in the second near-infrared region (NIR-II, 1000−1700 nm), which could provide accurate (0.2 °C resolution) and real-time thermal feedback, as well as regional thermal maps (Figure 7c).[83] As shown in Figure 7d,e, the fluorescence spectrum of nanocapsules varies with temperature. Eventually, it was shown that the combination of real-time detection with MHT facilitates precise treatment.

The ablation of tumors by MHT may induce the production of relevant antigens, thereby triggering and promoting immune responses.[84] For instance, Shi et al. combined MHT and checkpoint blockade immunotherapy for tumor ablation and inhibition of tumor growth.[85] Superparamagnetic NPs (DMSA-$CoFe_2O_4$@$MnFe_2O_4$) were synthesized by a thermal decomposition method and modified with 2,3-dimercaptosuccinic acid (DMSA) (**Figure** 8a). Due to exchange-coupling magnetism, DMSA-$CoFe_2O_4$@$MnFe_2O_4$ exhibited excellent performance in transforming magnetic energy into thermal energy and could completely ablate tumors. At the same time, the associated antigens produced simultaneously could activate dendritic cells (DCs) and T cells, resulting in T-cell immunity that killed tumors. Moreover, the therapeutic use of an immune checkpoint agonist that promoted T-cell function, such as anti-programmed death-ligand 1 (α-PD-L1), could effectively alleviate T-cell immune suppression, kill tumor cells, and inhibit tumor growth (Figure 8b). Overall, the combination therapy of MHT and α-PD-L1 has certain clinical application prospects. In addition, the synergistic treatment strategy of MHT and ferroptosis has also achieved complete tumor elimination and effective reduction

© 2024 The Authors. Advanced Materials published by Wiley-VCH GmbH

15214095, 2024, 27, Downloaded from https://onlinelibrary.wiley.com/doi/10.1002/adma.202402806 by Ewha Womans University Library, Wiley Online Library on [13/11/2024]. See the Terms and Conditions (https://onlinelibrary.wiley.com/terms-and-conditions) on Wiley Online Library for rules of use; OA articles are governed by the applicable Creative Commons License

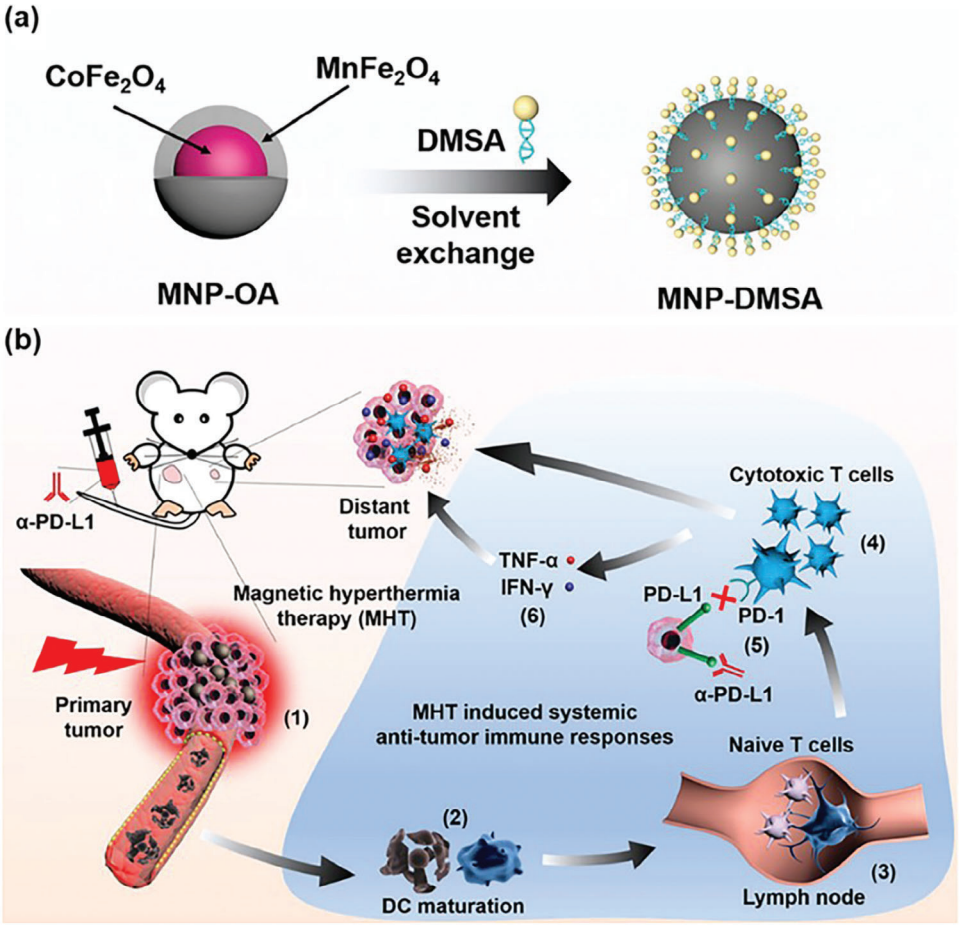


Figure 8. a) Schematic illustration of MNP-DMSA synthesis. b) Schematic illustration of antitumor immunity induced by MHT in combination with α-PD-L1 therapy. Reproduced with permission.[85] Copyright 2020, American Chemical Society.

of side effects.[86] Therefore, MHT-related combination therapy brings hope for the clinical practice of MHT.[87,88]

2.6. X-Ray-to-Chemical Energy Transformation: Radiation Therapy

After the discovery of radium and X-ray, radiation therapy (RT) underwent a century of development history and was soon used in the clinical treatment of malignant tumors. Radiotherapy is still an important local treatment for malignant tumors. RT is a method of treating malignant tumors using radiation such as α-, β-, and γ-rays produced by radioisotopes and X-rays, electron rays, proton beams, and other particle beams produced by various X-ray therapy machines or accelerators.[89] RT uses high-energy ionizing radiation to produce cytotoxic ROS through the radiation decomposition of water (H_2O) molecules, transforming X-ray energy into chemical energy to induce DNA damage, which is the main cause of apoptosis in cancer cells.[90,91] Although RT has a strong killing effect on tumors, it can affect the surrounding normal tissues and organs, which is currently the dilemma of RT.

Due to the radiation resistance of hypoxic cells and excessive radiation doses, tumors cannot be completely eradicated, leading to tumor recurrence and metastasis.[92,93] To address these issues, a ratio-based NIR-II fluorescence probe (BBT-IR/Se-MN) for detecting ROS levels was designed with a synergetic radiosensitization effect on cancer cells (**Figure 9a**).[94] X-rays can induce the generation of ROS, cleave diselenides, and cause significant fluorescence changes, thereby achieving the monitoring of ROS. Meanwhile, the released electron affinity nitro group effectively hinders DNA repair and improves the efficiency of RT. In addition to generating ROS for RT, H_2 therapy has also received attention. For example, Yang et al. designed an H_2 generation platform composed of Au-amorphous TiO_2 NPs coated with long afterglow particles (Figure 9b).[95] Meanwhile, its excellent PAI indicated that the maximum tumor enrichment time was 24 h, and it could effectively guide treatment. Moreover, the H_2 production platform can effectively treat cancer with low inflammatory side effects. Finally, this H_2 synergistic RT provided a new insight into the treatment and prognosis of cancer.

In RT, prolonged high-radiation exposure inevitably causes damage to normal tissues. In order to minimize the side effects caused by prolonged exposure to high levels of radiation, Chen et al. prepared Bi-doped TiO_2 NPs (TBR) to enhance X-ray absorption (**Figure 10**).[96] Even under low-dose X-ray irradiation, the high-Z element Bi doping enabled the NPs to produce

© 2024 The Authors. Advanced Materials published by Wiley-VCH GmbH

15214095, 2024, 27, Downloaded from https://onlinelibrary.wiley.com/doi/10.1002/adma.202402806 by Ewha Womans University Library, Wiley Online Library on [13/11/2024]. See the Terms and Conditions (https://onlinelibrary.wiley.com/terms-and-conditions) on Wiley Online Library for rules of use; OA articles are governed by the applicable Creative Commons License

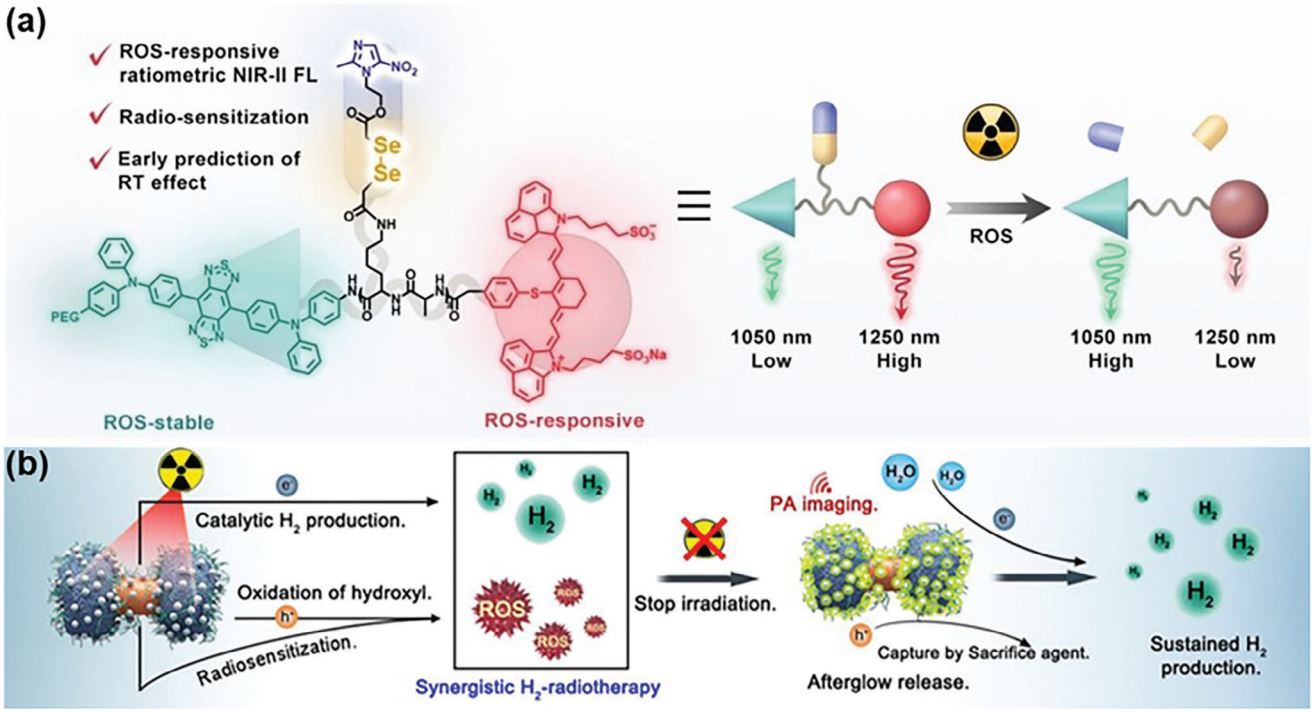


Figure 9. a) Schematic illustration of BBT-IR/Se-MN RT. Reproduced with permission.[94] Copyright 2023, Wiley-VCH. b) Schematic illustration of H_2 production under X-ray excitation. Reproduced with permission.[95] Copyright 2021, Wiley-VCH.

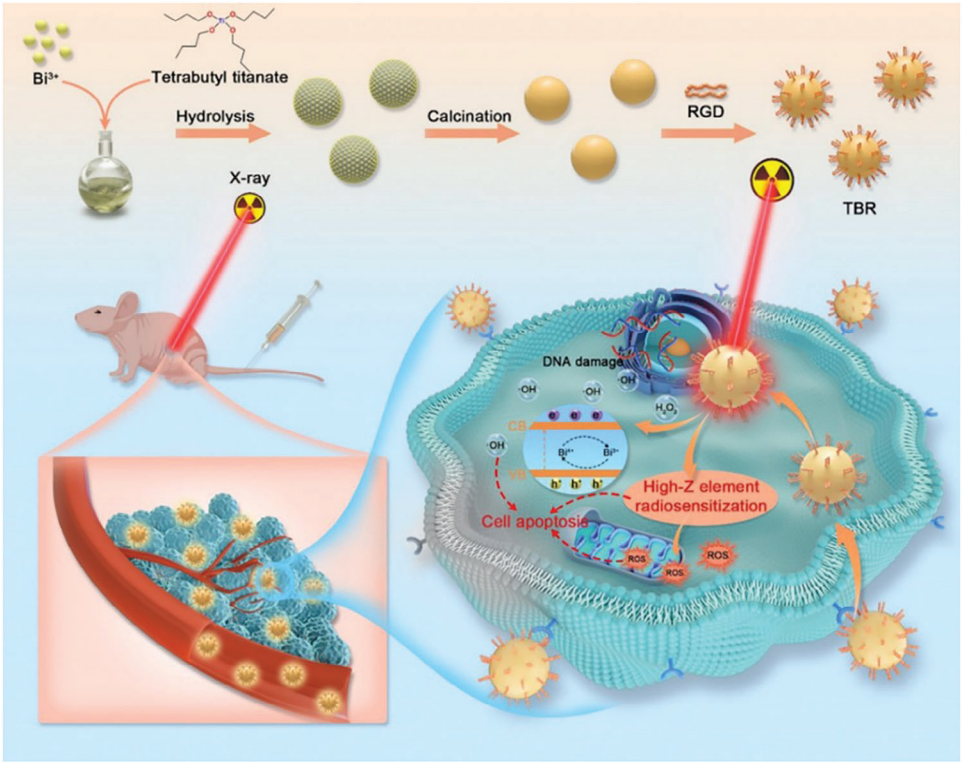


Figure 10. Schematic illustration of TBR preparation and RT. Reproduced with permission.[96] Copyright 2022, Springer Nature.

© 2024 The Authors. Advanced Materials published by Wiley-VCH GmbH

15214095, 2024, 27, Downloaded from https://onlinelibrary.wiley.com/doi/10.1002/adma.202402806 by Ewha Womans University Library, Wiley Online Library on [13/11/2024]. See the Terms and Conditions (https://onlinelibrary.wiley.com/terms-and-conditions) on Wiley Online Library for rules of use; OA articles are governed by the applicable Creative Commons License

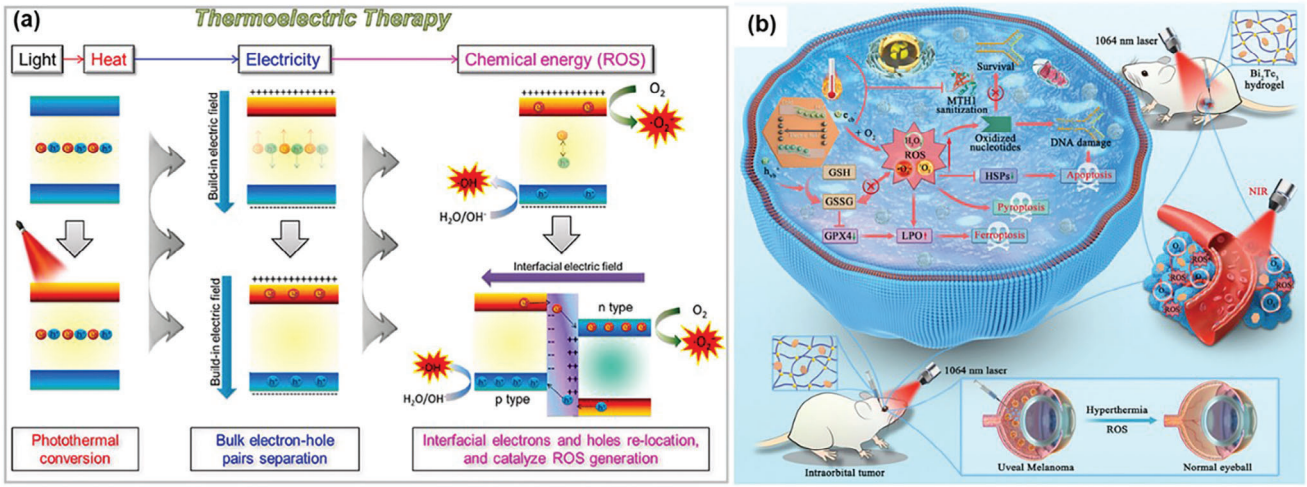


Figure 11. a) Schematic illustration of the SrTiO therapeutic mechanism. Reproduced with permission.[100] Copyright 2023, Elsevier Ltd. b) Schematic illustration of the Bi_2Te_3 NPs therapeutic mechanism. Reproduced with permission.[101] Copyright 2023, Wiley-VCH.

significant levels of ROS. Meanwhile, TBR could accumulate well at the U87MG tumor site through intravenous injection. Moreover, under low-dose X-ray activation, the electron–hole separation of TBR was effectively promoted, resulting in a large amount of ROS and irreversible apoptosis of tumor cells. Therefore, the application of low-dose X-rays has greatly reduced side effects, making these high-Z radiosensitizers promising as safer RT materials.

3. Multimodal Energy Transformation for Cancer Therapy

3.1. Photonic-to-Thermal (With Spatial Gradient)-to-Electrical-to-Chemical Energy Transformation: Thermoelectric Therapy

As mentioned above, thermal energy is used only as an output energy to ablate tumors, and ROS is triggered by a single chemical energy to kill tumors. However, in the process of clinical translation, it is difficult to eliminate tumors completely because of the complex TME. Due to the different energy transformation mechanisms and therapeutic mechanisms, it is difficult to simply integrate thermal energy and chemical energy to achieve synergistic therapeutic effects in the complex TME.[97] However, inspired by the photonic–thermal–electrical energy transformation, thermal energy can induce apoptosis in tumor cells by transforming thermal energy into electrical energy and promoting the production of ROS through thermoelectric materials. Overall, thermoelectric therapy is a cancer treatment strategy that kills tumors by transforming electrical currents or charge buildup generated when a temperature gradient is moved from a high- to a low-temperature zone into chemical energy.[98,99]

In 2023, Ji et al. constructed a thermoelectric material (SrTiO) composed of $SrTiO_3/Cu_2Se$ p–n heterojunction nanoplates that could effectively transform photonic–thermal–electrical–chemical energy (**Figure 11a**).[100] Under 808 nm laser irradiation and natural cooling, a temperature gradient of 35–45 °C was generated to form two self-built-in electric fields. Simultaneously, O_2 and H_2O generated superoxide anion ($O_2^{\bullet-}$) and $^{\bullet}OH$ radicals under the catalysis of separated electrons and holes, effectively killing tumor cells. Similarly, in order to improve the treatment efficiency, high-performance bismuth telluride nanoplates (Bi_2TE_3 NPs) with a photothermoelectric catalytic effect were designed. Under NIR-II light irradiation, Bi_2TE_3 NPs effectively transformed photonic energy into thermal energy, leading to an increase in tumor tissue temperature (Figure 11b).[101] Meanwhile, through the thermoelectric effect, thermal energy was transformed into electrical energy, and then, into chemical energy to generate ROS, causing pyroptosis of tumor cells. In addition, Bi_2TE_3 NPs could reduce the concentration of GSH and cause ferroptosis in tumor cells. Overall, this high-performance multifunctional energy transformation nanoplatform breaks the inherent limitations of traditional phototherapy and improves the tumor treatment effect of phototherapy.

3.2. Photonic-to-Thermal (With Temporal Gradient)-to-Electrical-to-Chemical Energy Transformation: Pyroelectric Therapy

Unlike thermoelectric therapy with temperature gradients, pyroelectric therapy (PCT) can generate usable positive and negative charges under repeated thermal stimulation, efficiently transforming thermal energy into electrical energy, and then, chemical energy, ultimately producing ROS to kill tumors.[98,102] In 2021, Zhang et al. prepared a high-performance nanorod (NR) pyroelectric biomaterial ($Bi_{13}S_{18}I_2$ NRs) with excellent photothermal and pyroelectric transformation capabilities (**Figure 12a**).[103] Under irradiation at 808 nm, $Bi_{13}S_{18}I_2$ NRs transformed photonic energy into thermal energy, causing a temperature increase and effectively performing PTT. At the same time, $Bi_{13}S_{18}I_2$ NRs effectively transformed the fluctuations of cold and hot changes into thermally released charges, which in turn, transformed into chemical energy to generate a large amount of ROS, thereby reducing the thermal resistance of tumor cells. On the whole, this

© 2024 The Authors. Advanced Materials published by Wiley-VCH GmbH

15214095, 2024, 27, Downloaded from https://onlinelibrary.wiley.com/doi/10.1002/adma.202402806 by Ewha Womans University Library, Wiley Online Library on [13/11/2024]. See the Terms and Conditions (https://onlinelibrary.wiley.com/terms-and-conditions) on Wiley Online Library for rules of use; OA articles are governed by the applicable Creative Commons License

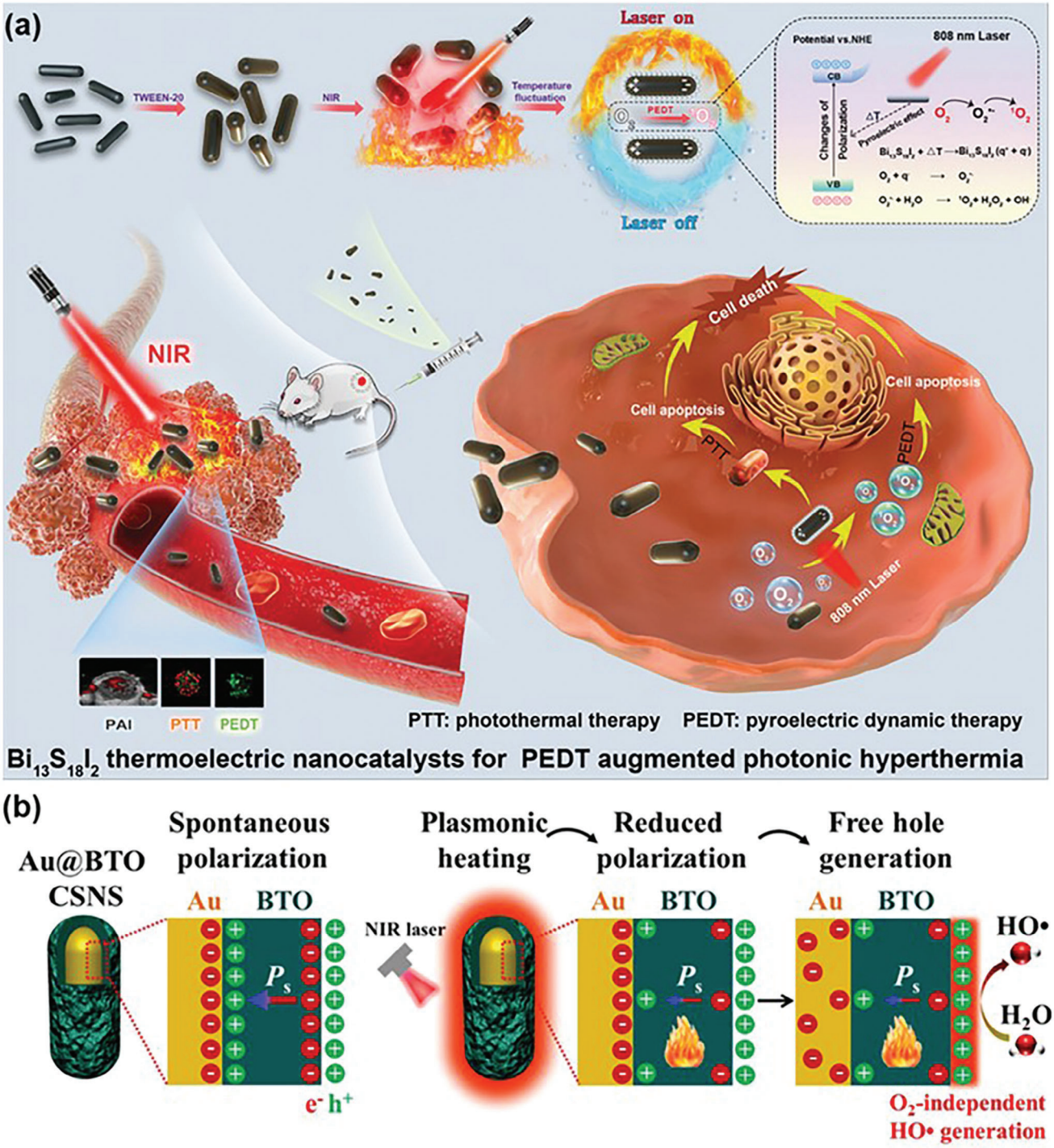


Figure 12. a) Schematic illustration of $Bi_{13}S_{18}I_2$ NRs for PEDT-augmented photonic hyperthermia. Reproduced with permission.[103] Copyright 2021, Wiley-VCH. b) Schematic illustration of pyroelectric effect and O_2-independent PDT property of Au@BTO CSNSs. Reproduced with permission.[104] Copyright 2021, Elsevier Ltd.

work combined PCT with PTT to solve the heat resistance of tumor cells and effectively improved the therapeutic effect of PTT.

In order to address the low efficiency of ROS generation in the hypoxic TME, Zhang et al. embedded NIR laser-activated photothermal gold NRs into the pyroelectric material barium titanate (BTO) to obtain plasma pyroelectric core–shell nanostructures (Au@BTO CSNSs) (Figure 12b).[104] Under 808 nm laser irradiation, the plasma Au core could transform photonic energy into thermal energy, heating the pyroelectric BTO shell. Meanwhile, BTO nanomaterials were affected

© 2024 The Authors. Advanced Materials published by Wiley-VCH GmbH

15214095, 2024, 27, Downloaded from https://onlinelibrary.wiley.com/doi/10.1002/adma.202402806 by Ewha Womans University Library, Wiley Online Library on [13/11/2024]. See the Terms and Conditions (https://onlinelibrary.wiley.com/terms-and-conditions) on Wiley Online Library for rules of use; OA articles are governed by the applicable Creative Commons License

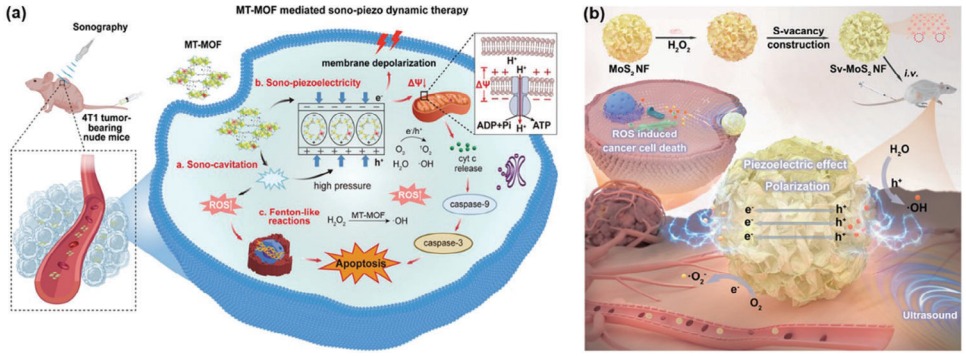


Figure 13. a) Schematic illustration of the MT-MOF-mediated piezoelectric therapy. Reproduced with permission.[109] Copyright 2023, Wiley-VCH. b) Schematic illustration of MoS_2 NF piezoelectric SDT. Reproduced with permission.[110] Copyright 2023, Wiley-VCH.

by temperature changes, thereby promoting the release of free holes and the generation of ROS. Finally, Au@BTO CSN_S showed excellent therapeutic effects in the treatment of hypoxic tumors.

3.3. Ultrasonic-to-Mechanical-to-Electrical-to-Chemical Energy Transformation: Piezoelectric Therapy

SDT transforms US directly into chemical energy through sensitizers activated by US, producing ROS to kill tumor cells. However, the scarcity of sonodynamic sensitizers severely limits the development of SDT. It can be seen that the development of sonodynamic sensitizers is a bottleneck problem that urgently needs to be overcome in SDT. Surprisingly, some studies have proven that piezoelectric materials can become a new type of sonodynamic sensitizer. It is worth noting that under the activation of external US, piezoelectric materials undergo deformation, and the formed piezoelectric field can promote redox reactions on the surface of piezoelectric materials to generate ROS, thereby killing tumor cells. Meanwhile, piezoelectric catalysis has been introduced into cancer therapy in recent years.[105,106]

Under US, piezoelectric sonosensitizers can transform ultrasonic energy into mechanical energy, thereby generating charges and promoting the generation of ROS. Therefore, piezoelectric sonosensitizers that overcome bandgap barriers and directly generate charges are urgently needed.[107,108] To solve this problem, Liu et al. designed and prepared Mn–Ti bimetallic organic framework tetragonal nanosheets (MT-MOF TNSs) (**Figure 13a**).[109] The nanosheets (NSs) exhibited high specific surface area and a high porosity-induced ultrasonic cavitation effect, as well as an in situ-induced MT-MOF TNS piezoelectric effect, generating high voltage. Meanwhile, the mechanism of acoustic excitation charge was verified by acoustic pressure-induced luminescence spectroscopy. In addition, the generated voltage and charge depolarized the mitochondrial and plasma membrane potentials, resulting in excessive ROS and damage to tumor cells. Moreover, by combining chemodynamic therapy and chemotherapy, MT-MOF TNS could be modified with targeted molecules and chemotherapy drugs to treat tumors. Finally, this novel MT-MOF piezoelectric nano-semiconductor provided a new strategy for tumor treatment. Similarly, in order to obtain an efficient piezoelectric sonosensitizer, a piezoelectric sonosensitizer (Sv-MoS_2NF) introducing sulfur vacancies on molybdenum disulfide nanoflowers (MoS_2NFs) was constructed (Figure 13b).[110] Meanwhile, under the action of US, the piezoelectric sonosensitizer enhanced the separation and migration of charge carriers, improving the efficiency of ROS generation and exhibiting good anticancer effects both in vivo and in vitro.

3.4. Synergistic Dual Energy Transformation

Similar to the synergistic combinations of anticancer drugs applied in clinical practice to achieve maximal therapeutic efficacy and minimal side effects by the simultaneous or sequential administration of two or more drugs,[111,112] there is multimodal energy transformation to release synergistic therapeutic elements/effects (e.g., cytotoxic ROS, mechanical effect, thermal effect, photoelectric effect, or cavitation effect) for cancer therapies. The transformation of a single energy into multiple energies, or the transformation of multiple energies into a single energy for cancer treatment, has been studied and reported. Most reported results indicated that the therapeutic effect of multiple energy transformations was better than that of single energy transformations.[113–115]

PDT and PTT transform photonic energy into chemical or thermal energy to eliminate tumors, and single photonic energy transformation has been extensively reported for cancer treatment.[116–119] Due to the oxygen consumption of tumor tissue during PDT, the efficacy of PDT gradually decreases, making it suitable for early cancer treatment. However, the thermal effect of PTT will show better efficacy with prolonged treatment time. Therefore, the two treatment modalities activated by the same energy have been widely used in cancer treatment in recent years. For example, Yoon et al. reported a NIR-photoexcited PDT/PTT synergistic therapy platform (B4 NPs) composed of self-assembled NPs from a heavy-atom-free B(0) dipyrromethene (BODIPY) derivative B4 (**Figure 14a**).[26] The B4 NPs had a high photothermal conversion efficiency (PCE) of 47.17% in aqueous solution and excellent NIR absorption ability; while, B4 had excellent protein-binding ability. Meanwhile, the binding of bovine serum protein to B4 enhanced the NIR absorption, promoting the efficiency of PTT and PDT, and thereby, effectively

© 2024 The Authors. Advanced Materials published by Wiley-VCH GmbH

15214095, 2024, 27, Downloaded from https://onlinelibrary.wiley.com/doi/10.1002/adma.202402806 by Ewha Womans University Library, Wiley Online Library on [13/11/2024]. See the Terms and Conditions (https://onlinelibrary.wiley.com/terms-and-conditions) on Wiley Online Library for rules of use; OA articles are governed by the applicable Creative Commons License

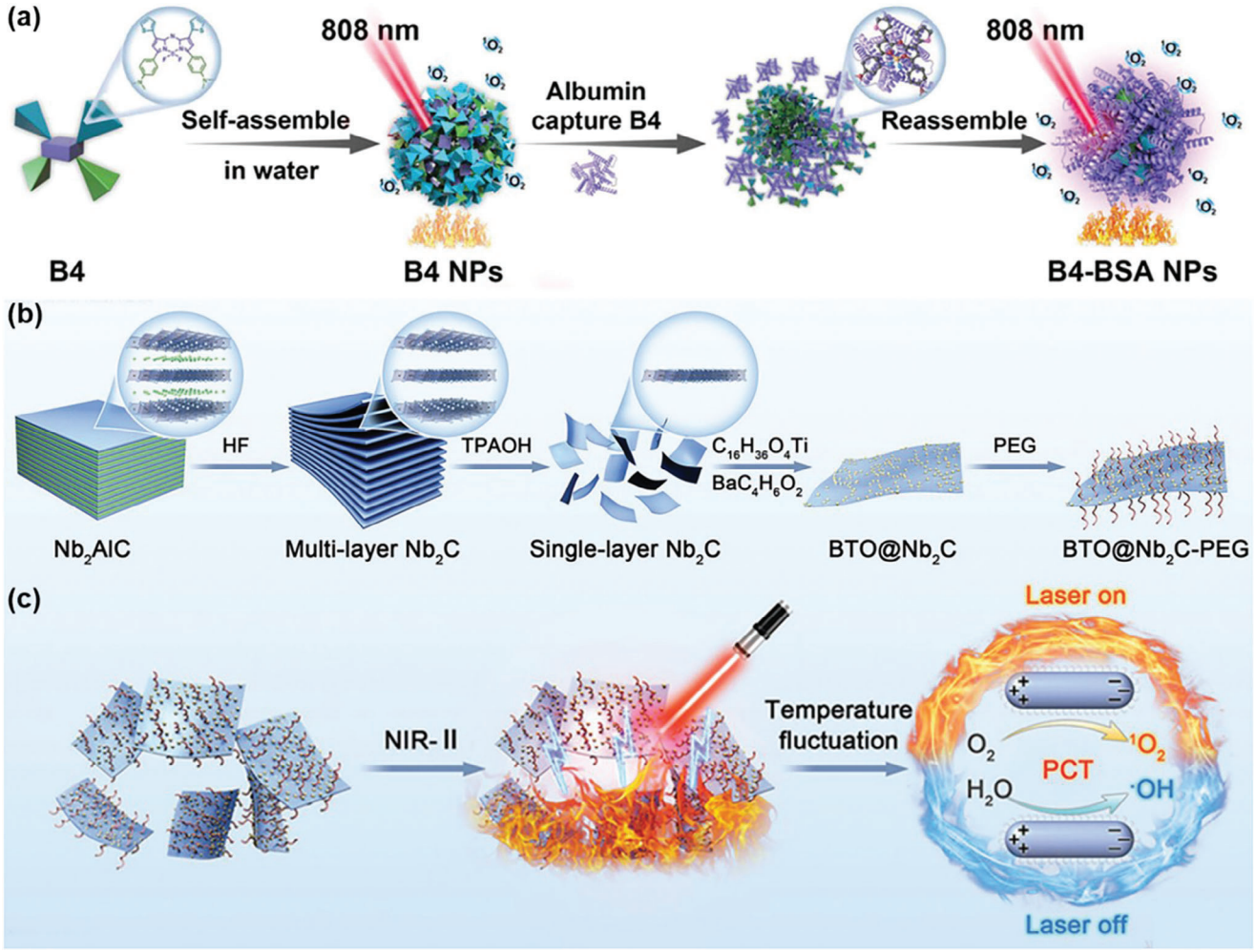


Figure 14. a) Schematic illustration of the assembly and disassembly of B4 NPs. Reproduced with permission.[26] Copyright 2022, Wiley-VCH. b) Synthesis of BTO@Nb_2C-PEG NSs. c) Schematic illustration of the PTT and PCT mechanisms of BTO@Nb_2C-PEG. Reproduced with permission.[120] Copyright 2023, Wiley-VCH.

inhibiting tumor growth. In addition, the PAI further enhanced the application prospects in tumor diagnosis and treatment. Based on the fact that hypoxic conditions in the TME are not conducive to the progression of PDT, Zhang et al. constructed an NS (BTO@Nb_2C-PEG) for the synergistic treatment of PTT and PCT (Figure 14b).[120] Under NIR-II irradiation, the 2D niobium carbide (Nb_2C) MXene shell effectively transformed photonic energy into thermal energy, regulating the temperature changes around BTO to cause electron–hole spatial separation, promoting its pyroelectric catalysis to produce excessive ROS and kill tumor cells (Figure 14c). In short, the synergistic therapy of PTT and PCT overcame the challenges of a hypoxic environment and had efficient therapeutic effects in both in vitro cells and tumor-bearing mice.

RT can transform hydrogen peroxide (H_2O_2) and H_2O inside tumors into highly toxic free radicals, but insufficient intracellular H_2O_2 can hinder its treatment.[121,122] In order to solve this problem, Gu et al. integrated the piezoelectric and radio-catalytic properties of BiOCl piezoelectric NSs (BiOCl@PAA) for synergistic treatment of tumors by PCT and RT (**Figure 15**a).[123] Under US, BiOCl could catalyze the production of free radicals and H_2O_2, and the increase in H_2O_2 concentration accelerated the radio-catalytic production of $^{\bullet}OH$ from H_2O_2. Therefore, this efficient collaborative therapy provided high levels of H_2O_2 that amplified the production of radio-catalytic free radicals, increased DNA damage levels, and was beneficial for tumor treatment. Similarly, in order to solve the problem of reduced ROS caused by hypoxia, Cheng et al. synthesized a Mxene-based sonosensitizer (H-Ti_3C_2-PEG NSs) through a two-step method, which extended blood circulation through a mild photothermal effect and effectively improved oxygen supply to enhance SDT (Figure 15b).[124] Moreover, under the condition of 1064 nm light and US acting together on H-Ti_3C_2-PEG NSs, the tumor growth was completely inhibited, and the survival of mice was greatly prolonged.

A single energy type can also be transformed into different energies when applied in different forms to the same type of nanomaterial. For instance, Cheng et al. synthesized bi-functional

© 2024 The Authors. Advanced Materials published by Wiley-VCH GmbH

15214095, 2024, 27, Downloaded from https://onlinelibrary.wiley.com/doi/10.1002/adma.202402806 by Ewha Womans University Library, Wiley Online Library on [13/11/2024]. See the Terms and Conditions (https://onlinelibrary.wiley.com/terms-and-conditions) on Wiley Online Library for rules of use; OA articles are governed by the applicable Creative Commons License

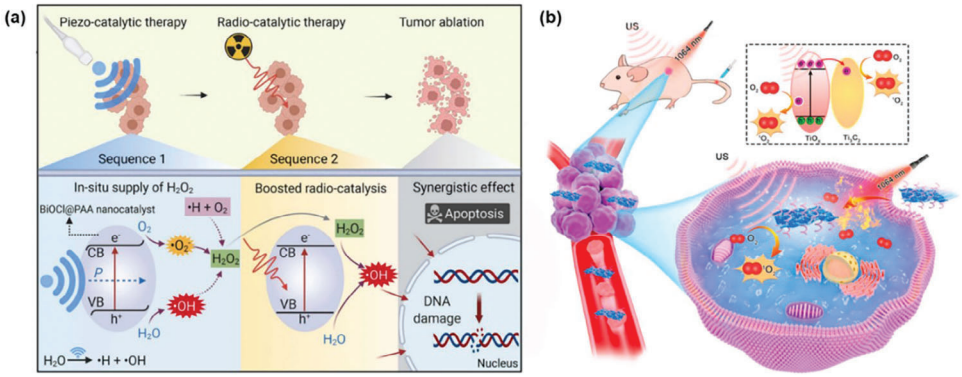


Figure 15. a) Schematic illustration of BiOCl@PAA synergistic piezoelectric and radio-catalytic cancer therapy. Reproduced with permission.[123] Copyright 2022, Elsevier Ltd. b) Schematic illustration of H-Ti_3C_2-PEG NSs for photothermal enhanced sonodynamic cancer therapy. Reproduced with permission.[124] Copyright 2022, Elsevier Ltd.

Ar-Gly-Asp (RGD)-modified iron oxide magnetic nanocubes (RGD-IONs) (**Figure 16a**).[125] Under a rotating magnetic field (15 Hz), the RGD-IONs transformed magnetic energy into mechanical energy through linear aggregation, interacted with organelles, and produced ROS. Subsequently, under high-frequency alternating magnetic fields (375 kHz), the RGD-IONs could transform magnetic energy into thermal energy, further accelerating the death of tumors. Finally, this synergistic treatment method of transforming magnetic energy into mechanical energy and thermal energy achieved good therapeutic effects in a tumor mouse model. Moreover, in order to further promote the therapeutic effect of MHT, Lin et al. constructed a hollow MNP (HP-HIONs@PDA-PEG) that catalyzed the production of O_2 from endogenous H_2O_2, overcoming the hypoxic environment of tumors (Figure 16b).[126] Under US, sound sensitizers produced a large amount of ROS to eliminate tumors. At the same time, a large amount of ROS would reduce the expression of heat shock protein (HSP) and promote the therapeutic effect of MHT. Therefore, these NPs overcame the shortcomings of both the hypoxic environment of SDT and the heat resistance of MHT, achieving the best synergistic effect of SDT and MHT in the treatment of cancer.

4. Single Energy Transformation for Cancer Imaging-Guided Therapy

4.1. Ultrasonic-to-Ultrasonic Energy Transformation: Ultrasound Imaging

Ultrasound imaging (USI) is achieved by transmitting and receiving US waves. Due to the different impedances of different human tissues to sound waves, different degrees of transmission and reflection occur at the junctions between different tissues. Then, by analyzing the reflected signals, information on the tissue structure in the body can be obtained. Meanwhile, compared with magnetic resonance imaging (MRI) or X-ray technology, USI has low cost, strong penetration ability, and no ionizing radiation, making it widely used in clinical practice.[127–129] In addition, it has developed at an astonishing speed and has become the preferred method for diagnosing various diseases in clinical practice. Meanwhile, it is a very important multi-parameter diagnostic technique.

A US contrast agent is a liquid containing bubbles with diameters of several micrometers, which vibrates and scatters strong US signals under the action of US.[130] However, the

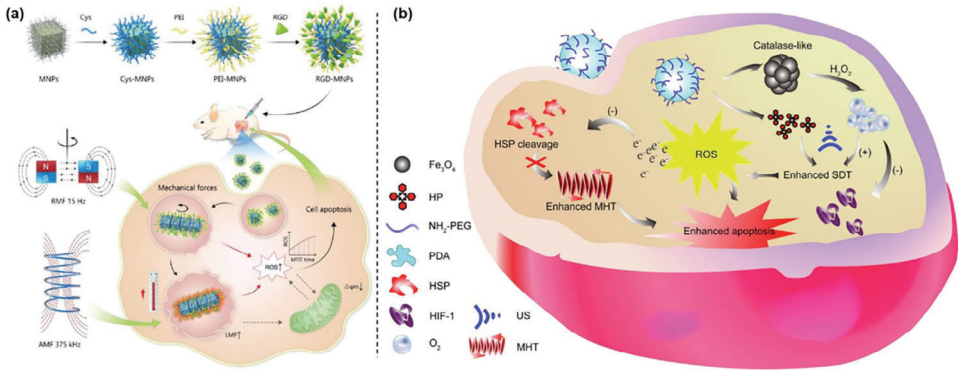


Figure 16. a) Schematic illustration of RGD-IONs synthesis and magneto–mechanical thermal induction therapy of alternating magnetic fields. Reproduced with permission.[125] Copyright 2020, Wiley-VCH. b) Schematic illustration of the synergistic treatment of MHT and SDT. Reproduced with permission.[126] Copyright 2020, Elsevier Ltd.

© 2024 The Authors. Advanced Materials published by Wiley-VCH GmbH

15214095, 2024, 27, Downloaded from https://onlinelibrary.wiley.com/doi/10.1002/adma.202402806 by Ewha Womans University Library, Wiley Online Library on [13/11/2024]. See the Terms and Conditions (https://onlinelibrary.wiley.com/terms-and-conditions) on Wiley Online Library for rules of use; OA articles are governed by the applicable Creative Commons License

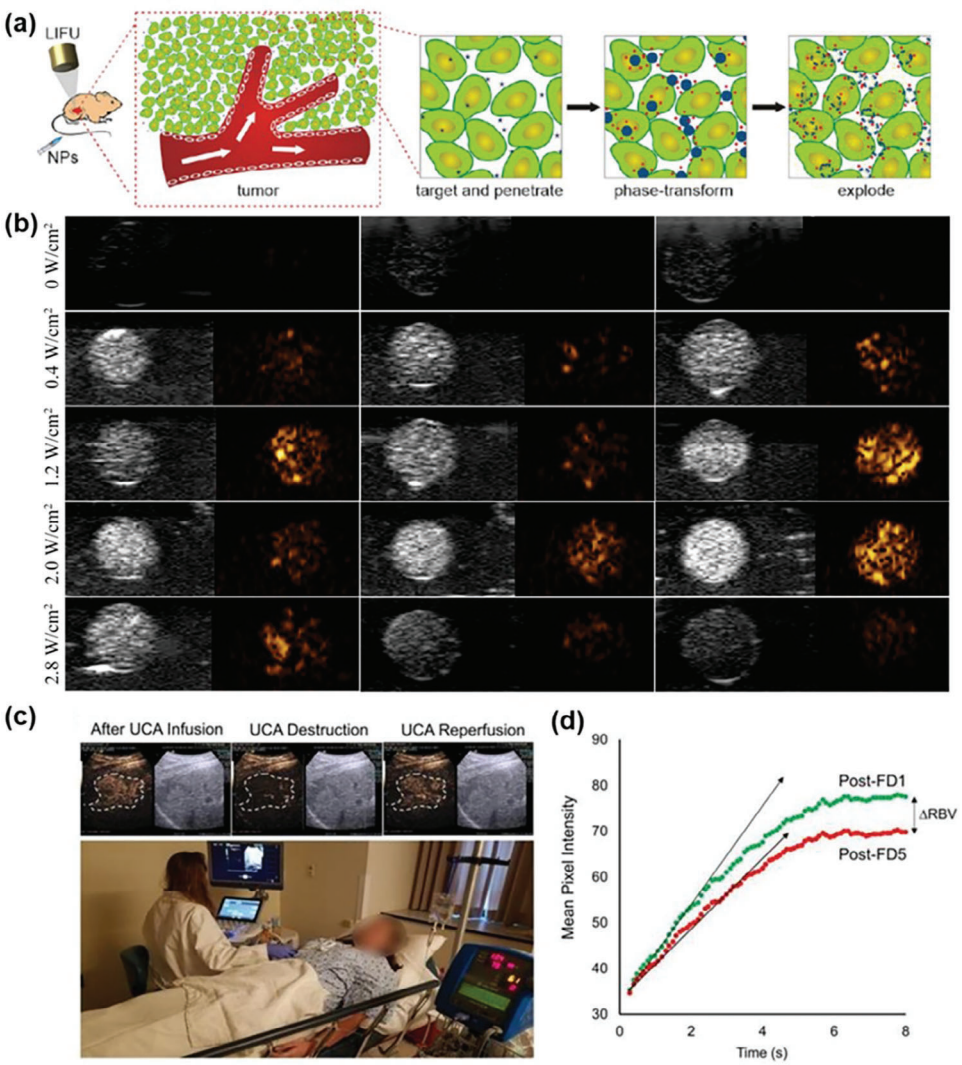


Figure 17. a) Schematic illustration of tLyP-1-10-HCPT-PFP NPs for LIFU-assisted tumor imaging and precise treatment. b) US images of tLyP-1-10-HCPT-PFP NPs. Reproduced with permission.[131] Copyright 2018, American Chemical Society. c) Representative images of contrast agent infusion, destruction, and reflow in hepatocellular carcinoma (outlined in white). d) The average pixel intensity that appears immediately after the flash destruction pulse. Reproduced with permission.[132] Copyright 2020, Ivyspring International.

extremely large particle size limits the infiltration into the tumor area. Cyclic tumor-targeting penetrating peptides, such as LyP-1 and its truncated form, tLyP-1, can promote tissue penetration, thereby increasing the delivery of drugs to the target site. In this context, tumor-homing-penetrating peptide-functionalized drug-loaded phase-transformation NPs (tLyP-1-10-HCPT-PFP NPs) have been developed and used for low-intensity focused ultrasound (LIFU)-assisted tumor imaging and precise treatment (**Figure 17a**).[131] With the assistance of LIFU, MBs can be formed, and the enhanced USI can be used for tumor diagnosis. As shown in Figure 17b, an increase in the particle size of tLyP-1-10-HCPT-PFP NPs was observed within the US range of 0.4–2 W cm^{-2}, and when the US intensity reached 2.8 W cm^{-2}, MB rupture led to a decrease in particle size. Moreover, tLyP-1-10-HCPT-PFP NPs can effectively accumulate in the tumor area, achieving USI of tumors, which is beneficial for early diagnosis. Interestingly, in order to detect the drug delivery capacity of FU, Sirsi et al. designed a 2D and 3D quantitative contrast-enhanced USI (qCEUS) system.[132] By combining FU therapy with "MB" US contrast agents, the drug payload was significantly improved. Moreover, the system imaging capability allowed effective monitoring of the US osmotic efficiency and prediction of drug uptake, making chemotherapy more efficient. Finally, US experiments on patients revealed a slight decrease in relative blood volume after US perfusion by qCEUS (Figure 17c,d).

4.2. Magnetic-to-Photonic Energy Transformation: MRI

MRI is a medical imaging technique that uses the principles of nuclear magnetic resonance (NMR) to form images of human anatomical structures and physiological processes, providing

© 2024 The Authors. Advanced Materials published by Wiley-VCH GmbH

15214095, 2024, 27, Downloaded from https://onlinelibrary.wiley.com/doi/10.1002/adma.202402806 by Ewha Womans University Library, Wiley Online Library on [13/11/2024]. See the Terms and Conditions (https://onlinelibrary.wiley.com/terms-and-conditions) on Wiley Online Library for rules of use; OA articles are governed by the applicable Creative Commons License

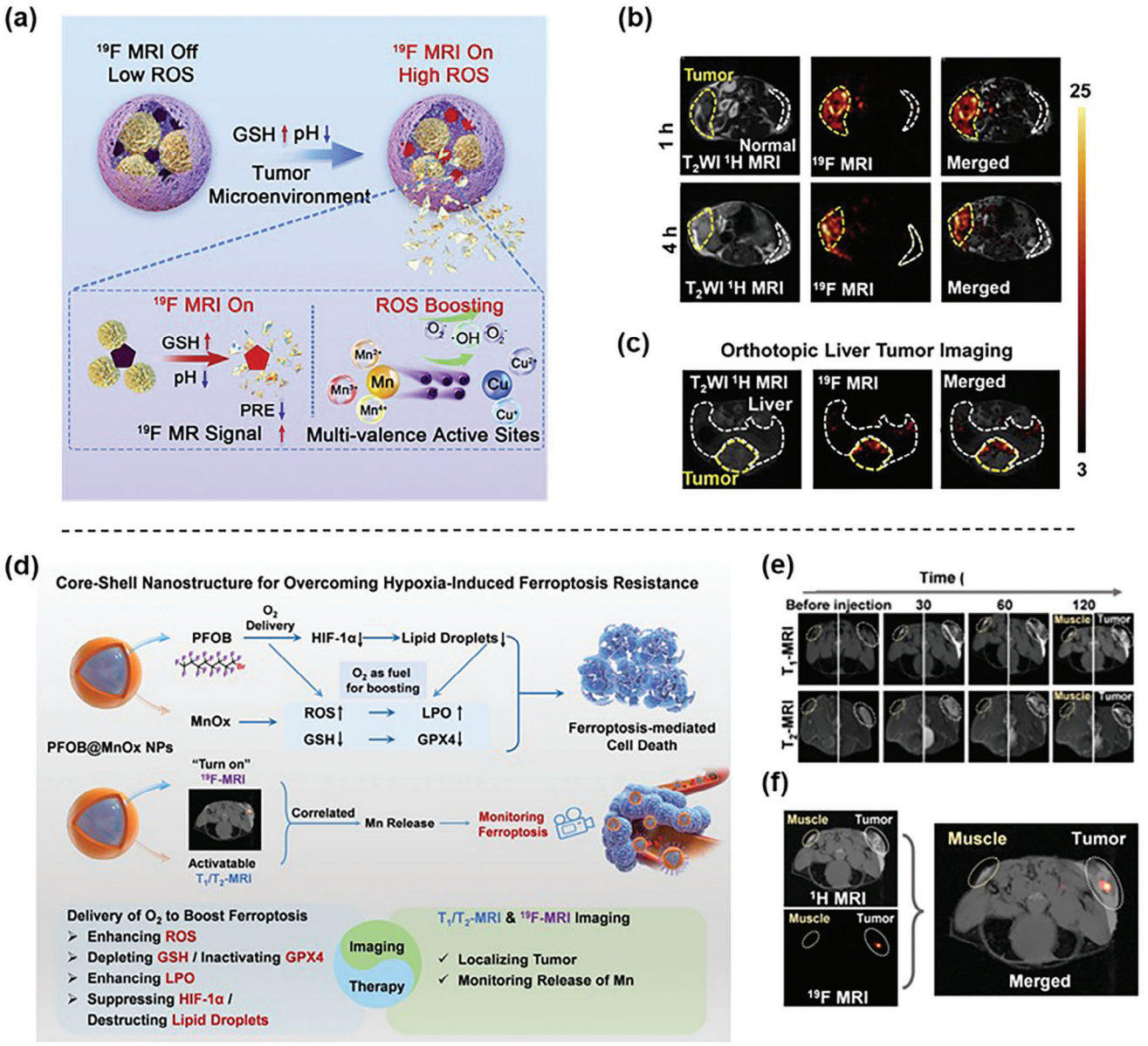


Figure 18. a) Schematic of TME-responsive mechanism of CMCF NCs. b) T_2-weighted ^{1}H MRI and ^{19}F MRI of tumors after injection of CMCF NCs. c) T_2-weighted ^{1}H MRI and ^{19}F MRI of orthotopic liver tumors at 12 h post-intravenous injection of CMCF NCs. Reproduced with permission.[138] Copyright 2022, Elsevier. d) Schematic illustration of PM-CS NPs for overcoming hypoxia-induced ferroptosis resistance. e) T_1/T_2-weighted MRI images of mice injected with PM-CS NPs over time. f) T_1-weighted MRI and ^{19}F MRI images of mice with injection of PM-CS NPs into muscle or tumor. Reproduced with permission.[141] Copyright 2022, Wiley-VCH.

accurate and reliable diagnostic information on physiology, pathology, and anatomy. MRI scanners use strong magnetic fields, magnetic field gradients, and radio waves to generate images of internal organs but do not involve X-rays or the use of ionizing radiation, which is different from computed tomography (CT) imaging and positron emission tomography (PET) imaging scans. Consequently, MRI has been widely used in hospitals and clinics for medical diagnosis, disease staging, and follow-up.[133–135] However, the growing demand for MRI in the health care system has raised concerns about cost-effectiveness and overdiagnosis.

The demand for precise diagnosis and efficient treatment of deep tumors in the medical field is increasing.[136,137] Based on this, Wang et al. developed a multifunctional nanoplatform containing Cu/Mn chalcogenide nanoflowers (CMCF NCs) and good ^{19}F MRI performance, which effectively killed tumors by promoting ROS generation and GSH depletion and provided guidance for tumor-targeted therapy (**Figure 18a**).[138] As shown in Figure 18b, there was a significant difference in the ^{19}F MRI signal between the tumor site and the normal site. Moreover, the signal at the tumor site was significantly enhanced and then gradually weakened over time. It is worth noting that significant ^{19}F

© 2024 The Authors. Advanced Materials published by Wiley-VCH GmbH

15214095, 2024, 27, Downloaded from https://onlinelibrary.wiley.com/doi/10.1002/adma.202402806 by Ewha Womans University Library, Wiley Online Library on [13/11/2024]. See the Terms and Conditions (https://onlinelibrary.wiley.com/terms-and-conditions) on Wiley Online Library for rules of use; OA articles are governed by the applicable Creative Commons License

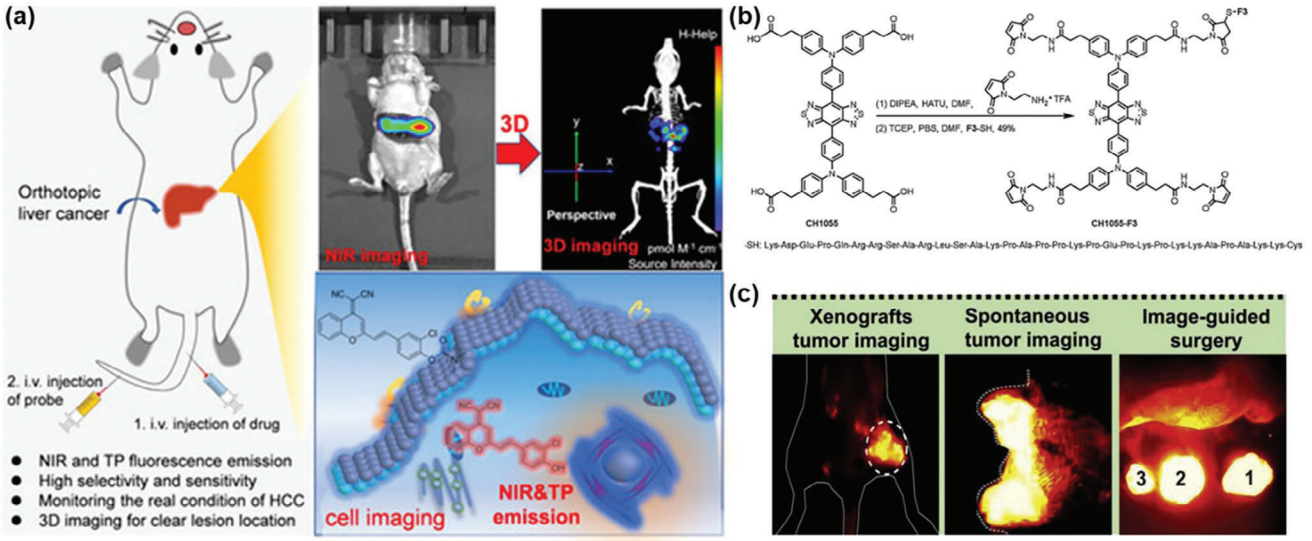


Figure 19. a) Schematic illustration of DCM-Cl-CE detection of CE and 3D imaging of liver cancer mouse. Reproduced with permission.[149] Copyright 2021, Wiley-VCH. b) The synthetic route of CH1055-F3. c) Imaging image of breast tumor with NIR-II fluorescence probe CH1055-F3. Reproduced with permission.[152] Copyright 2020, Elsevier Ltd.

MRI signals were observed in liver tumors in situ through intravenous injection (Figure 18c).

Ferroptosis is an effective pathway for cancer treatment, but the hypoxic TME reduces its efficacy.[139,140] In order to solve this problem, Song et al. designed NPs (PM-CS NPs) that directly deliver O_2 to the tumor (Figure 18d).[141] This activated ^{19}F MRI nanoplatform effectively demonstrates the process of iron-mediated cell death. From Figure 18e,f, it can be seen that tumor imaging can be efficiently achieved through T_1/T_2-weighted MRI and ^{19}F MRI signals, and PM-CS NPs can serve as MRI contrast agents activated by the TME.

4.3. Photonic-to-Photonic Energy Transformation: Fluorescence Imaging

Fluorescence is a phenomenon of photoluminescence in which high-energy excitation light excites fluorescent molecules, activating them into excited states. These excited-state fluorescent molecules are unstable and rapidly release energy in the form of light.[142] The light-triggered tunable photoluminescence avoids direct contact with cells at the microscopic level and is non-invasive, thereby allowing the selective observation of cells. Moreover, fluorescence imaging (FI) is widely used due to its advantages of advanced detection instruments, high sensitivity, high contrast, high resolution, intuitive imaging, fast imaging speed, and non-destructive detection.[143,144] The most valuable is that it has important practical significance and application prospects in exploring the pathogenesis, clinical manifestations, and genetic changes of diseases, understanding corresponding physiological and pathological information, disease diagnosis, and the development of new medical methods.[33,145–147]

Hepatocellular carcinoma is a primary cancer originating from liver cells in a hardened liver, and carboxylesterase (CE) is currently considered an important, relevant biomarker.[148] Based on this, Yoon et al. synthesized a highly selective NIR two-photon fluorescence probe (DCM-Cl-CE) for detecting CE.[149] The mechanism of this approach is the selective hydrolysis of DCM-Cl-CE by CE to afford fluorescent DCM-Cl-OH; thus, specifically recognizing CE. Meanwhile, DCM-Cl-CE has been successfully applied to detect the activity of CE in normal cells and liver cancer cells, and the distribution of CE in the deeper layers of cancer can be observed by 3D imaging (**Figure 19a**). Therefore, DCM-Cl-CE can be an important tool for surgical guidance and resection.

Based on the absorption and scattering of photons by biological tissues and the attenuation of spontaneous with increasing wavelength, the first near-infrared region (NIR-I, 700–950 nm) FI has limitations. In contrast, NIR-II FI can achieve deeper penetration and higher-quality imaging in vivo, further compensating for the lack of light in the NIR-I region.[150,151] For instance, Zhou et al. conjugated the peptide F3 ligand of the cell surface cell receptor, nucleolin, with CH1055 to prepare the NIR-II fluorescent probe CH1055-F3 for actively targeting triple-negative breast cancer cells (or breast cancer endothelial cells) (Figure 19b).[152] This probe could specifically visualize the transplanted and spontaneous breast cancer and successfully guide the surgical resection of spontaneous breast cancer in a mouse model (Figure 19c).

Given the advantages of FI in tumor imaging, Song et al. designed and synthesized a series of NIR-II photosensitizers (PSs) with A-D-A′-D-A configuration (NIR-II-H NPs) (**Figure 20a**).[153] Under 808 nm laser excitation, the PS exhibited excellent fluorescence emission and good photostability through intramolecular push–pull interactions and large conjugated systems. Meanwhile, the decreased singlet–triplet energy difference (ΔE_{ST}) promoted the effective catalysis of PSs for $^{\bullet}OH$ production. Excitingly, FI could accurately locate tongue tumors and distinguish between in situ tongue cancer and surrounding normal tissues, thereby guiding laser irradiation to achieve precise treatment effects and effectively reduce side effects. Compared to 808 nm excitation imaging, the NIR-II platform excited at

© 2024 The Authors. Advanced Materials published by Wiley-VCH GmbH

15214095, 2024, 27, Downloaded from https://onlinelibrary.wiley.com/doi/10.1002/adma.202402806 by Ewha Womans University Library, Wiley Online Library on [13/11/2024]. See the Terms and Conditions (https://onlinelibrary.wiley.com/terms-and-conditions) on Wiley Online Library for rules of use; OA articles are governed by the applicable Creative Commons License

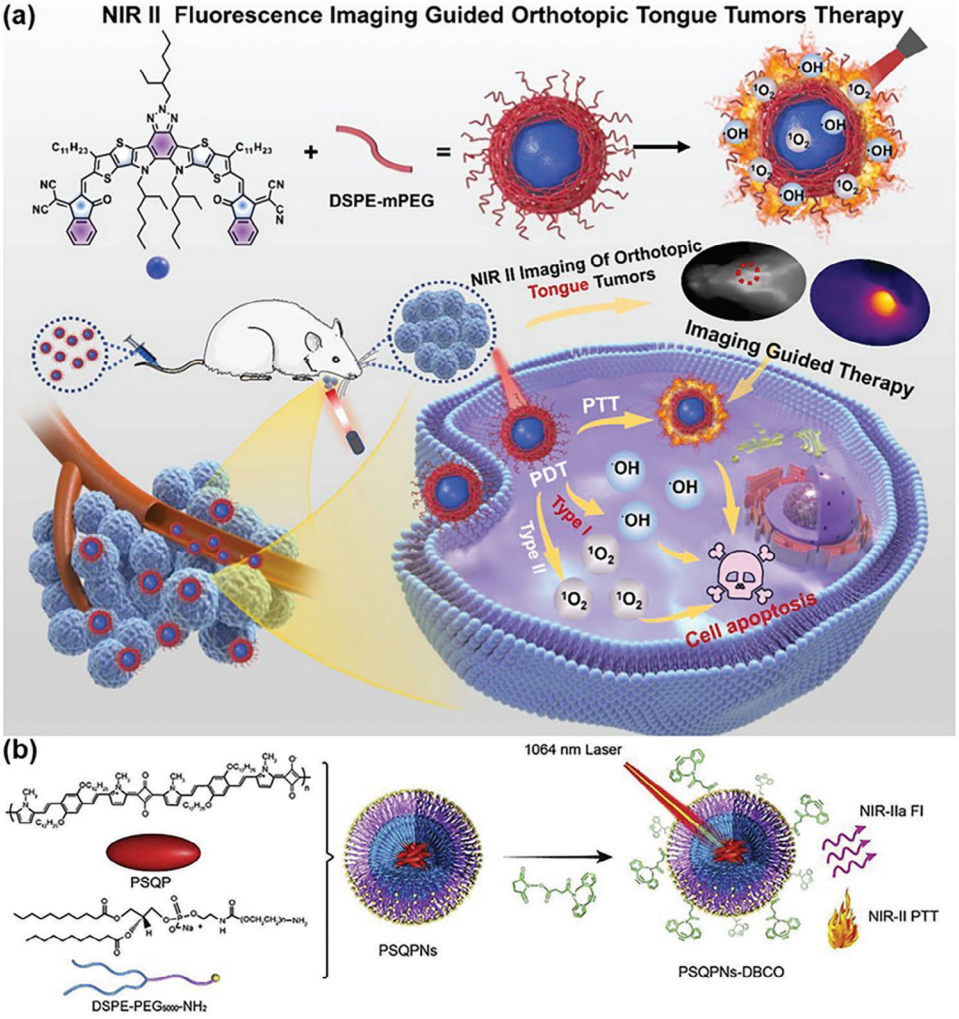


Figure 20. a) Schematic illustration of FI-guided precise treatment of NIR-II-H NPs. Reproduced with permission.[153] Copyright 2022, Elsevier Ltd. b) Schematic illustration of FI-guided precise treatment of PSQPNs-DBCO. Reproduced with permission.[154] Copyright 2020, Elsevier.

1064 nm had a higher signal-to-background ratio (SBR) and better deep tissue imaging, making it more effective for the precise treatment of deep tissue tumors. Based on this, Huang et al. developed a NIR-II imaging-guided PTT therapy using biorthogonal-labeled squaraine-based semiconducting polymer (SP) NPs (PSQPNs-DBCO) (Figure 20b).[154] Moreover, by increasing the π-conjugation length on the squaraine-based SP, the NPs could be excited at 1064 nm, thereby improving the imaging SBR. At the same time, biological orthogonal labeling enabled PSQPNs-DBCO to be significantly enriched in tumors, and the imaging SBR was further increased by 2.5 times. Therefore, PSQPNs-DBCO proved to be efficient and accurate for NIR-II imaging-guided PTT of colorectal tumors in mice.

4.4. X-Ray-to-X-Ray Energy Transformation: CT Imaging

X-rays are high-energy rays with strong penetrating power, but some of their energy is absorbed during the process of penetrating objects. CT imaging makes use of the absorption characteristics of radiation energy in biological tissues and engineering materials samples to perform tomography imaging without damaging the sample, thereby obtaining internal structural information of the sample. Meanwhile, based on the excellent 3D structural imaging ability of CT imaging through the principle of X-ray attenuation, X-ray CT imaging has been used for the diagnosis of routine clinical diseases, such as central nervous system diseases, head and neck diseases, chest diseases, heart diseases, and abdominal diseases,[155] and has become the most commonly used medical imaging equipment for tumor screening.[156,157]

Imaging of a primary tumor and sentinel lymph nodes (SLNs) is of therapeutic and prognostic importance in patients with newly diagnosed cancer.[158] With this in mind, a method combining CT imaging and FI for detecting SLNs was proposed.[159] Specifically, HfO_2 nanocrystals were coupled with NIR fluorescent dye IRDye 800CW to perform dual-mode imaging of SLNs. As shown in **Figure 21**a, after injecting the nanocrystals for 5 min, the contrast enhancement at the SLN could be observed in the CT image, and the signal intensified after 75 and 150 min. Therefore, these bimodal HfO_2

© 2024 The Authors. Advanced Materials published by Wiley-VCH GmbH

15214095, 2024, 27, Downloaded from https://onlinelibrary.wiley.com/doi/10.1002/adma.202402806 by Ewha Womans University Library, Wiley Online Library on [13/11/2024]. See the Terms and Conditions (https://onlinelibrary.wiley.com/terms-and-conditions) on Wiley Online Library for rules of use; OA articles are governed by the applicable Creative Commons License

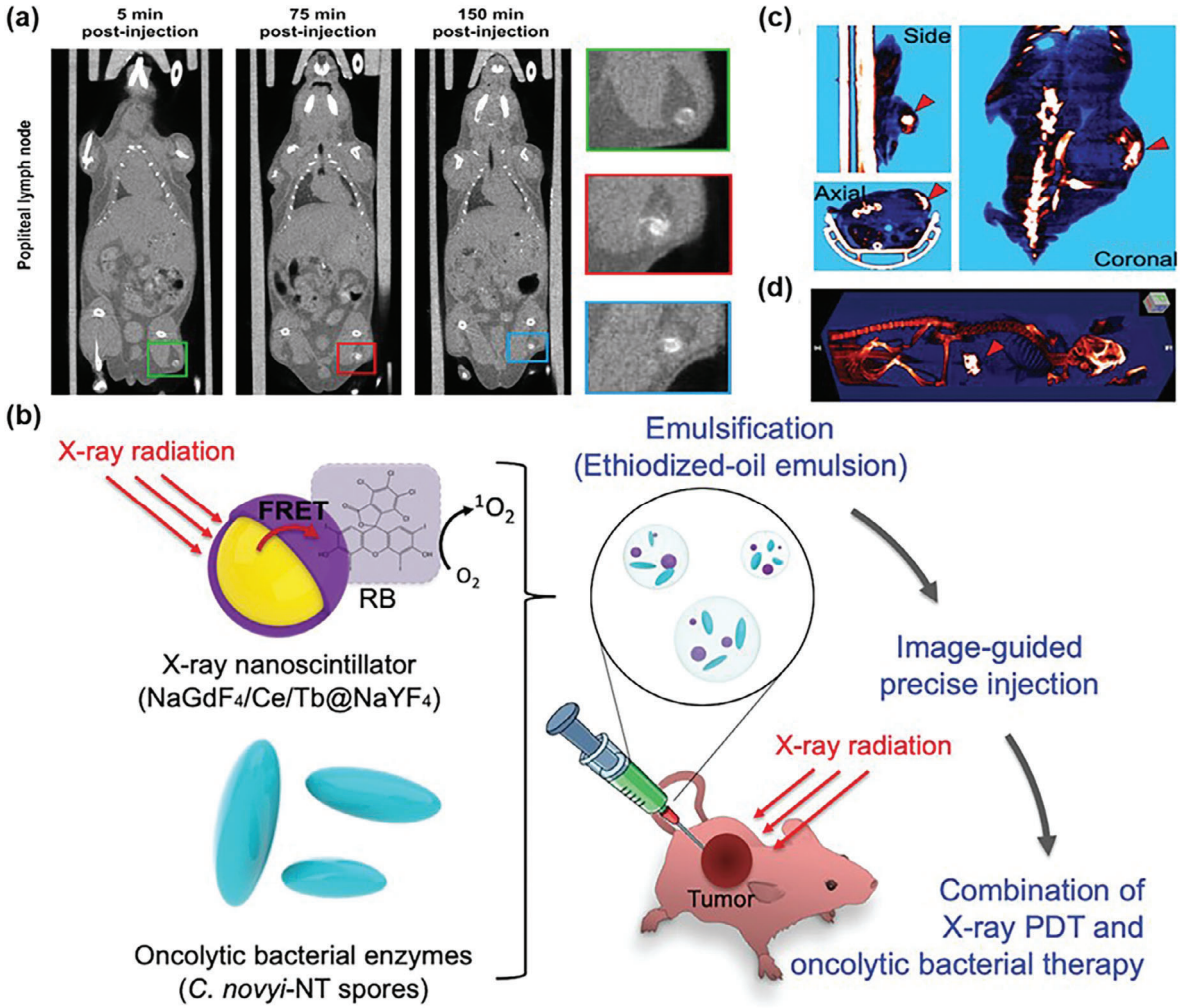


Figure 21. a) Coronal slices of CT scans taken at different time points. The SLN area has been highlighted with green, red, and blue rectangles, respectively. Reproduced with permission.[159] Copyright 2023, American Chemical Society. b) Schematic illustration of nano–bio therapeutic emulsion formulated for the synergistic combination of X-ray photodynamic and anaerobic bacteriolytic therapy. c) Micro-CT and d) 3D images after the infusion of the nano-bio therapeutic emulsion into the tumor site. Reproduced with permission.[160] Copyright 2020, Wiley-VCH.

nanocrystals can efficiently recognize SLNs, providing a good approach for the accuracy of tumor resection surgery. Similarly, in order to achieve image-guided cancer therapy, Kim et al. emulsified PS-coated core–shell-structured lanthanide-doped nanoscintillators (PS-NSs) and *Clostridium novyi*-NT spores with ethiodized oil to achieve internal injection under CT imaging guidance (Figure 21b).[160] A catheter was placed in the center of the tumor; and then, the nano-bio therapeutic emulsion was injected. From the CT image (Figure 21c,d), the nano-bio therapeutic emulsion aggregation at the tumor site could be observed. Therefore, the nano-bio therapeutic emulsion can be successfully injected into the tumor site under the guidance of CT imaging.

4.5. Radioactive-to-γ-Ray Energy Transformation: PET Imaging

PET imaging is a nuclear medicine clinical examination imaging technique that relies on radioactive isotope labeling. This imaging technique is currently the only anatomical and morphological imaging technique for functional, metabolic, and receptor imaging, which is non-invasive and can provide 3D and functional images of the whole body.[161] Consequently, PET imaging is both a scientific research tool and a medical diagnostic tool and has a large number of applications in oncology clinical medical imaging and cancer proliferation research.[162,163] The high value of PET in detecting tumors and identifying any areas of metastasis enables monitoring of the effectiveness of radiation or chemotherapy treatments by measuring the reduction in metabolic or tumor volume.[164,165]

Immune checkpoint inhibitor (ICI) cancer immunotherapy combined with PD-L1 can effectively improve the therapeutic effect in a variety of tumors, and PD-L1 expression has become a key factor.[166] In view of the lack of dynamic detection of PD-L1 positivity by immunohistochemistry, Nimmagadda et al. investigated the relationship between PD-L1 expression and cancer changes by PET imaging based on [18F]DK222 as an imaging agent.[167] Experiments have shown that [18F]DK222 uptake depends on the expression of PD-L1, which was consistent with

© 2024 The Authors. Advanced Materials published by Wiley-VCH GmbH

15214095, 2024, 27, Downloaded from https://onlinelibrary.wiley.com/doi/10.1002/adma.202402806 by Ewha Womans University Library, Wiley Online Library on [13/11/2024]. See the Terms and Conditions (https://onlinelibrary.wiley.com/terms-and-conditions) on Wiley Online Library for rules of use; OA articles are governed by the applicable Creative Commons License

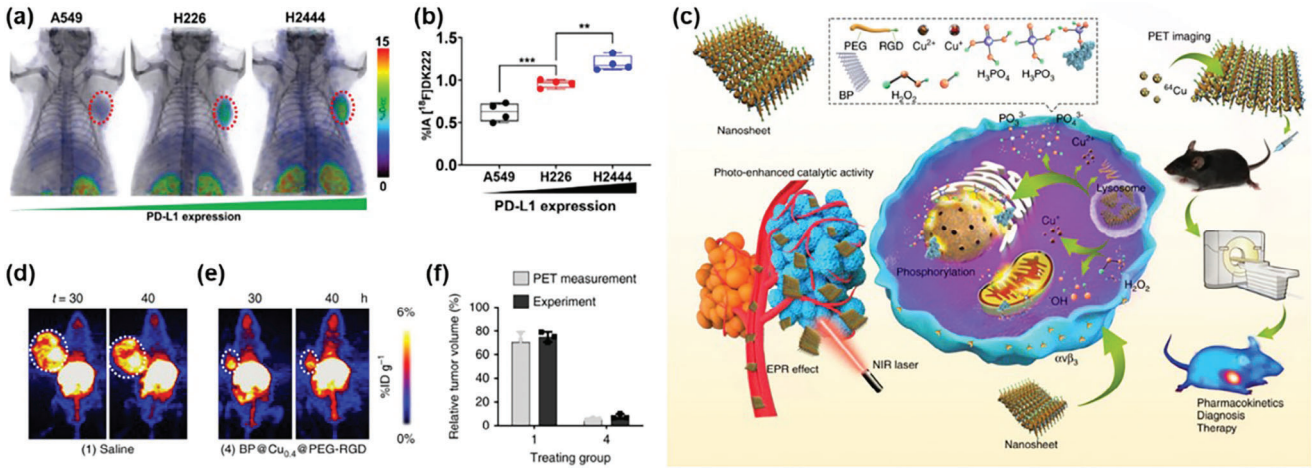


Figure 22. a) PET-CT images of mice bearing different tumors showing PD-L1 expression-dependent uptake. b) Incubation of cells with [18F]DK222 showing [18F]DK222 uptake to be PD-L1 expression-dependent. Reproduced with permission.[167] Copyright 2023, BMJ Ltd. c) Schematic diagram of multifunctional theranostic platform BP@Cu. d) PET images of B16F10 tumor-bearing mice with saline or e) BP@Cu0.4@PEG-RGD, respectively. f) Comparison of tumor volume measured by PET and experimentally. Reproduced with permission.[168] Copyright 2020, Springer Nature.

PD-L1 measurements by flow cytometry. Meanwhile, the PD-L1 shown by PET imaging was consistent with that of immunohistochemical analysis (**Figure 22**a,b). Remarkably, [18F]DK222 could accurately measure the level of PD-L1 expression and treatment-induced changes in different types of tumors by PET imaging, providing favorable support for combination immunotherapy and drug therapy.

Based on the excellent dynamic monitoring effect of PET imaging on tumors, Zhang et al. combined Cu^{2+} with black phosphorus (BP) NSs to achieve a synergistic photothermal effect through efficient loading of Cu^{2+} by BP NSs, further improving the performance of PTT (Figure 22c).[168] Notably, Cu^{2+} could undergo redox reactions with P(0), which promoted the degradation of BP NSs. Meanwhile, the generated Cu^{+} ions could catalyze the Fenton reaction of H_2O_2 in the TME, producing high concentrations of •OH radicals to kill cancer cells and achieving a combination of chemodynamic therapy and PTT. In addition, with $^{64}Cu^{2+}$ labeling, a comprehensive evaluation of the in vivo distribution, dynamics, tumor enrichment ability, and excretion pathways of BP NSs could be achieved through PET imaging (Figure 22d–f). Finally, the therapeutic effect was evaluated using PET imaging and the important role of PET as a diagnostic method in the development of nanomedicines and the evaluation of therapeutic effects was further emphasized.

5. Multimodal Energy Transformation for Cancer Imaging-Guided Therapy

5.1. Photonic-to-Chemical-to-Photonic Energy Transformation: Photoafterglow Imaging

In order to overcome the interference from the autoluminescent background of organisms and achieve high-sensitivity detection and low-background imaging of relevant disease markers, photoafterglow imaging relies on organic or inorganic materials as "photonic cells" to temporarily store the excited light energy and slowly release photons after cessation of the light irradiation.[169,170] Compared to FI, which relies on real-time excitation, photoafterglow imaging has higher SBR and sensitivity. Moreover, based on the flexible modification of the material structure, afterglow luminescence has the advantages of tunable visible-to-NIR emission, repeatable activation, and long lifespan.[171–173]

In 2022, Song et al. introduced pyridine pyrazine into thiophene-based SPs to induce a redshift in emission wavelength and introduced more thiophene as afterglow reaction sites to enhance the emission intensity; thus, developing various novel NIR organic afterglow NPs for monitoring cancer treatment (**Figure 23**a).[174] Meanwhile, the NIR afterglow luminescence relied on $^1O_2$; while, the SP NPs (NIR-3) could produce more $^1O_2$, resulting in the strongest fluorescence emission. Moreover, the SP NPs (NIR-3) could cause intracellular oxidative stress and induce ICD in tumor cells under laser irradiation. Therefore, SP NPs (NIR-3) afterglow imaging could provide real-time information on the degree of ICD occurrence during $^1O_2$-mediated cancer treatment, providing an intuitive detection tool for precise immunotherapy.

Based on the excellent biocompatibility and tunable chemical structure of organic afterglow materials, Song et al. designed activatable afterglow probes containing hemicyanine dyes (HDs) with different halogens (Figure 23b).[29] The HD absorbed photons to produce $^1O_2$, which participated in the afterglow fluorescence emission process. After testing the different halogen-substituted HDs, an activatable HD-Br afterglow probe with stimuli-responsive afterglow luminescence was designed by integrating a stimuli-responsive unit (pH stimulus, $O_2^{\bullet-}$-generating unit, and leucine aminopeptidase [LAP]), which could simultaneously control the initiation of fluorescence emission and $^1O_2$ generation, thereby enhancing the imaging sensitivity and SBR amplification. Based on this, the afterglow probe was successfully used for dynamic detection of $O_2^{\bullet-}$ and LAP in drug-induced hepatotoxicity of mice; while, enabling continuous occurrence of oxidative stress and sensitive imaging of upregulation of LAP. Given these promising results, this approach may provide a new method for early diagnosis of hepatotoxicity.

© 2024 The Authors. Advanced Materials published by Wiley-VCH GmbH

15214095, 2024, 27, Downloaded from https://onlinelibrary.wiley.com/doi/10.1002/adma.202402806 by Ewha Womans University Library, Wiley Online Library on [13/11/2024]. See the Terms and Conditions (https://onlinelibrary.wiley.com/terms-and-conditions) on Wiley Online Library for rules of use; OA articles are governed by the applicable Creative Commons License

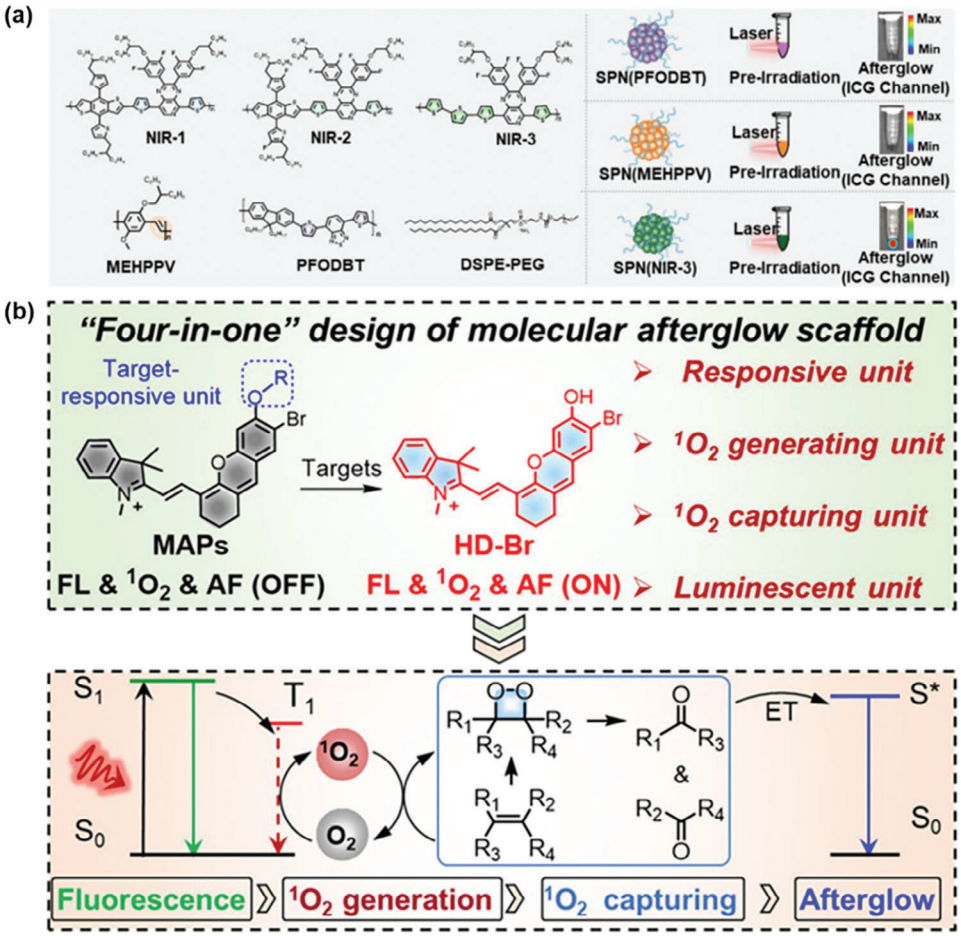


Figure 23. a) Molecular structure and preparation of various SP NPs. Reproduced with permission.[174] Copyright 2022, Ivyspring International. b) Schematic illustration of the design of HDs and the afterglow luminescence mechanism. Reproduced with permission.[29] Copyright 2023, American Chemical Society.

However, organic afterglow probes based on simpler organic molecular compositions, where the reaction site can be easily tuned, the spectra do not need to overlap, and which can exhibit a wider dynamic range and provide an open signal response, are still urgently needed.[175,176] In order to fulfill these requirements, Song et al. designed and synthesized a novel molecular afterglow scaffold (MAS) based on rhodamine–indole molecules, building upon previous research.[177] Meanwhile, this bracket integrated the structure of semi-cyanine and rhodamine dyes; while, retaining the NIR afterglow properties of semi-cyanine and the powerful optical switch adjustment function of rhodamine, achieving a powerful "OFF-to-ON" afterglow activation. Moreover, H_2O-soluble pH-responsive nanoprobes based on afterglow molecular scaffolds were developed to monitor changes in tumor pH; and thus, to evaluate the correlation between tumor glycolysis and chemotherapy (**Figure** 24a). Finally, by synergistically controlling the photodynamic effect and luminescence efficiency, the signal change with a larger dynamic range response and higher sensitivity was achieved.

Currently, most of the afterglow probes that have been reported are based on the molecular cascade reaction between probes and $^1O_2$, but there are very few reports on afterglow probes based on other mechanisms.[170] Therefore, considering both biosafety and clinical translational issues, an H_2O-soluble zwitterionic afterglow probe Cy5-NF with good biocompatibility and renal metabolic ability and afterglow luminescence was reported (Figure 24b).[178] The probe relied on the intramolecular cascade reaction of $O_2^{\bullet-}$ to release afterglow luminescence, and the renal metabolic rate was fast (half-life [$t_{1/2}$] ≈ 10 min). Most importantly, it showed a relatively longer renal retention time ($t_{1/2}$ more than 15 min) in mice with renal failure and could also be quickly metabolized ($t_{1/2}$ ≈ 25–30 min), improving biosafety. Ultimately, the H_2O-soluble zwitterionic Cy5-NF based on an $O_2^{\bullet-}$-mediated afterglow mechanism has great potential for clinical application, especially for the rapid detection of renal failure.

5.2. X-Ray-to-Chemical-to-Photonic Energy Transformation: X-Ray Afterglow Imaging

Recently, photoluminescence imaging has been developed and widely used for the precise diagnosis of tumors, monitoring of therapeutic drugs, and intraoperative imaging guidance. However, due to the scattering and absorption of excitation light by

© 2024 The Authors. Advanced Materials published by Wiley-VCH GmbH

15214095, 2024, 27, Downloaded from https://onlinelibrary.wiley.com/doi/10.1002/adma.202402806 by Ewha Womans University Library, Wiley Online Library on [13/11/2024]. See the Terms and Conditions (https://onlinelibrary.wiley.com/terms-and-conditions) on Wiley Online Library for rules of use; OA articles are governed by the applicable Creative Commons License

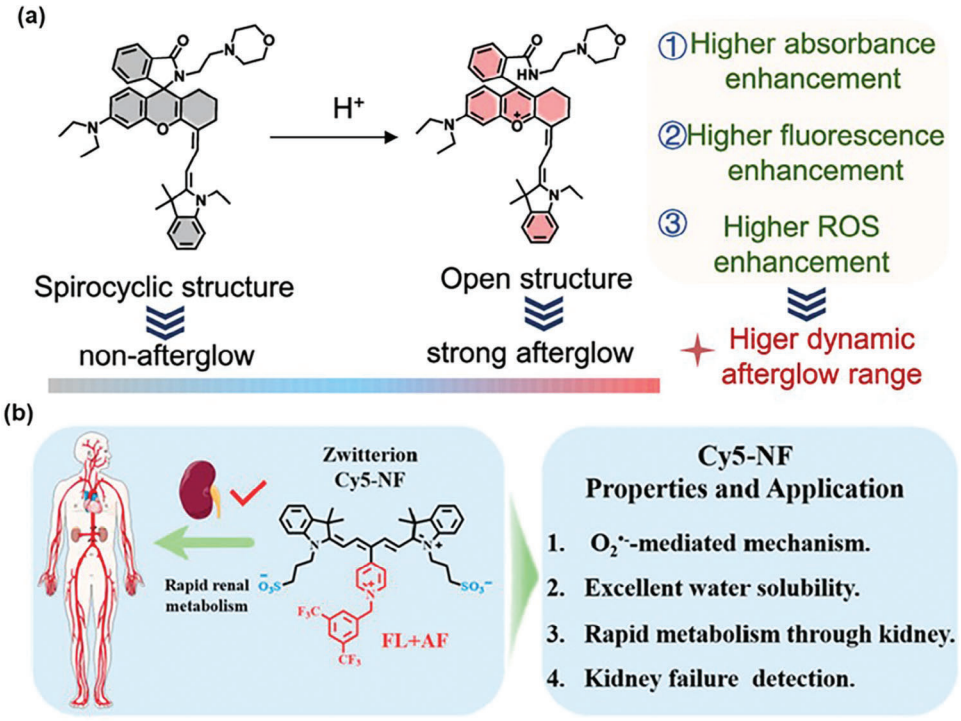


Figure 24. a) Responsive mechanism of MAS-pH for afterglow imaging of pH. Reproduced with permission.[177] Copyright 2023, American Chemical Society. b) Schematic illustration of Cy5-NF afterglow imaging. Reproduced with permission.[178] Copyright 2023, American Chemical Society.

biological tissues, it is difficult for excitation light to penetrate deep tissues, and the application of photo-induced afterglow in deep tissue imaging is greatly limited. In addition, exposure of tissues to external excitation light sources generates potential overheating, which can easily cause damage to biological tissues. Therefore, solving the transformation of initial photonic energy is a challenge faced by researchers.[179]

In response to the above challenges, Zhang's team used fluorides with high-energy band gaps and low phonon energy as matrix materials and, for the first time, designed and synthesized a series of size-, structure-, and wavelength-adjustable NIR-II rare-earth long afterglow nanoprobes (Ln-PLNPs) using a high-temperature solvent thermal decomposition method (**Figure 25a**).[180] By adjusting the type of rare earth ions in the luminescent center, a series of long afterglow NPs with emission wavelengths ranging from 1000 to 1700 nm was obtained under high-energy X-ray excitation. Moreover, by optimizing the luminescence center ion concentration, matrix crystal phase, and particle size, as well as constructing a core–shell structure of long afterglow NPs, the persistent luminescence (PL) time could be extended to over 72 h. Finally, the long afterglow imaging probe had a high signal-to-noise ratio and resolution in distinguishing mouse blood vessels, tumor imaging, and ureteral intraoperative recognition applications (Figure 25b).

However, the radiation function of inorganic nanomaterials is not related to biomarkers, resulting in poor specificity, which is not conducive to the specific diagnosis of tumors. Based on this, Pu et al. successfully prepared a series of adamantylidene-based X-ray afterglow dynamic luminescent materials (IDPAs) (Figure 25c).[181] Under X-ray irradiation, the X-ray afterglow brightness of the IDPAs was more than 25 times that of reported inorganic afterglow nanomaterials, and the production of $^1O_2$ was improved by more than 5.7 times. In addition, the X-ray afterglow dynamics of IDPAs could be induced at a tissue depth of 15 cm with ultra-high sensitivity. Moreover, due to the radioactive afterglow triggered by its intelligent biomarkers, the tissue imaging penetration depth reached 5 cm, and the signal-to-noise ratio was as high as 234. Ultimately, it could detect ultra-small tumors (0.64 mm) with ultra-sensitivity and improve the molecular-level specificity of radiotherapy.

5.3. Ultrasonic-to-Chemical-to-Photonic Energy Transformation: Sonoafterglow Imaging

Although X-rays solve the problem of light-induced penetration to a certain extent, prolonged exposure of patients to X-rays increases the risk of cell mutations and poses a threat to their health. According to the strong penetration performance of US in the therapeutic field, US-activated afterglow (sonoafterglow) imaging has become a research hotspot.[182] Sonoafterglow imaging uses a sonosensitizer as an initiator to generate $^1O_2$, which subsequently activates the substrate to produce afterglow luminescence. Moreover, the sonoafterglow is brighter than previously reported photoafterglow and can be detected at greater tissue depths (4 cm).[183]

In 2023, Pu et al. developed a sonoafterglow nanoprobe (Q-SNAP) composed of a sonosensitizer that could generate $^1O_2$, an afterglow substrate (DPA) that could emit afterglow during oxidation, and the quencher BBQ-650 (**Figure 26a**).[184] Under

© 2024 The Authors. Advanced Materials published by Wiley-VCH GmbH

15214095, 2024, 27, Downloaded from https://onlinelibrary.wiley.com/doi/10.1002/adma.202402806 by Ewha Womans University Library, Wiley Online Library on [13/11/2024]. See the Terms and Conditions (https://onlinelibrary.wiley.com/terms-and-conditions) on Wiley Online Library for rules of use; OA articles are governed by the applicable Creative Commons License

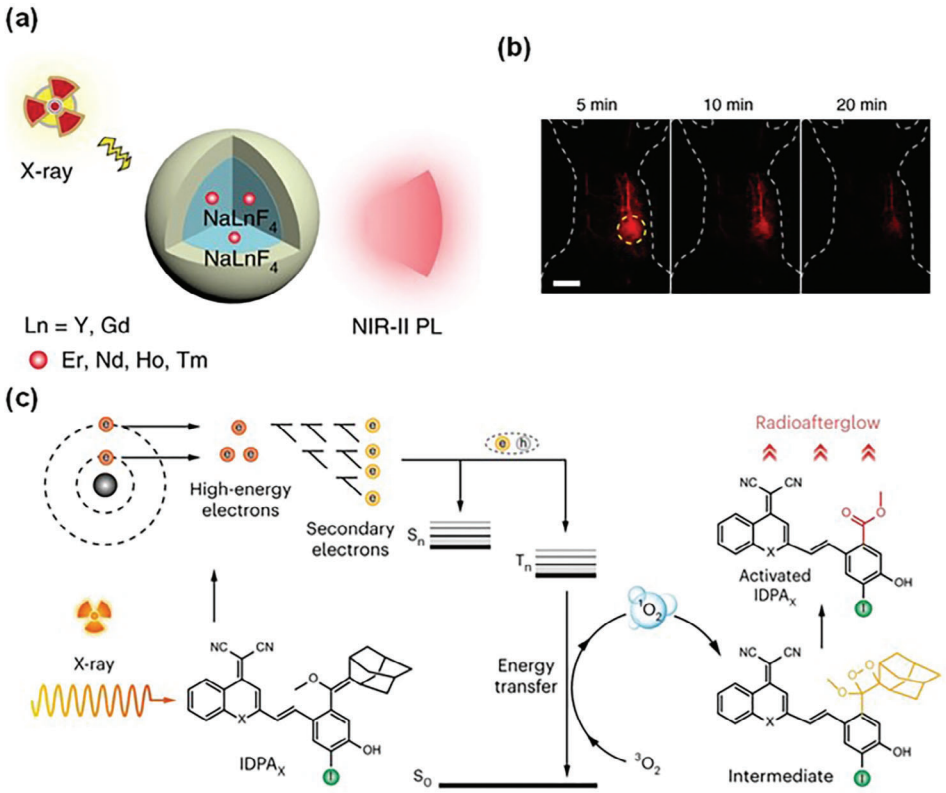


Figure 25. a) Schematic illustration of the X-ray afterglow mechanism of the Ln-PLNPs. Reproduced with permission.[180] Copyright 2021, Springer Nature. b) Time-dependent NIR-II PL images of tumors in living mice after multiple injections of Er-PLNPs. c) Schematic illustration of the radio afterglow mechanism of the IDPA$_x$. Reproduced with permission.[181] Copyright 2023, Springer Nature.

US irradiation, the sonosensitizer generated $^1O_2$ to transform the substrate into high-energy intermediates that gradually released energy after cessation of US. Due to the proximity, energy from DPA could be transferred to BBQ-650, leading to afterglow quenching. Afterglow emission occurred only in the presence of granzyme B, which indicated that Q-SNAP could be used to detect granzyme B. Therefore, given the strong tissue penetrating ability of US, Q-SNAP achieved real-time in situ monitoring and therapeutic evaluation of T cell-mediated autoimmune hepatitis. In the same year, Song et al. directly attached a sonosensitive agent, protoporphyrin IX (PpIX), to the afterglow substrate structure to obtain a US-activated NIR chemiluminescence probe (PNCL) (Figure 26b), which provided US-activated imaging of deep tumor tissues (≈20 mm).[185] US-activated afterglow imaging is expected to become a new diagnostic method for cancer imaging.

5.4. Photonic-to-Thermal-to-Ultrasonic Energy Transformation: Photoacoustic Imaging

PAI is an emerging imaging modality that combines the advantages of optical imaging and USI. When the tissue is irradiated with light, it absorbs a large amount of light energy, most of which is transformed into thermal energy. Meanwhile, the released thermal energy causes the local temperature of the absorber to rise, which in turn, leads to thermal expansion and the generation of pressure waves. The process of generating photoacoustic signals is the transformation process of photonic energy–thermal energy–mechanical energy (ultrasonic energy). Based on its high-resolution imaging performance, it has broad application value in early diagnosis of cancer, oxygen supply testing of various organs, detection of other diseases, and scientific research.[186–188]

An excellent PAI agent can greatly improve the effectiveness of PAI; so, high-performance PAI agents require NIR absorption, excellent light stability, and a strong PA signal (**Figure 27**a).[189,190] In 2023, Kim et al. designed a high-performance PAI agent (BDP1-NEt$_2$) based on the BODIPY structure (Figure 27b).[191] By using trifluoromethyl groups and two adjacent methyl groups in the excited state, the BODIPY framework was bent, activating low-frequency vibrations within the molecule and promoting the PA effect. Meanwhile, the introduction of electron-donating groups further enhanced the push–pull ability and reduced the optical gap of the PAI reagent. Notably, BDP1-NEt$_2$ can be used for rapid tumor diagnosis and persistent imaging, providing reliable information for tumor diagnosis.

Based on the energy transformation process of PAI and PTT, these modalities can be easily combined.[192–194] In this regard, Yoon et al. developed a phototherapy diagnostic agent (PcS4-PcN4) self-assembled from two H_2O-soluble phthalocyanine derivatives (PcS4 and PcN4) (Figure 27c).[18] Compared to the individual PcS4 and PcN4, the self-assembled PcS4-PcN4 had a significantly enhanced signal in the tumor area, and its

© 2024 The Authors. Advanced Materials published by Wiley-VCH GmbH

15214095, 2024, 27, Downloaded from https://onlinelibrary.wiley.com/doi/10.1002/adma.202402806 by Ewha Womans University Library, Wiley Online Library on [13/11/2024]. See the Terms and Conditions (https://onlinelibrary.wiley.com/terms-and-conditions) on Wiley Online Library for rules of use; OA articles are governed by the applicable Creative Commons License

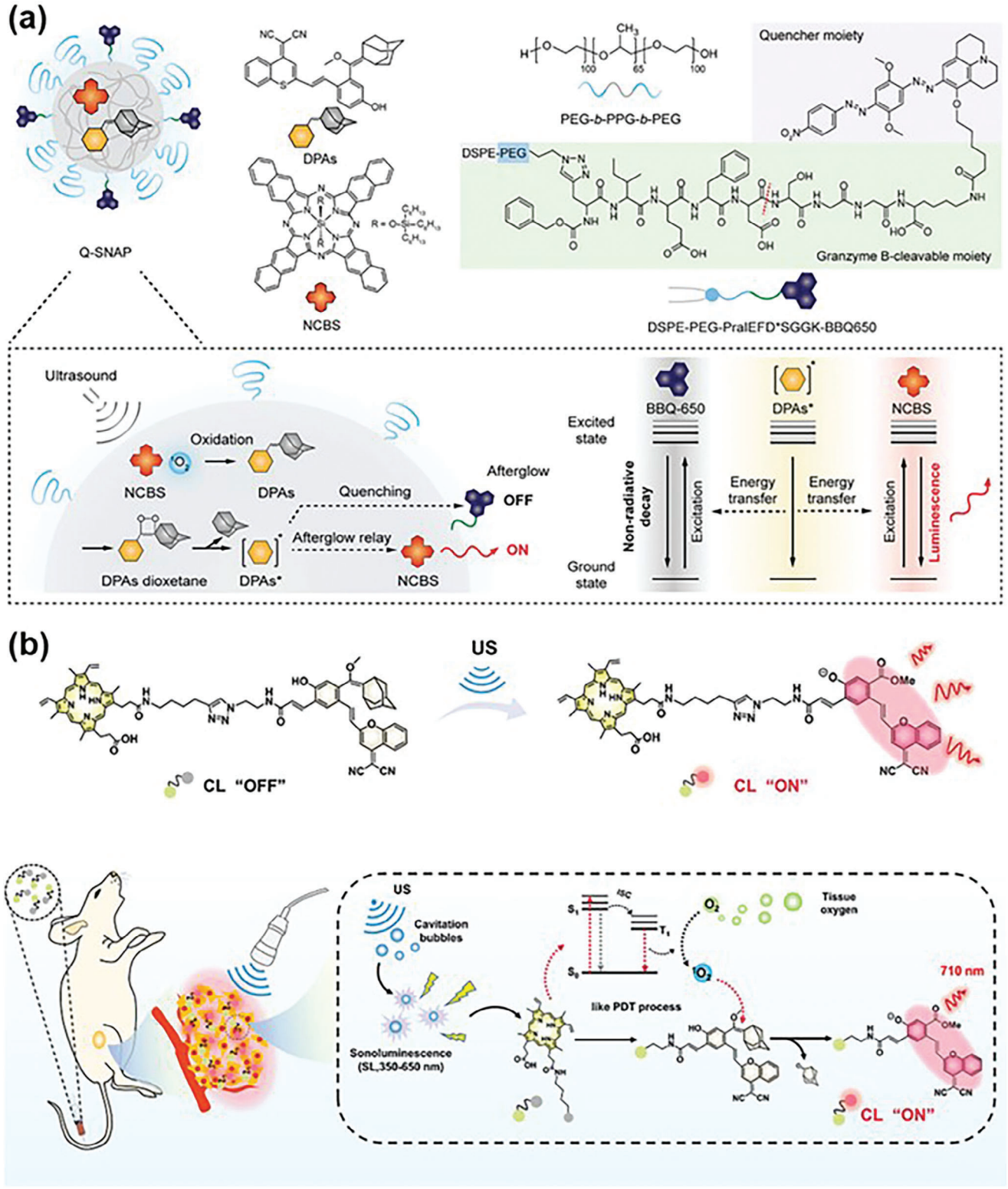


Figure 26. a) Schematic illustration of the composition of Q-SNAP and the quenching mechanism of sonoafterglow. Reproduced with permission.[184] Copyright 2023, Wiley-VCH. b) Schematic illustration of US-activated PNCL. Reproduced with permission.[185] Copyright 2023, American Chemical Society.

© 2024 The Authors. Advanced Materials published by Wiley-VCH GmbH

15214095, 2024, 27, Downloaded from https://onlinelibrary.wiley.com/doi/10.1002/adma.202402806 by Ewha Womans University Library, Wiley Online Library on [13/11/2024]. See the Terms and Conditions (https://onlinelibrary.wiley.com/terms-and-conditions) on Wiley Online Library for rules of use; OA articles are governed by the applicable Creative Commons License

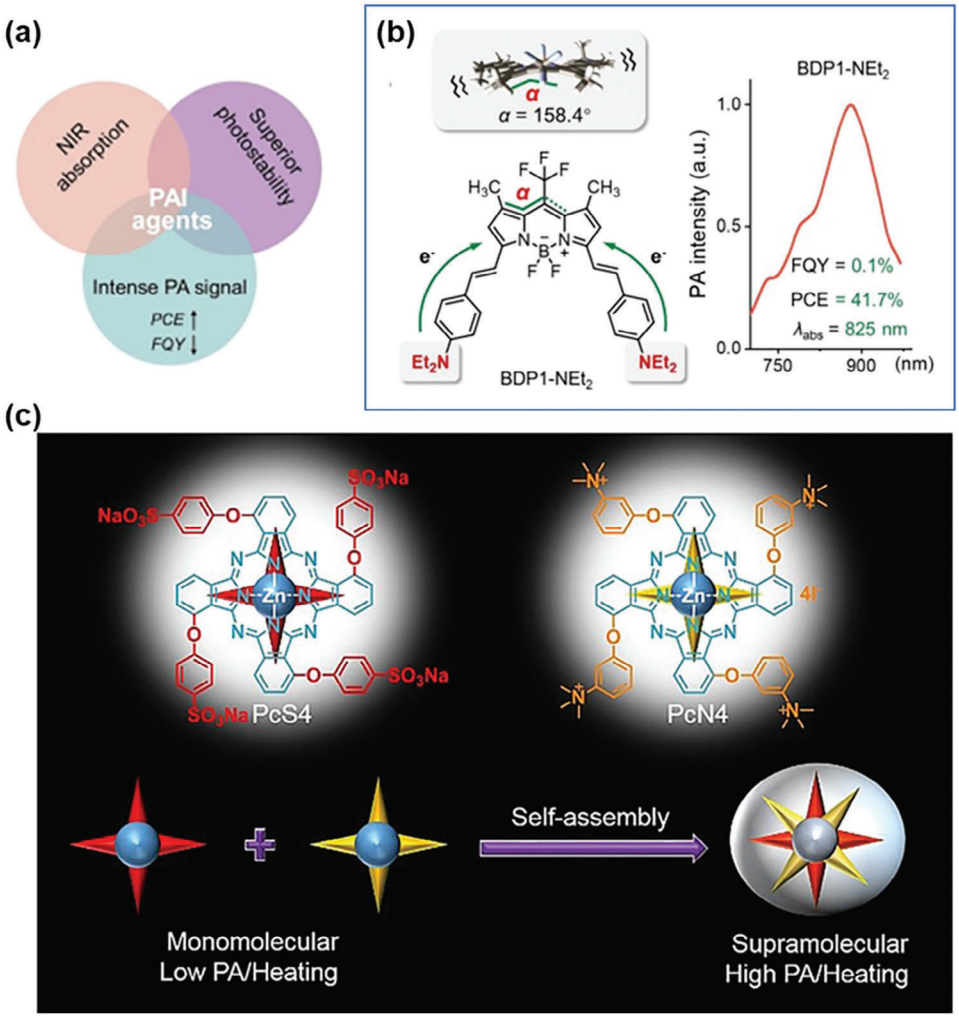


Figure 27. a) Key requirements of PAI agents. b) Schematic illustration of the BDP1-NE_2 design. Reproduced with permission.[191] Copyright 2023, Wiley-VCH. c) Schematic illustration of supramolecular self-assembly based on PcS4 and PcN4. Reproduced with permission.[18] Copyright 2020, Wiley-VCH.

good photothermal transformation enabled it to ablate the tumor effectively. However, PAI agents with NIR-II absorption ability have more advantages when it comes to the TME and deep tissue treatment.[195] In this light, Dong et al. developed two types of charge-transfer composite NPs (TMB-F4TCNQ and TMB-TCNQ) with NIR-II absorption, between which TMB-F4TCNQ exhibited a higher charge-transfer degree and stronger NIR-II absorption ability (**Figure** 28a).[196] Moreover, the high PCE of TMB-F4TCNQ (greater than 42%) endowed it with good tumor ablation ability; while, effectively reducing intracellular GSH through specific cysteine reaction, leading to redox imbalance and inducing ferroptosis, which promoted more efficient tumor elimination.

Similarly, PAI has good application prospects in guiding other tumor treatment modalities.[197,189] For instance, Xiao et al. synthesized a dual prodrug molecule (DOA) of sulfur dioxide (SO_2) and 5-aminolevulinic acid (ALA), which was then co-assembled with methoxyl-poly(ethylene glycol)-*b*-poly(L-lysine) to generate the dual prodrug (P-DOA NPs) for the treatment of skin cancer (Figure 28b).[198] In response to GSH overexpression in tumor cells, the P-DOA NPs simultaneously released SO_2 and ALA under US. The released ALA was metabolically transformed into PpIX for SDT and PAI; while, the SO_2, together with consumption of intracellular GSH based on the reaction between DOA in the P-DOA NPs with intracellular GSH, increased the intracellular ROS content, resulting in an enhanced SDT effect. Most importantly, real-time PAI enabled the P-DOA NPs to achieve good inhibition of melanoma and squamous cell carcinoma in vivo.

5.5. Synergistic Dual Energy Transformation

At present, biopsy, as the gold standard for diagnosis, only provides partial tumor data due to the heterogeneity of tumors and the complexity of the TME.[199,200] Therefore, in clinical settings, treatment decisions regarding patients with cancer are often based on incomplete or even misleading information. Although significant achievements have been made in single

© 2024 The Authors. Advanced Materials published by Wiley-VCH GmbH

15214095, 2024, 27, Downloaded from https://onlinelibrary.wiley.com/doi/10.1002/adma.202402806 by Ewha Womans University Library, Wiley Online Library on [13/11/2024]. See the Terms and Conditions (https://onlinelibrary.wiley.com/terms-and-conditions) on Wiley Online Library for rules of use; OA articles are governed by the applicable Creative Commons License

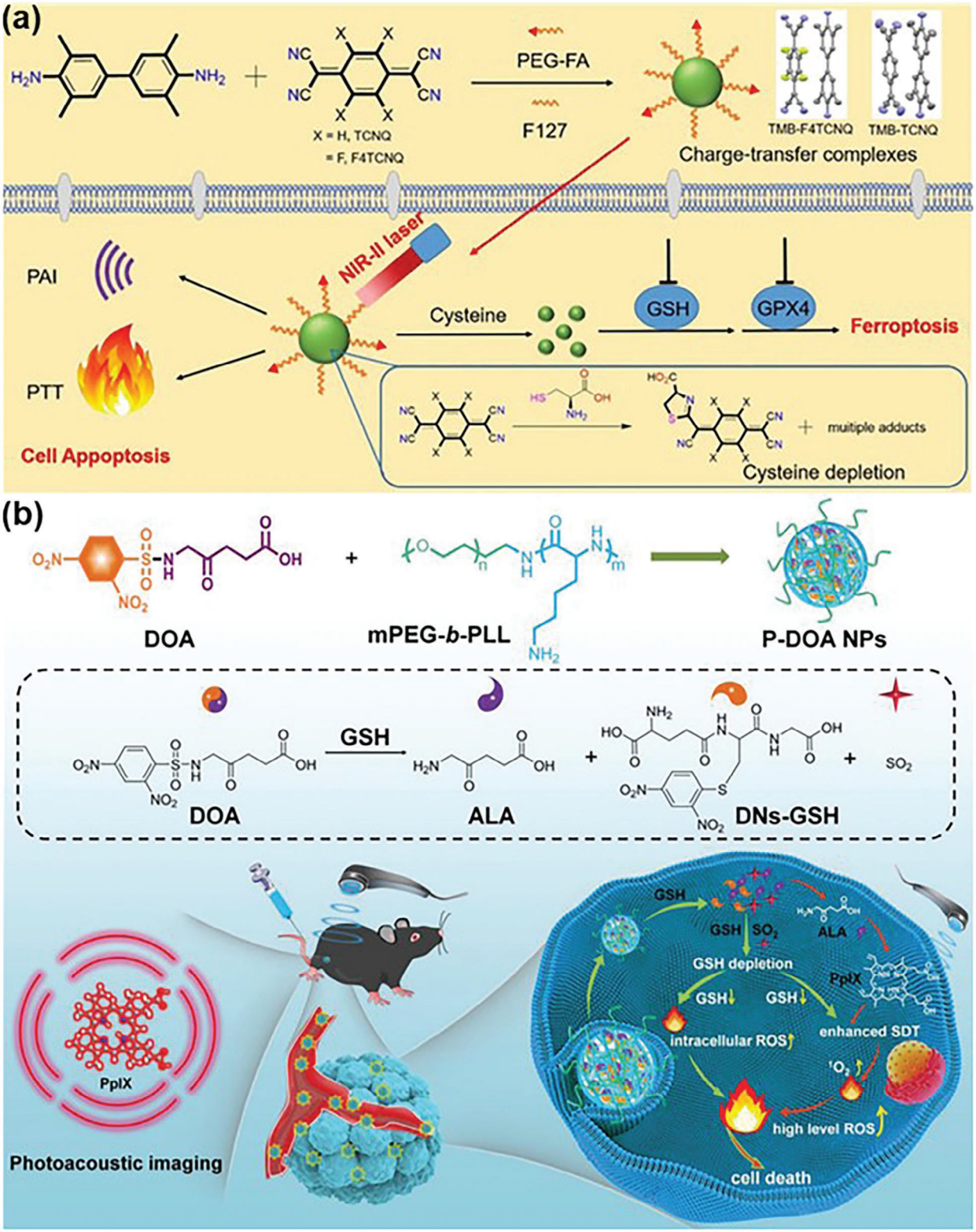


Figure 28. a) Schematic of the preparation of complex NPs (TMB-F4TCNQ and TMB-TCNQ) and illustration of ferroptosis and PTT. Reproduced with permission.[196] Copyright 2021, Wiley-VCH. b) Schematic illustration of P-DOA NPs preparation and PAI-guided enhanced SDT. Reproduced with permission.[198] Copyright 2022, Wiley-VCH.

© 2024 The Authors. Advanced Materials published by Wiley-VCH GmbH

15214095, 2024, 27, Downloaded from https://onlinelibrary.wiley.com/doi/10.1002/adma.202402806 by Ewha Womans University Library, Wiley Online Library on [13/11/2024]. See the Terms and Conditions (https://onlinelibrary.wiley.com/terms-and-conditions) on Wiley Online Library for rules of use; OA articles are governed by the applicable Creative Commons License

tumor imaging, there are still many limitations; for example, poor tissue penetration in FI, insufficient resolution in MRI, and motion artifacts in CT imaging. However, multi-imaging, a multidimensional analysis technique that can effectively distinguish the spatiotemporal changes of tumors, has great potential in achieving personalized and precise treatment of patients with tumors.[201,202] The reason is that multiple detections can improve the detection of spatial correlations between biomarkers to determine drug distribution and receptor occupancy or they can quantify the activation of frequently overexpressed signaling pathways in cancer. It should be noted that the value of multiple detections depends on the spatial resolution of basic imaging techniques and the clinical problems faced, and doctors or researchers need to choose the most suitable tools for disease-specific environments. It is clear that the rapid detection that currently constitutes the backbone of medical imaging still has limitations in terms of resolution and multiple detectability. However, it is precisely the many limitations of a single technology that have prompted the combination of multiple technologies to overcome each other's shortcomings, forming multiple imaging technologies.[203,204]

In 2022, Pu et al. constructed an SP nanoprobe (SPCy) by coupling and self-assembly of an amphiphilic SP and HD (hemi-Cy) (**Figure 29a**).[205] By specifically hydrolyzing the amide bonds of peptide substrates through neutrophil elastase (NE), the fluorescence and PA signal of SPCy were altered. Notably, SPCy only turned on the near-infrared fluorescence (NIRF) and PAI signals of semi-anthocyanin dyes after reacting with NE in the tumor, but the signal of polymer SP remained unchanged (Figure 29b). Finally, this enhanced PAI signal and ratiometric NIRF signal during cancer immunotherapy could effectively detect neutrophils in live mouse tumors, providing a new approach to non-invasive detection of cancer immunotherapy.[206] Similarly, Peng et al. designed a nano-micelle system containing amphiphilic dendritic polymers (Gd-1@ and DiR/Gd-1@).[207] This nanosystem possessed the multivalent properties of dendritic polymers and readily approached Gd^{3+} on the surface of dendritic polymers. Meanwhile, because of the toxicity and stability issues of free Gd^{3+}, a macrocyclic chelating agent was used to coordinate with Gd^{3+} to form Gd−DOTA complexes with high thermal and kinetic stability. The results demonstrated the potential of self-assembled dendritic molecular nanosystems in constructing modular and multimodal imaging contrast agents for MRI and MRI/NIRF bimodality imaging for tumor detection, respectively (Figure 29c). Ultimately, combining the advantages of both imaging systems compensates for the shortcomings of single-modality imaging and provides more complete imaging data for precision medicine.

Multifunctional nanomaterials have always been popular, and their unique chemical properties require specific ways to integrate them harmoniously.[208–210] For instance, Qiu et al. constructed a composite material (CBS&DC-ZIF8@DOX) using zeolite imidazolate framework-8 (ZIF8) to encapsulate copper bismuth sulfide (CBS) semiconductor NPs and rare-earth down-conversion (DC) NPs and loaded the material with the anticancer drug DOX for four-mode imaging (**Figure 30a**).[211] Before and after injection of CBS&DC-ZIF8@DOX, there were significant changes in the signal of the tumor area in MRI, PAI, FI, and CT imaging, demonstrating the practicality of these four imaging methods for tumor model imaging, which provided an excellent platform for multimodal imaging diagnostic strategies.

In cancer treatment, combination therapy with different treatment mechanisms often demonstrates satisfactory results.[212,213] For example, Zhou et al. constructed a nanoplatform (Cro-Fe@BSA NPs) to elicit ferroptosis and photothermal effects using the croconaine (Cro) molecule and an iron-chelating agent with bovine serum albumin (BSA) (Figure 30b,c).[214] In order to determine the optimal window for Cro-Fe@BSA NPs treatment of tumors, PAI and MRI were used in the study of tumor models. As shown in Figure 30d,e, after the injection of Cro-Fe@BSA NPs, the PAI and T_1-weighted MRI signals in the tumor reached their highest levels within 24 h, indicating that Cro-Fe@BSA NPs could efficiently target the tumor, and PAI and MRI imaging provided safe and reliable support for the tumor treatment process.

Distinguishing tumor margins and improving blood–brain barrier (BBB) permeability in surgical resection of glioblastoma is challenging, and better imaging methods are urgently needed to guide diagnosis. Based on this, Zhang et al. constructed nanocapsules (P@GMT-R) and modified their surface with the rabies virus glycoprotein (RVG29) (**Figure 31a**).[215] The P@GMT-R nanocapsules had good biodegradability, could efficiently penetrate the BBB and specifically target in situ gliomas, and guided surgical treatment through NIR-II fluorescence and MRI dual-mode imaging. Finally, these P@GMT-R nanocapsules could effectively distinguish between normal tissue and glioma; thus, providing efficient radiotherapy for glioma.

Multimodal imaging-guided multimodal therapy has made significant progress in tumor treatment.[216,217] For instance, Lan et al. synthesized a BODIPY derivative (B-2TPA) with aggregation-induced emission and twisted intramolecular charge transfer (TICT) properties, which was encapsulated in poly(ethylene glycol-2000)-grafted 1,2-distearoyl-*sn*-glycero-3-phosphatidylethanolamine (DSPE-PEG-2000) to form a nanophotosensitizer (B-2TPA NPs) for NIR FI- and PAI-guided synergistic PDT and PTT for cancer treatment (Figure 31b).[218] Notably, the fluorescence and absorption spectra underwent a red shift; while, the $^1O_2$ yield (6.7%) and PCE (60.1%) were higher than those of the B-2TPA in their non-aggregated state, effectively improving the phototherapy effect and imaging quality (Figure 31c). Results obtained from in vivo experiments, guided by NIR FI and PAI, showed that the B-2TPA NPs could accurately and effectively eliminate tumors through the combination of PTT and PDT.

6. Conclusion and Future Outlook

This review emphasized the aspects of energy transformation in cancer imaging and therapy that are beneficial for clinical cancer therapy, along with clinical trial examples that potentially offer safe, targetable, efficient, and long-term cancer treatment. Various combinations of energy transformation can be further advanced by developing novel nanomaterials in accordance with devising energy production devices and medical imaging equipment. The efficiency of energy transformation needs to be considered and improved for each imaging and treatment modality. This energy transformation can further harness various kinds of energy existing in the endogenous environment of the human

© 2024 The Authors. Advanced Materials published by Wiley-VCH GmbH

15214095, 2024, 27, Downloaded from https://onlinelibrary.wiley.com/doi/10.1002/adma.202402806 by Ewha Womans University Library, Wiley Online Library on [13/11/2024]. See the Terms and Conditions (https://onlinelibrary.wiley.com/terms-and-conditions) on Wiley Online Library for rules of use; OA articles are governed by the applicable Creative Commons License

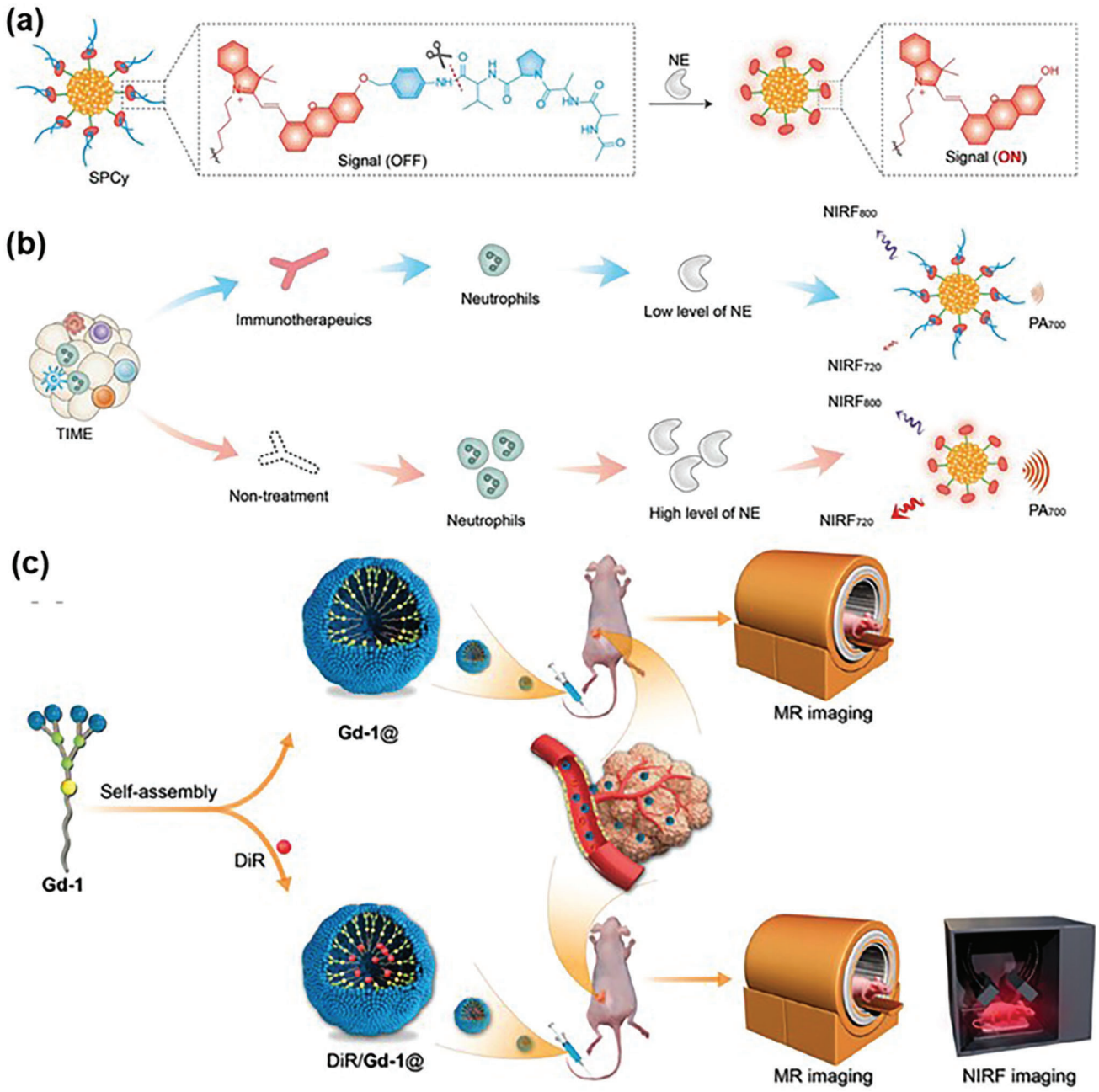


Figure 29. a) Schematic illustration of SPCy in response to NE. b) Mechanism of SPCy-based real-time NIRF and PA imaging of tumor-associated neutrophils (TANs) during cancer immunotherapy in vivo. Reproduced with permission.[205] Copyright 2022, Wiley-VCH. c) Schematic illustration of Gd-1@ and DiR/Gd-1@ for MRI and MR/NIRF bimodality imaging, respectively. Reproduced with permission.[207] Copyright 2023, Wiley-VCH.

body to enable biofriendly solutions for cancer imaging and therapy.

Although research into the precise diagnosis of cancer with remote energy stimulation has recently made surprising progress (**Table 1**), its translation into clinical applications is still a huge challenge. Meanwhile, the interaction and dynamic changes between tumors and the microenvironment make the detection and treatment of tumors highly complex and arduous. However, energy transformation for new diagnostic and treatment modalities provides new tools and support for cancer diagnosis and treatment and will also make tumor treatment more accurate and effective. Although nanomaterial-based systems for imaging and therapy using energy transformation have made rapid progress in cancer treatment, there are still many problems that need to be solved for their clinical translation.

1) Nanomaterials, in energy transformation applications, play a decisive role in imaging and therapy. However, there are

© 2024 The Authors. Advanced Materials published by Wiley-VCH GmbH

15214095, 2024, 27, Downloaded from https://onlinelibrary.wiley.com/doi/10.1002/adma.202402806 by Ewha Womans University Library, Wiley Online Library on [13/11/2024]. See the Terms and Conditions (https://onlinelibrary.wiley.com/terms-and-conditions) on Wiley Online Library for rules of use; OA articles are governed by the applicable Creative Commons License

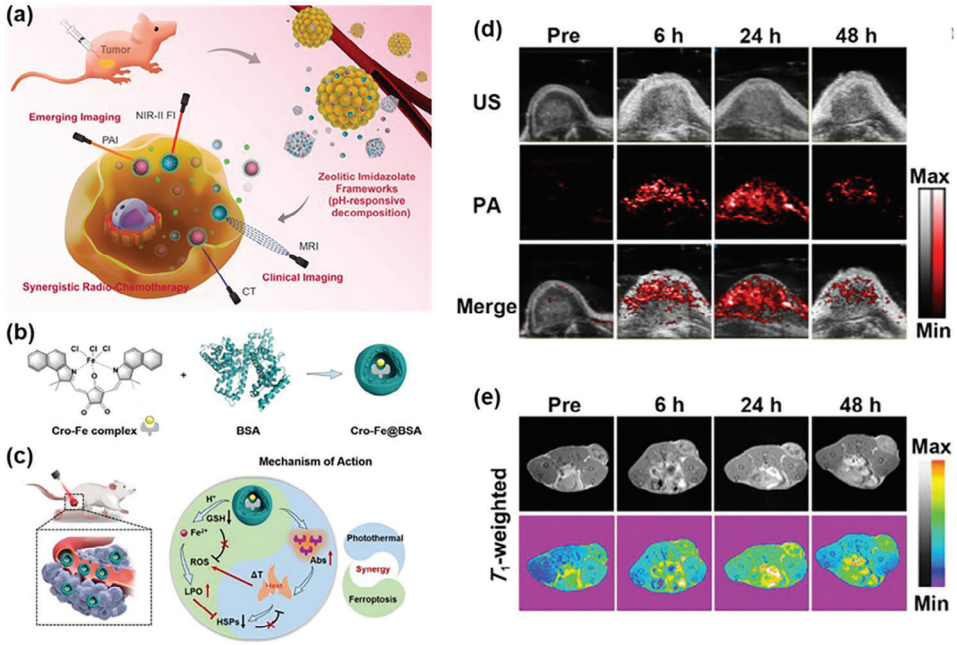


Figure 30. a) Schematic illustration of tetramodal imaging and synergistic cancer radio–chemotherapy enabled by CBS&DC-ZIF8@DOX. Reproduced with permission.[211] Copyright 2020, American Chemical Society. b) Schematic illustration of Cro-Fe@BSA preparation. c) Mechanism of the mutually beneficial combination of ferroptosis and the photothermal effect. d) T_1-weighted in vivo US/PA and e) MRI images of tumor mice after intravenous injection of Cro-Fe@BSA. Reproduced with permission.[214] Copyright 2022, Wiley-VCH.

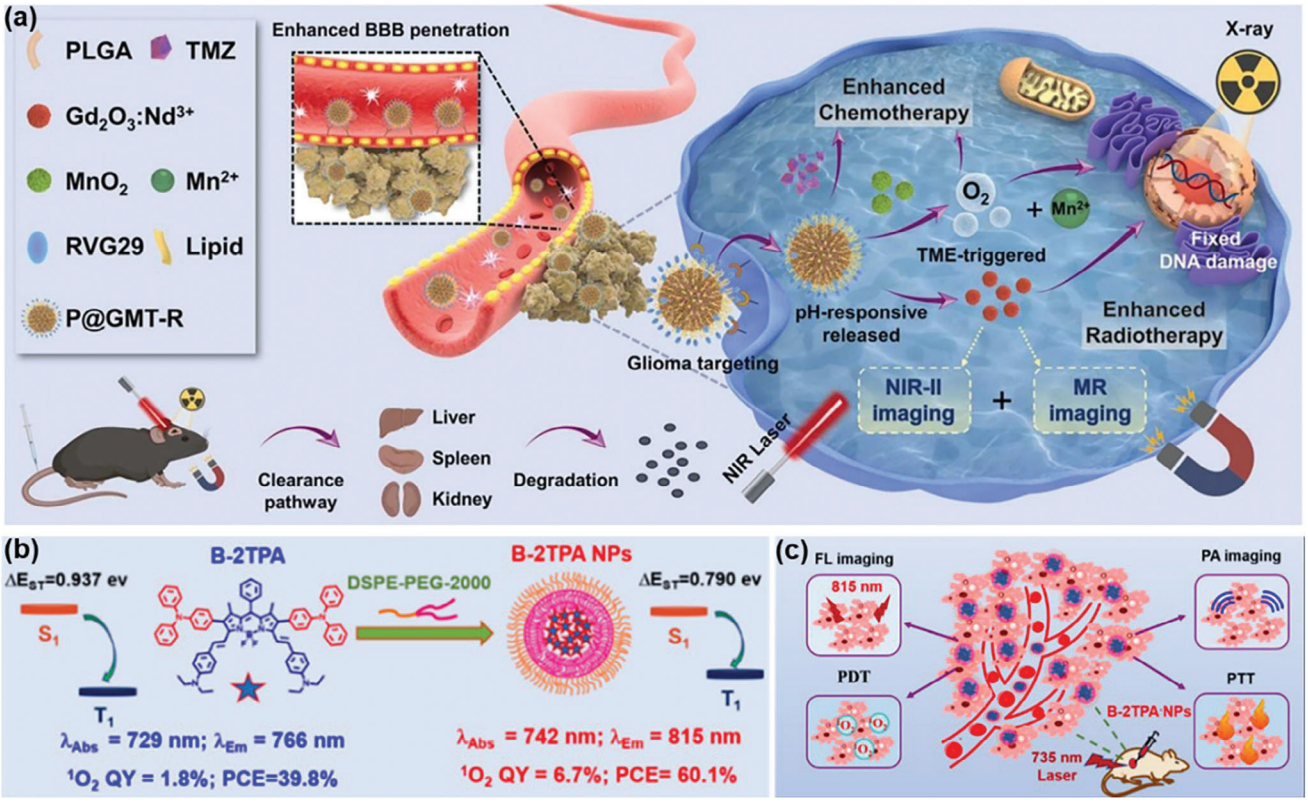


Figure 31. a) Illustration of the therapeutic and imaging mechanisms of P@GMT-R NPs.[215] Reproduced with permission. Copyright 2022, Elsevier. b) Preparation of B-2TPA NPs and main optical properties. c) Schematic illustration of B-2TPA NPs in FL and PA imaging-guided synergistic PDT and PTT of tumors. Reproduced with permission.[218] Copyright 2023, Elsevier Ltd.

© 2024 The Authors. Advanced Materials published by Wiley-VCH GmbH

15214095, 2024, 27, Downloaded from https://onlinelibrary.wiley.com/doi/10.1002/adma.202402806 by Ewha Womans University Library, Wiley Online Library on [13/11/2024]. See the Terms and Conditions (https://onlinelibrary.wiley.com/terms-and-conditions) on Wiley Online Library for rules of use; OA articles are governed by the applicable Creative Commons License

Table 1. Summary of various energy transformation-based cancer imaging and therapy modalities.

Energy transformation	Therapy or imaging mechanisms	Nanomaterial	Cancer type	Refs.
Ultrasonic-to-chemical	SDT	Sensitizer-anchored MOF sonosensitizers	CT26 and 4T1	[42]
–	–	B(0)-doped organic sonosensitizers	4T1	[45]
–	–	Sonosensitizers–nanovaccine integration platform	B16-OVA	[48]
–	–	Artificial polyphenol-based sonosensitizer complexes	4T1	[51]
Ultrasonic-to-mechanical	Ultrasonic mechanical therapy	siRNA nanoparticles-decorated microbubbles	SCC-7	[55]
–	–	Nucleotide nanocomplex-decorated microbubbles	EO771 and 4T1	[56]
Ultrasonic-to-thermal	HIFU	Doxorubicin-loaded thermosensitive liposome	Sarcomas	[60]
–	–	Temperature-sensitive plateletsomes	HeLa	[61]
Ultrasonic-to-ultrasonic	USI	Phase-transformation nanoparticles	MDA-MB-231	[131]
–	–	Liposomal doxorubicin nanoparticles	Neuroblastoma	[132]
Ultrasonic-to-mechanical-to-electrical-to-chemical	Piezoelectric therapy	Versatile sono-piezoelectric nanosheets	4T1	[109]
–	–	Sulfur vacant piezo-sonosensitizers	4T1	[110]
Ultrasonic-to-chemical-to-photonic	Sonoafterglow imaging	Sonosensitizer- and afterglow substrate-loaded nanomaterials	–	[184]
–	–	Sonosensitizer- and afterglow substance-coupled nanomaterials	4T1	[185]
Magnetic-to-mechanical	MMT	Zn-doped iron oxide magnetic nanocubes	U87 and MDA-MB-231	[68]
–	–	Zn-doped iron oxide magnetic nanocubes	U87	[70]
Magnetic-to-thermal	MHT	Zn^{2+}-doped superparamagnetic nanoparticles	HepG2	[79]
–	–	Nanothermometers-based magnetic nanocapsules	MCF-7	[83]
–	–	Superparamagnetic $CoFe_2O_4$@$MnFe_2O_4$ nanoparticles	4T1	[85]
Magnetic-to-photonic	MRI	Photosensitizer and ^{19}F MRI nanoplatform	4T1	[138]
–	–	Ferroptosis core–shell nanoparticles	4T1	[141]
X-ray-to-chemical	RT	Synergetic radiosensitizers	U87	[94]
–	–	H_2 generation radio-platform	MC38	[95]
–	–	Bi-doped TiO_2 radiosensitizers	U87MG	[96]
X-ray-to-X-ray	CT imaging	Dual-modality HfO_2 nanocrystals	Breast cancer (SLNs)	[159]
–	–	X-ray nanoscintillator	PC3	[160]
X-ray-to-chemical-to-photonic	X-ray afterglow imaging	La-doped nanoparticles	4T1	[180]
		Organic radio-luminophore	U87-Luc	[181]
Photonic-to-photonic	FI	Resorufin-based fluorescence probes	HepG2	[149]
–	–	NIR-II fluorescent probes	4T1	[152]
–	–	NIR-II photosensitizers	CAL-27	[153]
–	–	NIR-II semiconducting polymer nanoparticles	CT26	[154]
Photonic-to-thermal (with spatial gradient)-to-electrical-to-chemical	Thermoelectric therapy	$SrTiO_3$/Cu_2Se nanoplates	MCF 7	[100]
–	–	Bismuth telluride nanoplates	B16F10	[101]
Photonic-to-thermal (with temporal gradient)-to-electrical-to-chemical	Pyroelectric therapy	$Bi_{13}S_{18}I_2$ nanorod-pyroelectric biomaterials	4T1	[103]
–	–	Plasmon-pyroelectric nanomaterials	4T1	[104]
Photonic-to-chemical-to-photonic	Photoafterglow imaging	Semiconductor polymer nanomaterials	CT26	[174]
–	–	Hemicyanine-based afterglow materials	–	[29]
–	–	Hemicyanine and rhodamine dye-based afterglow materials	MCF-7	[177]
–	–	Cyanine-based afterglow materials	–	[178]
Photonic-to-thermal-to-ultrasonic	PAI	High-contrast PAI agents	CT26	[191]

(*Continued*)

© 2024 The Authors. Advanced Materials published by Wiley-VCH GmbH

15214095, 2024, 27, Downloaded from https://onlinelibrary.wiley.com/doi/10.1002/adma.202402806 by Ewha Womans University Library, Wiley Online Library on [13/11/2024]. See the Terms and Conditions (https://onlinelibrary.wiley.com/terms-and-conditions) on Wiley Online Library for rules of use; OA articles are governed by the applicable Creative Commons License

Table 1. (Continued)

Energy transformation	Therapy or imaging mechanisms	Nanomaterial	Cancer type	Refs.
–	–	Phthalocyanine self-assembled nanomaterials	4T1	[18]
–	–	Charge-transfer complex nanoparticles	4T1	[196]
–	–	Prodrug nanoparticles	B16F10	[198]
Radioactive-to-γ-ray	PET imaging	Peptide-based PD-L1 imaging agent	NSCLCs and UCs	[167]
–	–	Cu^{2+}-doped black phosphorus nanosheets	B16F10	[168]
–	PDT/PTT	Photosensitizers self-assembling nanoparticles	4T1	[26]
–	PTT/PCT	Photothermal and pyroelectric nanosheets	4T1	[120]
–	PCT/RCT	BiOCl piezoelectric nanosheets	4T1	[123]
–	SDT/PTT	Ti_3C_2 nanosheets	4T1	[124]
–	MMT/MHT	Self-assembling magnetic nanocubes	MDA-MB-231 and U87	[125]
–	SDT/MHT	Hollow magnetic nanosystem	PC-3	[126]
–	FI/PAI	Semiconducting polymer nanoprobes	4T1	[205]
–	FI/MRI	Self-assembling dendrimer nanosystems	L-IPC	[207]
–	MRI/FI/PAI/CT	Zeolitic imidazolate frameworks	4T1	[211]
–	PAI/USI/MRI/PTT	Ferroptosis and photothermal nanoplatform	4T1	[214]
–	FI/MRI/RT	Theranostic nanocapsules	GL261	[215]
–	FI/PAI/PDT/PTT	Multifunctional BODIPY photosensitizers	4T1	[218]

currently bottlenecks in the application of nanomaterials in clinical cancer treatment.[219–221] Although the vast majority of reported nanomaterials have high energy conversion efficiency and good cancer treatment effects, the clinical translation rate of nanomedicines is still low. Currently, only 14% of FDA-approved nanomedicines have shown clinical efficacy, which is unbalanced with the current hot topic of nanomedicine therapy. In addition, several points need to be considered for the clinical use of nanomaterials. First, the reported nanomaterials can only be synthesized in small batches in the laboratory, and it is challenging to ensure the same performance in industrial mass production.[222,223] Further, the stability and storage conditions of nanomaterials must be considered, among which are the high cost and low return on investment, which are of concern to investors. Finally, the biological toxicity of nanomaterials also needs to be studied, and the FDA's strict drug standards compound the challenge for clinical translation of nanomaterials.

2) Advanced energy generation devices and medical imaging equipment provide strong support for remote imaging and therapy modalities based on energy transformation. Although the rapid development of science and technology has led to the rapid updating of medical equipment, there are still many problems in clinical translation. For example, different energy transformation experiments may be conducted smoothly in the laboratory, but in clinical practice, the generation and reception of multiple energies pose challenges for the manufacturing of large-scale medical equipment, and the expensive testing and treatment costs deter many ordinary patients. Moreover, in the medical industry, there are very high standards for the reliability of test data and the safety of instruments. However, with the development of science and technology, new medical equipment has created the possibility of early diagnosis of tumors. For example, PET-CT imaging integrates PET imaging and CT imaging, which can simultaneously reflect the pathological and physiological changes and morphological structure of lesions, improving diagnostic accuracy.[224]
3) There are various types of energy transformation, and biologically friendly as well as efficient energy transformation imaging and therapy are desired. Among them, due to its mature theory and practice, cancer phototherapy has developed beyond other energy transformation modes. However, its biggest problem is that the penetration depth of light in tumor tissue is limited, and only superficial tumors can be imaged and treated. It is exciting that recent NIR-II and afterglow imaging promise to resolve this dilemma. Although US, magnetic field, and radiation have strong tissue penetration ability, they all have corresponding problems;[225,226] for example, the treatment mechanisms of SDT and HIFU are unclear, low magnetocaloric transformation efficiency in MHT, inability to feedback the actual temperature in real-time, and side effects caused by long-term radiation.[227,228] Moreover, different types of cancer and different external environments have different demands for energy transformation, and it is necessary to design reasonably according to these demands. Finally, using endogenous energy in the human body to induce biofriendly energy transformation has great application prospects, such as bioluminescence (transforming biological energy to photon energy), transforming body heat into electrical energy, transforming mechanical energy into electrical energy (triboelectric nanogenerators), and hypothermal PTT.[229–236]

In summary, remote control of energy transformation-based cancer imaging and therapy has shown unique advantages in

© 2024 The Authors. Advanced Materials published by Wiley-VCH GmbH

15214095, 2024, 27, Downloaded from https://onlinelibrary.wiley.com/doi/10.1002/adma.202402806 by Ewha Womans University Library, Wiley Online Library on [13/11/2024]. See the Terms and Conditions (https://onlinelibrary.wiley.com/terms-and-conditions) on Wiley Online Library for rules of use; OA articles are governed by the applicable Creative Commons License

cancer treatment. Although this article focused primarily on the energy transformation of cancer imaging and therapy, there is a similar demand in many other types of diseases.[237,238] Ultimately, we hope that this summary of systematic energy transformation can guide the design of new imaging and therapy methods to achieve precise remote imaging and therapy in clinical practice.

Acknowledgements

H.X. and D.K. contributed equally to this work. This work was supported by the Natural Science Foundation of Shandong Province (No. ZR2022YQ12, Q.H.) and the National Research Foundation of Korea (NRF) grant funded by the Korean government (MSIT) (No. RS-2023-00208427, H.K., No. RS-2023-00217701 and No. 2022M3E5F3080873, J.Y.).

Conflict of Interest

The authors declare no conflict of interest.

Keywords

cancer therapy, energy transformation, imaging, nanomaterials, synergistic treatment

Received: February 23, 2024
Revised: March 24, 2024
Published online: April 5, 2024

[1] I. Gunnarsdottir, B. Davidsdottir, E. Worrell, S. Sigurgeirsdottir, *Renewable Sustainable Energy Rev.* **2021**, *141*, 110770.
[2] N. A. C. Lah, *Renewable Sustainable Energy Rev.* **2021**, *145*, 111103.
[3] J. An, H. Hong, M. Won, H. Rha, Q. Ding, N. Kang, H. Kang, J. S. Kim, *Chem. Soc. Rev.* **2023**, *52*, 30.
[4] J. Li, Y. Luo, K. Pu, *Angew. Chem., Int. Ed.* **2021**, *60*, 12682.
[5] N. Kang, S. Son, S. Min, H. Hong, C. Kim, J. An, J. S. Kim, H. Kang, *Chem. Soc. Rev.* **2023**, *52*, 3955.
[6] X. Li, H. Yang, P. Zheng, D. Lin, Z. Zhang, M. Kang, D. Wang, B. Z. Tang, *J. Mater. Chem. A* **2023**, *11*, 4850.
[7] J. Kim, S. Lee, Y. Kim, M. Choi, I. Lee, E. Kim, C. G. Yoon, K. Pu, H. Kang, J. S. Kim, *Nat. Rev. Mater.* **2023**, *8*, 710.
[8] H. Xiang, Y. Chen, *Small* **2019**, *15*, 1805339.
[9] J. Chen, Y. Zhu, C. Wu, J. Shi, *Chem. Soc. Rev.* **2020**, *49*, 9057.
[10] X. Song, Q. Zhang, M. Chang, L. Ding, H. Huang, W. Feng, T. Xu, Y. Chen, *Adv. Mater.* **2023**, *35*, 2212259.
[11] J. Shin, N. Kang, B. Kim, H. Hong, L. Yu, J. Kim, H. Kang, J. S. Kim, *Chem. Soc. Rev.* **2023**, *52*, 4488.
[12] Q. Zhou, L. Zhang, H. Wu, *Nanotechnol. Rev.* **2017**, *6*, 473.
[13] M. Ermis, N. Falcone, N. R. D. Barros, M. Mecwan, R. Haghniaz, A. Choroomi, M. Monirizad, Y. Lee, J. Song, H. Cho, Y. Zhu, H. Kang, M. R. Dokmeci, A. Khademhosseini, J. Lee, H. Kim, *Bioact. Mater.* **2023**, *25*, 360.
[14] R. Thangam, M. S. Kim, G. Bae, Y. Kim, N. Kang, S. Lee, H. J. Jung, J. Jang, H. Choi, N. Li, M. Kim, S. Park, S. Y. Kim, T. M. Koo, H. E. Fu, Y. S. Jeon, A. Ambrović-Ristov, J. Song, S. Y. Kim, S. Park, Q. Wei, C. Ko, K. Lee, R. Paulmurugan, Y. K. Kim, H. Kang, *Adv. Funct. Mater.* **2021**, *31*, 2008698.
[15] W. Jin, C. Dong, D. Yang, R. Zhang, T. Jiang, D. Wu, *Curr. Drug Delivery* **2020**, *17*, 577.
[16] C. Yin, X. Li, Y. Wang, Y. Liang, S. Zhou, P. Zhao, C. Lee, Q. Fan, W. Huang, *Adv. Funct. Mater.* **2021**, *31*, 2104650.
[17] Y. Zhao, X. Zhang, Z. Chen, Y. Xu, H. Kim, H. Jeong, Y. R. Lee, J. Lee, X. Li, J. Yoon, *Aggregate* **2024**, e514, https://doi.org/10.1002/agt2.514.
[18] X. Li, E. Park, Y. Kang, N. Kwon, M. Yang, S. Lee, W. J. Kim, C. Kim, J. Yoon, *Angew. Chem., Int. Ed.* **2020**, *59*, 8630.
[19] Y. Liu, Z. Zhou, J. Hou, W. Xiong, H. Kim, J. Chen, C. Zheng, X. Jiang, J. Yoon, J. Shen, *Adv. Mater.* **2022**, *34*, 2206121.
[20] Y. Li, J. Xie, W. Um, D. G. You, S. Kwon, L. Zhang, J. Zhu, J. H. Park, *Adv. Funct. Mater.* **2021**, *31*, 2008061.
[21] S. Wang, G. Yu, W. Yang, Z. Wang, O. Jacobson, R. Tian, H. Deng, L. Lin, X. Chen, *Adv. Sci.* **2021**, *8*, 2002927.
[22] N. Mohaghegh, A. Ahari, F. Zehtabi, C. Buttles, S. Davani, H. Hoang, K. Tseng, B. Zamanian, S. Khosravi, A. Daniali, N. H. Kouchehbaghi, I. Thomas, H. S. Nouri, D. Khorsandi, R. Abbasgholizadeh, M. Akbari, R. Patil, H. Kang, V. Jucaud, A. Khademhosseini, A. H. Najafabadi, *Acta Biomater.* **2023**, *172*, 67.
[23] Q. Wu, M. Qu, H. Kim, X. Zhou, X. Jiang, Y. Chen, J. Zhu, L. Ren, T. Wolter, H. Kang, C. Xu, Z. Gu, W. Sun, A. Khademhosseini, *ACS Appl. Mater. Interfaces* **2022**, *14*, 35309.
[24] R. Wang, K. Kim, J. Yoo, X. Li, N. Kwon, Y. Jeon, S. Shin, S. S. Han, D. Lee, J. Yoon, *ACS Nano* **2022**, *16*, 3045.
[25] X. Li, J. F. Lovell, J. Yoon, X. Chen, *Nat. Rev. Clin. Oncol.* **2020**, *17*, 657.
[26] H. Cheng, H. Dai, X. Tan, H. Li, H. Liang, C. Hu, M. Huang, J. Y. Lee, J. Zhao, L. Zhou, Y. Wang, L. Zhang, J. Yong, *Adv. Mater.* **2022**, *34*, 2109111.
[27] L. Yu, Y. Xu, Z. Pu, H. Kang, M. Li, J. L. Sessler, J. S. Kim, *J. Am. Chem. Soc.* **2022**, *144*, 11326.
[28] R. Blau, O. Shelef, D. Shabat, R. Satchi-Fainaro, *Nat. Rev. Bioeng.* **2023**, *1*, 648.
[29] Y. Liu, L. Teng, X. Lou, X. Zhang, G. Song, *J. Am. Chem. Soc.* **2023**, *145*, 5134.
[30] Z. Feng, X. Xiang, J. Huang, L. Wang, B. Zhu, H. Zhou, H. Pang, C. Cheng, L. Ma, L. Qiu, *Adv. Funct. Mater.* **2023**, *33*, 2302579.
[31] S. Son, J. Kim, J. Kim, B. Kim, J. Lee, Y. Kim, M. Li, H. Kang, J. S. Kim, *Chem. Soc. Rev.* **2022**, *51*, 8201.
[32] S. Chen, P. Zhu, L. Mao, W. Wu, H. Lin, D. Xu, X. Lu, J. Shi, *Adv. Mater.* **2023**, *35*, 2208256.
[33] J. S. D. Mieog, F. B. Achterberg, A. Zlitni, M. Hutteman, J. Burggraaf, R. Swijnenburg, S. Gioux, A. L. Vahrmeijer, *Nat. Rev. Clin. Oncol.* **2022**, *19*, 9.
[34] E. Natera-Villalba, M. Matarazzo, R. Martinez-Fernandez, *Curr. Opin. Neurol.* **2022**, *35*, 525.
[35] A. Ma, H. Chen, Y. Cui, Z. Luo, R. Liang, Z. Wu, Z. Chen, T. Yin, J. Ni, M. Zheng, L. Cai, *Small* **2019**, *15*, 1804028.
[36] G. Canavese, A. Ancona, L. Racca, M. Canta, B. Dumontel, F. Barbaresco, T. Limongi, V. Cauda, *Chem. Eng. J.* **2018**, *340*, 155.
[37] C. Dong, P. Yang, X. Wang, H. Wang, Y. Tang, H. Zhang, L. Yu, Y. Chen, W. Wang, *Bioconjug. Chem.* **2022**, *33*, 1035.
[38] K. M. Nowak, M. R. Schwartz, V. R. Breza, R. J. Price, *Cancer Lett.* **2022**, *532*, 215592.
[39] X. Pan, H. Wang, S. Wang, X. Sun, L. Wang, W. Wang, H. Shen, H. Liu, *Sci. China: Life Sci.* **2018**, *61*, 415.
[40] D. Li, Y. Yang, D. Li, J. Pan, C. Chu, G. Liu, *Small* **2021**, *17*, 2101976.
[41] X. Liang, M. Chen, P. Bhattarai, S. Hameed, Z. Dai, *ACS Nano* **2020**, *14*, 13569.
[42] G. Lin, G. T. Nash, T. Luo, I. Ghosh, S. Sohoni, A. J. Christofferson, G. Liu, G. S. Engel, W. Lin, *Adv. Mater.* **2023**, *35*, 2212069.
[43] Y. He, S. Hua Liu, J. Yin, J. Yoon, *Coord. Chem. Rev.* **2021**, *429*, 213610.
[44] X. Xing, S. Zhao, T. Xu, L. Huang, Y. Zhang, M. Lan, C. Lin, X. Zheng, P. Wang, *Coord. Chem. Rev.* **2021**, *445*, 214087.

© 2024 The Authors. Advanced Materials published by Wiley-VCH GmbH

15214095, 2024, 27, Downloaded from https://onlinelibrary.wiley.com/doi/10.1002/adma.202402806 by Ewha Womans University Library, Wiley Online Library on [13/11/2024]. See the Terms and Conditions (https://onlinelibrary.wiley.com/terms-and-conditions) on Wiley Online Library for rules of use; OA articles are governed by the applicable Creative Commons License

[45] K. Liu, Z. Jiang, F. Zhao, W. Wang, F. Jäkle, N. Wang, X. Tang, X. Yin, P. Chen, *Adv. Mater.* **2022**, *34*, 2206594.
[46] X. Zhong, X. Wang, L. Cheng, Y. Tang, G. Zhan, F. Gong, R. Zhang, J. Hu, Z. Liu, X. Yang, *Adv. Funct. Mater.* **2019**, *30*, 1907954.
[47] P. Zhu, Y. Chen, J. Shi, *ACS Nano* **2018**, *12*, 3780.
[48] G. Zhan, Q. Xu, Z. Zhang, Z. Wei, T. Yong, N. Bie, X. Zhang, X. Lin, J. Li, L. Gan, X. Yang, *Nano Today* **2021**, *38*, 101195.
[49] P. C. Zhang, Y. H. Zhai, Y. Cai, Y. L. Zhao, Y. P. Li, *Adv. Mater.* **2019**, *31*, 1904156.
[50] J. Li, Z. Yue, M. Tang, W. Wang, Y. Sun, T. Sun, C. Chen, *Adv. Healthcare Mater.* **2024**, *13*, 2302028.
[51] Z. Zhang, B. Li, L. Xie, W. Sang, H. Tian, J. Li, G. Wang, Y. Dai, *ACS Nano* **2021**, *15*, 16934.
[52] Q. Xia, J. Tian, X. Y. Chen, *Biomaterials* **2016**, *79*, 56.
[53] S. Wilhelm, A. J. Tavares, Q. Dai, S. Ohta, J. Audet, H. F. Dvorak, W. C. W. Chan, *Nat. Rev. Mater.* **2016**, *1*, 16014.
[54] C. M. Newman, T. Bettinger, *Gene Ther.* **2007**, *14*, 465.
[55] H. Han, D. Kim, Y. Jang, M. Seo, K. Kim, J. B. Lee, H. Kim, *J. Controlled Release* **2020**, *322*, 346.
[56] X. Li, S. Khorsandi, Y. Wang, J. Santelli, K. Huntoon, N. Nguyen, M. Yang, D. Lee, Y. Lu, R. Gao, B. Y. S. Kim, C. D. G. Lux, R. F. Mattrey, W. Jiang, J. Lux, *Nat. Nanotechnol.* **2022**, *17*, 891.
[57] Y. Cai, Y. Sun, F. Xu, Y. Wu, C. Ren, X. Hao, B. Gao, Q. Cao, *Sci. Rep.* **2023**, *13*, 9903.
[58] P. Liu, J. Foiret, Y. Situ, N. Zhang, A. J. Kare, B. Wu, M. N. Raie, K. W. Ferrara, L. S. Qi, *Nat. Commun.* **2023**, *14*, 6575.
[59] Q. Li, J. Zhang, J. Li, H. Ye, M. Li, W. Hou, H. Li, Z. Wang, *ACS Appl. Mater. Interfaces* **2021**, *13*, 26808.
[60] L. C. Sebeke, J. D. C. Gómez, E. Heijman, P. Rademann, A. C. Simon, S. Ekdawi, S. Vlachakis, D. Toker, B. L. Mink, C. Schubert-Quecke, S. Y. Yeo, P. Schemidt, C. Lucas, S. Brodesser, M. Hossann, L. H. Lindner, H. Grüll, *J. Controlled Release* **2022**, *343*, 798.
[61] D. Wu, X. Jin, X. Wang, B. Ma, C. Lou, H. Qu, J. Zheng, B. Zhang, X. Yan, Y. Wang, L. Jing, *Theranostics* **2019**, *9*, 3966.
[62] Y. Li, Z. Cong, L. Xie, S. Tang, C. Ren, X. Peng, D. Tang, F. Wan, H. Han, X. Zhang, W. Gao, S. Wu, *Small* **2023**, *19*, 2301489.
[63] M. Hasan, J. Choi, H. Akter, H. Kang, M. Ahn, S. Lee, *Adv. Sci.* **2024**, *11*, 2307148.
[64] S. Y. Kim, R. Thangam, N. Kang, H. Hong, C. Kim, S. Lee, S. Son, H. Lee, K. Tag, S. Min, D. Jeong, J. Hwang, K. Kim, D. Kim, Y. Kim, J. Joo, B. H. Kim, Y. Zhu, S. Park, H. Song, W. Sun, J. Ahn, W. Y. Jang, R. Paulmurugan, H. Kim, J. S. Kim, H. Kang, *Adv. Funct. Mater.* **2023**, *33*, 2215166.
[65] Y. Kim, T. Myeongseok, k. R. Thangam, M. S. Kim, W. Y. Jang, N. Kang, S. Min, S. Y. Kim, L. Yang, H. Hong, H. J. Jung, E. K. Koh, K. D. Patel, S. Lee, H. E. Fu, Y. S. Jeon, B. C. Park, S. Y. Kim, S. Park, J. Lee, L. Gu, D. Kim, T. Kim, K. Lee, W. K. Jeong, R. Paulmurugan, Y. K. Kim, H. Kang, *Adv. Mater.* **2022**, *34*, 2110340.
[66] P. Wang, C. Chen, Q. Wang, H. Chen, C. Chen, J. Xu, X. Wang, T. Song, *J. Controlled Release* **2022**, *351*, 941.
[67] M. Sun, K. F. Chan, Z. Zhang, L. Wang, Q. Wang, S. Yang, S. M. Chan, P. W. Y. Chiu, J. J. Y. Sung, L. Zhang, *Adv. Mater.* **2022**, *34*, 2201888.
[68] Y. Shen, W. Zhang, G. Li, P. Ning, Z. Li, H. Chen, X. Wei, X. Pan, Y. Qin, B. He, Z. Yu, Y. Cheng, *ACS Nano* **2021**, *15*, 20020.
[69] G. Bae, Y. S. Jeon, M. J. Ko, Y. Kim, S. Han, R. Thangam, W. Kim, H. J. Jung, S. Lee, H. Choi, S. Min, H. Hong, S. Park, S. Y. Kim, K. D. Patel, N. Li, J. E. Shin, B. C. Park, H. S. Park, J. H. Moon, Y. J. Kim, U. K. Sukumar, J. Song, S. Y. Kim, S. Yu, Y. C. Kang, S. Park, S. M. Han, D.-H. Kim, K.-B. Lee, et al., *Adv. Funct. Mater.* **2021**, *31*, 2103409.
[70] M. Chen, J. Wu, P. Ning, J. Wang, Z. Ma, L. Huang, G. R. Plaza, Y. Shen, C. Xu, Y. Han, M. S. Lesniak, Z. Liu, Y. Cheng, *Small* **2020**, *16*, 1905424.
[71] M. Wang, Q. Chen, D. Xu, Z. Yang, J. Chen, Y. Zhang, H. Chen, *Nano Today* **2022**, *43*, 101374.
[72] X. Wang, Y. Qi, Z. Hu, L. Jiang, F. Pan, Z. Xiang, Z. Xiong, W. Jia, J. Hu, W. Lu, *Adv. Compos. Hybrid Mater.* **2022**, *5*, 1786.
[73] S. S. Laha, N. D. Thorat, G. Singh, C. I. Sathish, J. Yi, A. Dixit, A. Vinu, *Small* **2022**, *18*, 2104855.
[74] L. Zhang, Q. Zhang, D. T. Hinojosa, K. Jiang, Q. Pham, Z. Xiao, V. L. Colvin, G. Bao, *ACS Nano* **2022**, *16*, 18538.
[75] H. Fu, L. Chen, W. Fang, P. Hu, J. Shi, *Nano Today* **2023**, *52*, 101987.
[76] Y. Kim, H. J. Jung, Y. Lee, S. Koo, R. Thangam, W. Y. Jang, S. Y. Kim, S. Park, S. Lee, G. Bae, K. D. Patel, Q. Wei, K. Lee, R. Paulmurugan, W. K. Jeong, T. Hyeon, D. Kim, H. Kang, *J. Am. Chem. Soc.* **2022**, *144*, 5769.
[77] G. Bae, M. S. Kim, R. Thangam, T. M. Koo, W. Y. Jang, J. Yoon, S. Han, L. Yang, S. Y. Kim, N. Kang, S. Min, H. Hong, H. E. Fu, M. J. Ko, D. Kim, W. K. Jeong, D. Kim, T. Kim, J. Choi, K. Lee, R. Paulmurugan, Y. Zhu, H. Kim, J. Lee, J. S. Kim, A. Khademhosseini, Y. K. Kim, H. Kang, *Adv. Funct. Mater.* **2022**, *32*, 2200828.
[78] N. Feliu, D. Docter, M. Heine, P. del Pino, S. Ashraf, J. Kolosnjaj-Tabi, P. Macchiarini, P. Nielsen, D. Alloyeau, F. Gazeau, R. H. Stauber, W. J. Parak, *Chem. Soc. Rev.* **2016**, *45*, 2440.
[79] J. Pan, Y. Cu, Q. Wu, P. Hu, J. Shi, *J. Am. Chem. Soc.* **2021**, *143*, 8116.
[80] U. M. Engelmann, A. A. Roeth, D. Eberbeck, E. M. Buhl, U. P. Neumann, T. Schmitz-Rode, I. Slabu, *Sci. Rep.* **2018**, *8*, 13210.
[81] H. Hong, S. Min, S. Koo, Y. Lee, J. Yoon, W. Y. Jang, N. Kang, R. Thangam, H. Choi, H. J. Jung, S. Han, Q. Wei, S. Yu, D. Kim, R. Paulmurugan, W. K. Jeong, K. Lee, T. Hyeon, D. Kim, H. Kang, *Adv. Mater.* **2022**, *34*, 2105460.
[82] R. Thangam, S. Y. Kim, N. Kang, H. Hong, H. Lee, S. Lee, D. Jeong, K. Tag, K. Kim, Y. Zhu, W. Sun, H. Kim, S. Cho, J. Ahn, W. Y. Jang, J. S. Kim, R. Paulmurugan, A. Khademhosseini, H. Kim, H. Kang, *Adv. Funct. Mater.* **2023**, *33*, 2206673.
[83] E. Ximendes, R. Marin, Y. Shen, D. Ruiz, D. Gómez-Cerezo, P. Rodríguez-Sevilla, J. Lifante, P. X. Viveros-Méndez, F. Gámez, D. García-Soriano, G. Salas, C. Zalbidea, A. Espinosa, A. Benayas, N. García-Carrillo, L. Cussó, M. Desco, F. J. Teran, B. H. Juárez, D. Jaque, *Adv. Mater.* **2021**, *33*, 2100077.
[84] Y. Chao, G. Chen, C. Liang, J. Xu, Z. Dong, X. Han, C. Wang, Z. Liu, *Nano Lett.* **2019**, *19*, 4287.
[85] J. Pan, P. Hu, Y. Guo, J. Hao, D. Ni, Y. Xu, Q. Bao, H. Yao, C. Wei, Q. Wu, J. Shi, *ACS Nano* **2020**, *14*, 1033.
[86] X. Chen, H. Wang, J. Shi, Z. Chen, Y. Wang, S. Gu, Y. Fu, J. Huang, J. Ding, L. Yu, *Biomaterials* **2023**, *298*, 122139.
[87] J. Ge, N. Yang, Y. Yang, H. Yu, X. Yang, Y. Wang, T. Wang, S. Cheng, Y. Wang, Z. Han, Y. Teng, J. Zou, H. Yang, L. Cheng, *Bioact. Mater.* **2023**, *25*, 73.
[88] Q. Qin, Y. Zhou, P. Li, Y. Liu, R. Deng, R. Tang, N. Wu, L. Wan, M. Ye, H. Zhou, Z. Wang, *J. Nanobiotechnol.* **2023**, *21*, 131.
[89] a) M. A. Knoll, R. Jagsi, K. Rosenzweig, *JAMA Oncol.* **2019**, *5*, 442; b) S. Goel, D. Ni, W. Cai, *ACS Nano* **2017**, *11*, 5233.
[90] C. Zhao, Y. Cheng, P. Huang, C. Wang, W. Wang, M. Wang, W. Shan, H. Deng, *Adv. Mater.* **2023**, *35*, 2208059.
[91] L. Wang, H. Zhou, Q. Chen, Z. Lin, C. Jiang, X. Chen, M. Chen, L. Liu, L. Shao, X. Liu, J. Pan, J. Wu, J. Song, J. Wu, D. Zhang, *Adv. Sci.* **2024**, *11*, 2307858.
[92] L. Chan, P. Gao, W. Zhou, C. Mei, Y. Huang, X. Yu, P. K Chu, T. Chen, *ACS Nano* **2018**, *12*, 12401.
[93] C. Beckers, M. Pruschy, I. Vetrugno, *Semin. Cancer Biol.* **2024**, *98*, 19.
[94] X. Ge, L. Su, Z. Chen, K. Zhu, X. Zhang, Y. Wu, J. Song, *Angew. Chem., Int. Ed.* **2023**, *62*, 202305744.
[95] Y. Wu, L. Su, M. Yuan, T. Chen, J. Ye, Y. Jiang, J. Song, H. Yang, *Angew. Chem., Int. Ed.* **2021**, *60*, 12868.
[96] L. Chen, J. Zhang, L. Xu, L. Zhu, J. Jing, Y. Feng, Z. Wang, P. Liu, W. Sun, X. Liu, Y. Li, H. Chen, *J. Nanobiotechnol.* **2022**, *20*, 293.

© 2024 The Authors. Advanced Materials published by Wiley-VCH GmbH

15214095, 2024, 27, Downloaded from https://onlinelibrary.wiley.com/doi/10.1002/adma.202402806 by Ewha Womans University Library, Wiley Online Library on [13/11/2024]. See the Terms and Conditions (https://onlinelibrary.wiley.com/terms-and-conditions) on Wiley Online Library for rules of use; OA articles are governed by the applicable Creative Commons License

[97] C. Pan, M. Ou, Q. Cheng, Y. Zhou, Y. Yu, Z. Li, F. Zhang, D. Xia, L. Mei, X. Ji, *Adv. Funct. Mater.* **2020**, *30*, 1906466.
[98] P. Zang, Y. Du, C. Yu, D. Yang, S. Gai, L. Feng, S. Liu, P. Yang, J. Lin, *Chem. Mater.* **2023**, *35*, 7770.
[99] Y. Dong, S. Dong, C. Yu, J. Liu, S. Gai, Y. Xie, Z. Zhao, X. Qin, L. Feng, P. Yang, Y. Zhao, *Sci. Adv.* **2023**, *9*, eadi9980.
[100] Y. Kang, N. Kong, M. Ou, Y. Wang, Q. Xiao, L. Mei, B. Liu, L. Chen, X. Zeng, X. Ji, *Bioact. Mater.* **2023**, *20*, 663.
[101] X. Jiang, M. Yang, Y. Fang, Z. Yang, X. Dai, P. Gu, W. Feng, Y. Chen, *Adv. Healthcare Mater.* **2023**, *12*, 2300699.
[102] S. Hur, S. Kim, H. Kim, A. Kumar, C. Kwon, J. Shin, H. Kang, T. H. Sung, J. Ryu, J. M. Baik, H. Song, *Nano Energy* **2023**, *114*, 108596.
[103] Y. Wang, X. Dai, C. Dong, W. Guo, Z. Xu, Y. Chen, H. Xiang, R. Zhang, *Adv. Mater.* **2022**, *34*, 2106773.
[104] Y. Chang, Y. Cheng, R. Zheng, X. Wu, P. Song, Y. Wang, J. Yan, H. Zhang, *Nano Today* **2021**, *38*, 101110.
[105] Y. Wang, Q. Tang, R. Wu, S. Sun, J. Zhang, J. Chen, M. Gong, C. Chen, X. Liang, *ACS Nano* **2023**, *17*, 3557.
[106] Y. Kang, L. Lei, C. Zhu, H. Zhang, L. Mei, X. Ji, *Mater. Horiz.* **2021**, *8*, 2273.
[107] S. Cheng, Y. Luo, J. Zhang, R. Shi, S. Wei, K. Dong, X. Liu, S. Wu, H. Wang, *Chem. Eng. J.* **2022**, *442*, 136380.
[108] S. Lv, Z. Qiu, D. Yu, X. Wu, X. Yang, Y. Ren, Y. Huang, G. Jiang, F. Gao, *Small* **2023**, *19*, 2300976.
[109] Q. Wang, Y. Tian, M. Yao, J. Fu, L. Wang, Y. Zhu, *Adv. Mater.* **2023**, *35*, 2301784.
[110] Q. Wu, J. Zhang, X. Pan, Z. Huang, H. Zhang, J. Guo, Y. Xue, R. Shi, H. Liu, *Adv. Sci.* **2023**, *10*, 2301152.
[111] S. Zhu, T. Zhang, H. Gao, G. Jin, J. Yang, X. He, H. Guo, F. Xu, *Adv. Healthcare Mater.* **2023**, *12*, 2300103.
[112] A. M. Mallick, A. Biswas, S. Mishra, S. Jadhav, K. Chakraborty, A. Tripathi, A. Mukherjee, R. S. Roy, *Chem. Sci.* **2023**, *14*, 7842.
[113] M. He, Z. Cheng, Z. Wang, M. Li, H. Liang, H. Liu, L. Yu, L. Zhao, F. Yu, *Adv. Healthcare Mater.* **2023**, *12*, 2300752.
[114] M. overchuk, R. A Weersink, B. Wilson, G. Zheng, *ACS Nano* **2023**, *17*, 7979.
[115] H. Hu, J. Zhao, K. Ma, J. Wang, X. Wang, T. Mao, C. Xiang, H. Luo, Y. Cheng, M. Yu, Y. Qin, K. Yang, Q. Li, Y. Sun, S. Wang, *J. Controlled Release* **2023**, *359*, 188.
[116] J. Li, X. Du, X. Zhou, J. Yoon, *Adv. Healthcare Mater.* **2023**, *12*, 2301022.
[117] X. Ma, Y. Huang, S. A. A. Abedi, H. Kim, T. T. B. Davin, X. Liu, W. Yang, Y. Sun, S. H. Liu, J. Yin, J. Yoon, G. Yang, *CCS Chem.* **2022**, *4*, 1961.
[118] Y. Zhao, H. Kim, V. Nguyen, S. Jang, W. J. Jang, J. Yoon, *Coord. Chem. Rev.* **2024**, *501*, 215560.
[119] Y. Zhao, L. Zhang, Z. Chen, B. Zheng, M. Ke, X. Li, J. Huang, *J. Am. Chem. Soc.* **2021**, *143*, 13980.
[120] S. Zhang, L. Wu, W. Shi, J. Qin, W. Feng, Y. Chen, R. Zhang, *Adv. Funct. Mater.* **2023**, *33*, 2302360.
[121] Y. Sang, F. Cao, W. Li, L. Zhang, Y. You, Q. Deng, K. Dong, J. Ren, X. Qu, *J. Am. Chem. Soc.* **2020**, *142*, 5177.
[122] L. S. Lin, T. Huang, J. Song, X. Y. Ou, Z. Wang, H. Deng, R. Tian, Y. Liu, J. F. Wang, Y. Liu, G. Yu, Z. Zhou, S. Wang, G. Niu, H. H. Yang, X. Chen, *J. Am. Chem. Soc.* **2019**, *141*, 9937.
[123] Y. Liao, D. Wang, S. Zhu, R. Zhou, F. Rahbarizadeh, Z. Gu, *Nano Today* **2022**, *44*, 101510.
[124] G. Li, X. Zhang, X. Wang, F. Gong, H. Lei, Y. Zhou, C. Li, Z. Xiao, G. Ren, L. Zhang, Z. Dong, Z. Liu, L. Cheng, *Bioact. Mater.* **2022**, *8*, 409.
[125] J. Wu, P. Ning, R. Gao, Q. Feng, Y. Shen, Y. Zhang, Y. Li, C. Xu, Y. Qin, G. R. Plaza, Q. Bai, X. Fan, Z. Li, Yu, H., M. S. Lesniak, H. Fan, Y. Cheng, *Adv. Sci.* **2020**, *7*, 1902933.
[126] Y. Zhang, Y. Xu, D. Sun, Z. Meng, W. Ying, W. Gao, R. Hou, Y. Zheng, X. Cai, B. Hu, X. Lin, *Chem. Eng. J.* **2020**, *390*, 124521.
[127] L. J. Delaney, J. R. Eisenbrey, D. Brown, J. R. Brody, M. Jimbo, B. E. Oeffinger, M. Stanczak, F. Forsberg, J. Liu, M. A. Wheatley, *Acta Biomater.* **2021**, *130*, 385.
[128] C. Schnell, *Nat. Methods* **2018**, *15*, 159.
[129] C. Rabut, S. Yoo, R. C. Hurt, Z. Jin, H. Li, H. Guo, B. Ling, M. G. Shapiro, *Neuron* **2020**, *108*, 93.
[130] S. Sabuncu, R. J. Ramirez, J. M. Fischer, F. Civitci, A. Yildirim, *Nano Lett.* **2023**, *23*, 659.
[131] L. Zhu, H. Zhao, Z. Zhou, Y. Xia, Z. Wang, H. Ran, P. Li, J. Ren, *Nano Lett.* **2018**, *18*, 1831.
[132] A. Bellary, A. Villarreal, R. Eslami, Q. J. Undseth, B. Lec, A. M. Defnet, N. Bagrodia, J. J. Kandel, M. A. Borden, S. Shaikh, R. Chopra, T. W. Laetsch, L. J. Delaney, C. M. Shaw, J. R. Eisenbrey, S. L. Hernandez, S. R. Sirsi, *Theranostics* **2020**, *10*, 8143.
[133] Y. Zhang, K. Xi, X. Fu, H. Sun, H. Wang, D. Yu, Z. Li, Y. Ma, X. Liu, B. Huang, J. Wang, G. Li, J. Cui, X. Li, S. Ni, *Biomaterials* **2021**, *278*, 121163.
[134] N. Zhao, L. Yan, J. Xue, K. Zhang, F. Xu, *Nano Today* **2021**, *38*, 101118.
[135] R. Zhou, Y. Liu, Z. Wang, J. Lv, W. Liao, Z. Shen, X. Rong, *Adv. Healthcare Mater.* **2023**, *12*, 2300176.
[136] B. Yang, Y. Zhang, L. Sun, J. Wang, Z. Zhao, Z. Huang, W. Mao, R. Xue, R. Chen, J. Luo, T. Wang, J. Jiang, Y. Qin, *Adv. Funct. Mater.* **2023**, *33*, 2211251.
[137] P. Shou, Z. Yu, Y. Wu, Q. Feng, B. Zhou, J. Xing, C. Liu, J. Tu, O. U. Akakuru, Z. Ye, X. Zhang, Z. Lu, L. Zhang, A. Wu, *Adv. Healthcare Mater.* **2020**, *9*, 1900948.
[138] H. Zhu, X. Yin, Y. Zhou, S. Xu, T. D. James, L. Wang, *Chem* **2022**, *8*, 2498.
[139] G. Guan, C. Zhang, H. Liu, Y. Wang, Z. Dong, C. Lu, B. Nan, R. Yue, X. Yin, X. Zhang, G. Song, *Angew. Chem., Int. Ed.* **2022**, *61*, 202117229.
[140] B. Yu, B. Choi, W. Li, D. Kim, *Nat. Commun.* **2020**, *11*, 3637.
[141] Z. Dong, P. Liang, G. Guan, B. Yin, Y. Wang, R. Yue, X. Zhang, G. Song, *Angew. Chem., Int. Ed.* **2022**, *61*, 202206074.
[142] Y. Kim, R. Thangam, J. Yoo, J. Heo, J. Y. Park, N. Kang, S. Lee, J. Yoon, K. R. Mun, M. Kang, S. Min, S. Y. Kim, S. Son, J. Kim, H. Hong, G. Bae, K. Kim, S. Lee, L. Yang, J. Y. Lee, J. Kim, S. Park, D. Kim, K. Lee, W. Y. Jang, B. H. Kim, R. Paulmurugan, S. Cho, H. Song, S. J. Kim, et al., *Adv. Mater.* **2022**, *34*, 2205498.
[143] X. Liu, Y. Chang, *Chem. Soc. Rev.* **2022**, *51*, 1573.
[144] S. Samanta, Y. He, A. Sharma, J. Kim, W. Pan, Z. Yang, J. Li, W. Yan, L. Liu, J. Qu, J. S. Kim, *Cell* **2019**, *5*, 1697.
[145] J. Zhang, X. Chai, X. He, H. Kim, J. Yoon, H. Tian, *Chem. Soc. Rev.* **2019**, *48*, 683.
[146] Q. Duan, Z. Zhao, Y. Zhang, L. Fu, Y. Yuan, J. Du, J. Wang, *Adv. Drug Delivery Rev.* **2023**, *196*, 114793.
[147] N. Kwon, C. S. Lim, G. Ko, J. Ha, D. Lee, J. Yin, H. M. Kim, J. Yoon, *Anal. Chem.* **2021**, *93*, 11612.
[148] P. Chen, W. Kuang, Z. Zhen, S. Yang, Y. Liu, L. Su, K. Zhao, G. Liang, *Theranostics* **2019**, *9*, 7359.
[149] X. Wu, R. Wang, S. Qi, N. Kwon, J. Han, H. Kim, H. Li, F. Yu, J. Yong, *Angew. Chem., Int. Ed.* **2021**, *60*, 15418.
[150] Y. Ji, C. Jones, Y. Baek, G. K. Park, S. Kashiwagi, H. S. Choi, *Adv. Drug Delivery Rev.* **2020**, *167*, 121.
[151] X. Hu, C. Zhu, F. Sun, Z. Chen, J. Zou, X. Chen, Z. Yang, *Adv. Mater.* **2024**, *36*, 2304848.
[152] H. Zhou, S. Li, X. Zeng, M. Zhang, L. Tang, Q. Li, D. Chen, X. Meng, *Chin. Chem. Lett.* **2020**, *31*, 1382.
[153] B. Yin, Q. Qin, Z. Li, Y. Wang, X. Liu, Y. Liu, S. Huan, X. Zhang, G. Song, *Nano Today* **2022**, *45*, 101550.
[154] W. Zhang, W. Deng, H. Zhang, X. Sun, T. Huang, W. Wang, P. Sun, Q. Fan, W. Huang, *Biomaterials* **2020**, *243*, 119934.

© 2024 The Authors. Advanced Materials published by Wiley-VCH GmbH

15214095, 2024, 27, Downloaded from https://onlinelibrary.wiley.com/doi/10.1002/adma.202402806 by Ewha Womans University Library, Wiley Online Library on [13/11/2024]. See the Terms and Conditions (https://onlinelibrary.wiley.com/terms-and-conditions) on Wiley Online Library for rules of use; OA articles are governed by the applicable Creative Commons License

[155] N. Uchida, M. Sekino, A. Kimoto, T. Hara, *Intensive Care Med.* **2023**, *49*, 1544.
[156] C. Zhang, A. Vedadghavami, T. He, J. F. Charles, A. G. Bajpayee, *ACS Nano* **2023**, *17*, 6649.
[157] F. Shao, Z. Pan, Y. Long, Z. Zhu, K. Wang, H. Ji, K. Zhu, W. Song, Y. Song, X. Song, Y. Gai, Q. Liu, C. Qin, D. Jiang, J. Zhu, X. Lan, *J. Nanobiotechnol.* **2022**, *20*, 243.
[158] A. J. Cochran, R. Essner, D. M. Rose, E. C. Glass, *Langenbecks Arch. Surg.* **2000**, *385*, 252.
[159] L. Deblock, B. Descamps, I. Goemaere, E. Goossens, G. Vergauwen, J. Debacker, P. Tummers, K. Remaut, I. V. Driessche, K. D. Buysser, J. D. Roo, C. Vanhove, *Chem. Mater.* **2023**, *35*, 8883.
[160] W. Park, S. Cho, D. Kang, J. han, J. Park, B. Lee, J. Lee, D. Kim, *Adv. Healthcare Mater.* **2020**, *9*, 1901812.
[161] J. Dai, H. Wang, Y. Xu, X. Chen, R. Tian, *Semin. Cancer Biol.* **2023**, *91*, 124.
[162] D. Jiang, X. Lan, W. Cai, *Clin. Cancer Res.* **2023**, *29*, 3259.
[163] D. Ruan, L. Zhao, J. Cai, W. Xu, L. Sun, J. Li, J. Zhang, X. Chen, H. Chen, *Theranostics* **2023**, *13*, 4694.
[164] J. Schwenck, D. Sonanini, J. M. Cotton, H. Rammensee, C. la Fougère, L. Zender, B. J. Pichler, *Nat. Rev. Cancer* **2023**, *23*, 474.
[165] Y. Huang, T. W. Chen, L. Chen, Y. Huang, Y. Lu, *Clin. Nucl. Med.* **2023**, *48*, 785.
[166] C. Lin, K. Huang, S. Kao, M. Lin, C. Lin, S. Yang, W. Chung, Y. Chang, R. Chein, P. Yang, *Sci. Adv.* **2023**, *9*, eade9944.
[167] A. Mishra, K. Gupta, D. Kumar, G. Lofland, A. K. Sharma, L. B. Solnes, S. P. Rowe, P. M. Forde, M. G. Pomper, E. W. Gabrielson, S. Nimmagadda, *J. Immunother. Cancer* **2023**, *11*, 007535.
[168] K. Hu, L. Xie, Y. Zhang, M. Hanyu, Z. Yang, K. Nagatsu, H. Suzuki, J. Ouyang, X. Ji, J. Wei, H. Xu, O. C. Farokhzad, S. H. Liang, L. Wang, W. Tao, M. Zhang, *Nat. Commun.* **2020**, *11*, 2778.
[169] Z. Li, N. Yu, J. Zhou, Y. Li, Y. Zhang, L. Huang, K. Huang, Y. Zhao, S. Kelmar, J. Yang, G. Han, *Adv. Mater.* **2020**, *32*, 2070371.
[170] X. Wang, K. Pu, *Chem. Soc. Rev.* **2023**, *52*, 4549.
[171] Y. Wang, G. Song, S. Liao, Q. Qin, Y. Zhao, L. Shi, K. Guan, X. Gong, P. Wang, X. Yin, Q. Chen, X. Zhang, *Angew. Chem., Int. Ed.* **2021**, *60*, 19779.
[172] W. Chen, Y. Zhang, Q. Li, Y. Jiang, H. Zhou, Y. Liu, Q. Miao, M. Gao, *J. Am. Chem. Soc.* **2022**, *144*, 6719.
[173] L. Yang, M. Zhao, W. Chen, J. Zhu, W. Xu, Q. Li, K. Pu, Q. Miao, *Angew. Chem., Int. Ed.* **2024**, *63*, 202313117.
[174] S. Liao, Y. Wang, Z. Li, Y. Zhang, X. Yin, S. Huan, X. Zhang, S. Liu, G. Song, *Theranostics* **2022**, *12*, 6883.
[175] J. Zou, L. Li, J. Zhu, X. Li, Z. Yang, W. Huang, X. Chen, *Adv. Mater.* **2021**, *33*, 2103627.
[176] Y. Xu, W. Yang, D. Yao, K. Bian, W. Zeng, K. Liu, D. Wang, B. Zhang, *Chem. Sci.* **2020**, *11*, 419.
[177] L. Lei, F. Yang, X. Meng, L. Xu, P. Liang, Y. Ma, Z. Dong, Y. Wang, X. Zhang, G. Song, *J. Am. Chem. Soc.* **2023**, *145*, 24386.
[178] Z. Li, L. Xu, J. Li, L. Lei, P. Liang, Q. Wu, F. Yang, T. Ren, X. Yin, L. Yuan, X. Zhang, *J. Am. Chem. Soc.* **2023**, *145*, 26736.
[179] Z. Hong, Z. Chen, Q. Chen, H. Yang, *Acc. Chem. Res.* **2022**, *56*, 37.
[180] P. Pei, Y. Chen, C. Sun, Y. Fan, Y. Yang, X. Liu, L. Lu, M. Zhang, H. Zhang, D. Zhao, X. Liu, F. Zhang, *Nat. Nanotechnol.* **2021**, *16*, 1011.
[181] J. Huang, L. Su, C. Xu, X. Ge, R. Zhang, J. Song, K. Pu, *Nat. Mater.* **2023**, *22*, 1421.
[182] W. Zeng, D. Ye, *Nat. Biomed. Eng.* **2023**, *7*, 197.
[183] C. Xu, J. Huang, Y. Jiang, S. He, C. Zhang, K. Pu, *Nat. Biomed. Eng.* **2023**, *7*, 298.
[184] C. Xu, S. He, X. Wei, J. Huang, M. Xu, K. Pu, *Adv. Mater.* **2023**, *35*, 2211651.
[185] R. Wu, Z. Yao, Z. Chen, X. Ge, L. Su, S. Wang, Y. Wu, J. Song, *Anal. Chem.* **2023**, *95*, 11219.
[186] P. K. Upputuri, M. Pramanik, *Wiley Interdiscip. Rev.: Nanomed. Nanobiotechnol.* **2020**, *12*, e1618.
[187] B. Park, S. Park, J. Kim, C. Kim, *Adv. Drug Delivery Rev.* **2022**, *184*, 114235.
[188] Y. Zhao, Z. Chen, L. Zhang, X. Qin, H. Liu, B. Zheng, M. Ke, J. Huang, X. Li, *Chem. Eng. J.* **2023**, *474*, 145921.
[189] Z. Zhao, C. B. Swartchick, J. Chan, *Chem. Soc. Rev.* **2022**, *51*, 829.
[190] J. Qi, L. Feng, X. Zhang, H. Zhang, L. Huang, Y. Zhou, Z. Zhao, X. Duan, F. Xu, R. T. K. Kwok, J. W. Y. Lam, D. Ding, X. Xue, B. Z. Tang, *Nat. Commun.* **2021**, *12*, 960.
[191] L. Yu, S. A. A. Abedi, J. Lee, Y. Xu, S. Son, W. Chi, M. Li, X. Liu, J. H. Park, J. S. Kim, *Angew. Chem., Int. Ed.* **2023**, *62*, 202307797.
[192] H. Zhu, B. Li, C. Y. Chan, B. L. Q. Ling, J. Tor, X. Y. Oh, W. Jiang, E. Ye, Z. Li, X. J. Loh, *Adv. Drug Delivery Rev.* **2023**, *192*, 114644.
[193] Y. He, Y. Pan, X. Zhao, W. Fan, Y. Cai, X. Mou, *Acta Biomater.* **2022**, *152*, 546.
[194] C. Zhou, L. Zhang, T. Sun, Y. Zhang, Y. Liu, M. Gong, Z. Xu, M. Du, Y. Liu, G. Liu, D. Zhang, *Adv. Mater.* **2021**, *33*, 2006532.
[195] S. Jiang, J. Lin, P. Huang, *Adv. Healthcare Mater.* **2023**, *12*, 2202208.
[196] C. Ou, W. Na, W. Ge, H. Huang, F. Gao, L. Zhong, Y. Zhao, X. Dong, *Angew. Chem., Int. Ed.* **2021**, *60*, 8157.
[197] G. Wen, X. Li, Y. Zhang, X. Han, X. Xu, C. Liu, K. W. Y. Chan, C. Lee, C. Yin, L. Bian, L. Wang, *ACS Appl. Mater. Interfaces* **2020**, *12*, 33492.
[198] S. Sun, D. Wang, R. Yin, P. Zhang, R. Jiang, C. Xiao, *Small* **2022**, *18*, 2202558.
[199] Q. Ye, S. Ling, S. Zheng, X. Xu, *Mol. Cancer* **2019**, *18*, 114.
[200] H. Zhou, L. Zhu, J. Song, G. Wang, P. Li, W. Li, P. Luo, X. Sun, J. Wu, Y. Liu, S. Zhu, Y. Zhang, *Mol. Cancer* **2022**, *21*, 86.
[201] Q. Wei, Y. Chen, X. Ma, J. Ji, Y. Qiao, B. Zhou, F. Ma, D. Ling, H. Zhang, M. Tian, J. Tian, M. Zhou, *Adv. Funct. Mater.* **2018**, *28*, 1704634.
[202] Z. Zheng, Z. Jia, C. Qu, R. Dai, Y. Qin, S. Rong, Y. Liu, Z. Cheng, R. Zhang, *Small* **2021**, *17*, 2006508.
[203] J. Ju, D. Xu, X. Mo, J. Miao, L. Xu, G. Ge, X. Zhu, H. Deng, *Carbohydr. Polym.* **2023**, *317*, 121048.
[204] J. Yang, L. Xiao, X. Gao, Y. Tang, S. Hu, *Clin. Nucl. Med.* **2024**, *49*, 180.
[205] Y. Zhang, S. He, C. Xu, Y. Jiang, Q. Miao, K. Pu, *Angew. Chem., Int. Ed.* **2022**, *61*, 202203184.
[206] T. Chen, L. Su, X. Ge, W. Zhang, Q. Li, X. Zhang, J. Ye, L. Lin, J. Song, H. Yang, *Nano Res.* **2020**, *13*, 3268.
[207] L. Ding, Z. Lyu, T. Perles-Barbacaru, A. Y. Huang, B. Lian, Y. Jiang, T. Roussel, C. Galanakou, S. Giorgio, C. Kao, X. Liu, J. lovanna, M. Bernard, A. Viola, L. Peng, *Adv. Mater.* **2024**, *36*, 2308262.
[208] J. Cui, F. Zhang, D. Yan, T. Han, L. Wang, D. Wang, B. Z. Tang, *Adv. Mater.* **2023**, *35*, 2302639.
[209] P. Xiao, Y. Sun, M. Liang, S. Yang, J. Li, L. Zhang, X. Jiang, W. Wu, *Mater. Today Nano* **2023**, *24*, 100404.
[210] L. Xia, X. Meng, L. Wen, N. Zhou, T. Liu, X. Xu, F. Wang, Z. Cheng, Z. Yang, H. Zhu, *Small* **2021**, *17*, 2100378.
[211] Y. Kang, X. Xu, X. Fan, Aodenggerile, S. Z, C. Tu, Z. Yan, R. Wang, W. Li, H. Qiu, *ACS Nano* **2020**, *14*, 4336.
[212] W. Qin, J. Huang, C. Yang, Q. Yue, S. Chen, M. Wang, S. Gao, X. Zhou, X. Yang, Y. Zhang, *Adv. Funct. Mater.* **2023**, *33*, 2209748.
[213] K. Wu, H. Zhao, Z. Sun, B. Wang, X. Tang, Y. Dai, M. Li, Q. Shen, H. Zhang, Q. Fan, W. Huang, *Theranostics* **2019**, *9*, 7697.
[214] F. Zeng, L. Tang, Q. Zhang, C. Shi, Z. Huang, S. Nijiati, X. Chen, Z. Zhou, *Angew. Chem., Int. Ed.* **2022**, *61*, 202112925.
[215] N. Yin, Y. Wang, Y. Cao, Y. Huang, L. Jin, S. Zhang, J. Liu, T. Zhang, Z. Lv, Y. Liu, S. Song, D. Wang, H. Zhang, *Nano Today* **2022**, *46*, 101619.
[216] K. Yang, B. Yu, W. Liu, Z. Zhang, L. Huang, S. Zhao, B. Wang, J. Yi, J. Yuan, Y. Zou, C. Lin, X. Song, M. Lan, *Chin. Chem. Lett.* **2023**, *34*, 107889.

© 2024 The Authors. Advanced Materials published by Wiley-VCH GmbH

15214095, 2024, 27, Downloaded from https://onlinelibrary.wiley.com/doi/10.1002/adma.202402806 by Ewha Womans University Library, Wiley Online Library on [13/11/2024]. See the Terms and Conditions (https://onlinelibrary.wiley.com/terms-and-conditions) on Wiley Online Library for rules of use; OA articles are governed by the applicable Creative Commons License

[217] H. Gu, W. Liu, W. Sun, J. Du, J. Fan, X. Peng, *Chem. Sci.* **2022**, *13*, 9719.
[218] X. Xing, P. Zhu, E. Pang, S. Zhao, Y. Tang, Z. Hu, Q. Ouyang, M. Lan, *Chin. Chem. Lett.* **2023**, 109452, https://doi.org/10.1016/j.cclet.2023.109452.
[219] J. C. Hsu, Z. Tang, O. E. Eremina, A. M. Sofias, T. Lammers, J. F. Lovell, C. Zavaleta, W. Cai, D. P. Cormode, *Nat. Rev. Methods Primers* **2023**, *3*, 30.
[220] S. Hassan, G. Prakash, A. Ozturk, S. Saghazadeh, M. F. Sohail, J. Seo, M. Dockmeci, Y. S. Zhang, A. Khademhosseini, *Nano Today* **2017**,*15*, 91.
[221] S. Liang, J. Yao, D. Liu, L. Rao, X. Chen, Z. Wang, *Adv. Mater.* **2023**, *35*, 2211130.
[222] S. F. Tehrani, P. Bharadwaj, J. L. Chain, V. G. Roullin, *J. Controlled Release* **2023**, *360*, 591.
[223] Y. Huang, C. Liu, Q. Feng, J. Sun, *Nanoscale Horiz.* **2023**, *8*, 1610.
[224] E. A. S. Polomski, H. W. Kapiteijn, J. C. Heemelaar, T. Kalisvaart, P. Dibbets-Schneider, F. H. P. Van Der Velden, J. L. Stoger, J. W. Jukema, L. F. De Geus-Oei, M. L. Antoni, *Eur. Heart J.* **2023**, *44*, ehad655.2692.
[225] H. Choi, G. Bae, C. Khatua, S. Min, H. J. Jung, N. Li, I. Jun, H. Liu, Y. Cho, K. Na, M. Ko, H. Shin, Y. H. Kim, S. Chung, J. Song, V. P. Dravid, H. Kang, *Adv. Funct. Mater.* **2020**, *30*, 2001446.
[226] S. Lee, M. S. Kim, K. D. Patel, H. Choi, R. Thangam, J. Yoon, T. M. Koo, H. J. Jung, S. Min, G. Bae, Y. Kim, S. Han, N. Kang, M. Kim, N. Li, H. E. Fu, Y. S. Jeon, J. Song, D. Kim, S. Park, J. Choi, R. Paulmurugan, Y. C. Kang, H. Lee, Q. Wei, V. P. Dravid, K. Lee, Y. K. Kim, H. Kang, *Small* **2021**, *17*, 2102892.
[227] X. Wang, W. Sun, H. Shi, H. Ma, G. Niu, Y. Li, J. Zhi, X. Yao, Z. Song, L. Chen, S. Li, G. Yang, Z. Zhou, Y. He, S. Qu, M. Wu, Z. Zhao, C. Yin, C. Lin, J. Gao, Q. Li, X. Zhen, L. Li, X. Chen, X. Liu, Z. An, H. Chen, W. Huang, *Nat. Commun.* **2022**, *13*, 5091.
[228] Q. Liu, J. Zou, Z. Chen, W. He, W. Wu, *Acta Pharm. Sin. B* **2023**, *13*, 4391.
[229] M. B. Al-Handawi, S. Polavaram, A. Kurlevskaya, P. Commins, S. Schramm, C. Carrasco-López, N. M. Lui, K. M. Solntsev, S. P. Laptenok, I. Navizet, P. Naumov, *Chem. Rev.* **2022**, *122*, 13207.
[230] G. Wu, F. Liu, N. Li, Q. Fu, C. Wang, S. Yang, H. Xiao, L. Tang, F. Wang, W. Zhou, W. Wang, Q. Kang, Z. Li, N. Lin, Y. Wu, G. Chen, X. Tan, Q. Yang, *Adv. Sci.* **2023**, *10*, 2304104.
[231] H. Abadijoo, R. Shakibi, F. R. Pouria, N. Manoochehri, S. Moharamipour, M. Hasanloo, M. Ghaderinia, A. A. Moosavi-Movahedi, M. Abdolahad, M. A. Khayamian, *Nano Energy* **2024**, *120*, 109157.
[232] A. J. Syed, J. C. Anderson, *Chem. Soc. Rev.* **2021**, *50*, 5668.
[233] E. S. Shakhova, T. A. Karataeva, N. M. Markina, T. Mitiouchkina, K. A. Palkina, M. M. Perfilov, M. G. Wood, T. T. Hoang, M. P. Hall, L. I. Fakhranurova, A. E. Alekberova, A. K. Malyshevskaia, D. A. Gorbachev, E. N. Bugaeva, L. K. Pletneva, V. V. Babenko, D. I. Boldyreva, A. Y. Gorokhovatsky, A. V. Balakireva, F. Gao, V. V. Choob, L. P. Encell, K. V. Wood, I. V. Yampolsky, K. S. Sarkisyan, A. S. Mishin, *Nat. Methods* **2024**, *21*, 406.
[234] W. Kim, D. Kim, H. M. Lee, Y. Choi, *Nano Energy* **2022**, *100*, 107485.
[235] X. Fu, X. Pan, Y. Liu, J. Li, Z. Zhang, H. Liu, M. Gao, *Adv. Funct. Mater.* **2023**, *33*, 2306749.
[236] B. Zhang, X. Li, W. Shu, Y. Yang, H. Zhu, C. Shao, *Mater. Design* **2022**, *222*, 111067.
[237] A. H. C. Anthis, S. Kilchenmann, M. Murdeu, P. J. LeValley, M. Wolf, C. Meyer, O. Cipolato, M. W. Tibbitt, J. Rosendorf, V. Liska, T. Rduch, I. K. Herrmann, *Adv. Mater.* **2024**, https://doi.org/10.1002/adma.202310301.
[238] B. Li, J. Mao, J. Wu, K. Mao, Y. Jia, F. Chen, J. Liu, *Small* **2024**, *20*, 2306135.



Hai Xu received his Ph.D. degree from the Southwest Jiaotong University in 2023. Then, he joined Prof. Juyoung Yoon's group as a postdoctoral researcher. His current interests include the design and development of fluorescent chemosensors, molecular recognition, and NIR-II imaging and therapy.



Dahee Kim received her B.S. degree in Materials Science and Engineering from the Korea University, Seoul, in 2023. She is pursuing her MS/Ph.D. degree in Prof. Heemin Kang's laboratory since 2023.

© 2024 The Authors. Advanced Materials published by Wiley-VCH GmbH

15214095, 2024, 27, Downloaded from https://onlinelibrary.wiley.com/doi/10.1002/adma.202402806 by Ewha Womans University Library, Wiley Online Library on [13/11/2024]. See the Terms and Conditions (https://onlinelibrary.wiley.com/terms-and-conditions) on Wiley Online Library for rules of use; OA articles are governed by the applicable Creative Commons License



Yuan-Yuan Zhao received his Ph.D. degree from the Fuzhou University in 2021 under the supervision of Prof. Jiandong Huang and Prof. Xingshu Li. Then, he joined Prof. Juyoung Yoon's group as a postdoctoral researcher. His current interests include the design and development of activatable photosensitizers, nanoprobes, and multifunctional theranostic agents.



Chowon Kim received her B.S. degree in Materials Science and Engineering from the Korea University, Seoul, in 2022. She is pursuing her MS/Ph.D. degree in Prof. Heemin Kang's laboratory since 2022.



Guosheng Song received his Ph.D. degree from the Donghua University in 2014. He did postdoctoral research at the Soochow University and then at Stanford University from 2014 to 2018. In 2018, he joined the College of Chemistry and Chemical Engineering, Hunan University. His research mainly focuses on the design of activatable nanoplatforms for multimode imaging and cancer therapy.



Qiongzheng Hu received his B.Sc. in Applied Chemistry from the Shandong University in 2009, his M.Eng. in Nanosystem from the Gachon University in 2011, and his Ph.D in Chemistry from the University of Houston in 2017. He also worked as postdoctoral fellow in the Salk Institute for Biological Studies and University of Washington at Seattle. Currently, he is a professor in the College of Chemistry and Pharmacy at the Qilu University of Technology (Shandong Academy of Sciences).

© 2024 The Authors. Advanced Materials published by Wiley-VCH GmbH

15214095, 2024, 27, Downloaded from https://onlinelibrary.wiley.com/doi/10.1002/adma.202402806 by Ewha Womans University Library, Wiley Online Library on [13/11/2024]. See the Terms and Conditions (https://onlinelibrary.wiley.com/terms-and-conditions) on Wiley Online Library for rules of use; OA articles are governed by the applicable Creative Commons License



Heemin Kang received his M.S. at Stanford University in 2008 and Ph.D. at UC San Diego in 2016. Currently, he is an associate professor in the Department of Materials Science and Engineering (joint: College of Medicine) and the director of the Dynamic Nanobioengineering Laboratory at Korea University in Seoul.



Juyoung Yoon received his Ph.D. in 1994 at the Ohio State University and conducted his postdoctoral work at the UCLA and Scripps Research Institute. Currently, he is a distinguished professor at the Department of Chemistry and Nanoscience, Ewha Womans University. His research interests include the investigation of fluorescent chemosensors, activatable photosensitizers, and organic functional materials for cancer therapy and imaging. He has been a "Highly-Cited Researcher" by Clarivate Analytics/Thomson Reuters since 2014 with an h-index of 125.

© 2024 The Authors. Advanced Materials published by Wiley-VCH GmbH

15214095, 2024, 27, Downloaded from https://onlinelibrary.wiley.com/doi/10.1002/adma.202402806 by Ewha Womans University Library, Wiley Online Library on [13/11/2024]. See the Terms and Conditions (https://onlinelibrary.wiley.com/terms-and-conditions) on Wiley Online Library for rules of use; OA articles are governed by the applicable Creative Commons License